STRATEGIES FOR CONTROLLING THE INNATE IMMUNE RESPONSES TO IN VITRO TRANSCRIBED MESSENGER RNAS

A Dissertation
Presented to
The Academic Faculty

by

Kristin Helene Loomis

In Partial Fulfillment
Of the Requirements for the Degree
Doctor of Philosophy in Biomedical Engineering in the
Wallace H. Coulter Department of Biomedical Engineering

Georgia Institute of Technology

May, 2016

STRATEGIES FOR CONTROLLING THE INNATE IMMUNE RESPONSES TO IN VITRO TRANSCRIBED MRNAS

Dr. Ravi Bellamkonda, Ph.D., Advisor
Department of Biomedical Engineering
Georgia Institute of Technology

Philip J. Santangelo, Ph.D.
Department of Biomedical Engineering
Georgia Institute of Technology

Dr. Julia Babensee, Ph.D.
Department of Biomedical Engineering
Georgia Institute of Technology

Dr. Krishnendu Roy, Ph.D.
Department of Biomedical Engineering
Georgia Institute of Technology

Dr. Susan Thomas, Ph.D.
School of Mechanical Engineering
Georgia Institute of Technology

Date Approved:
January 29, 2016

To my family

who inspire me in so many ways

ACKNOWLEDGEMENTS

It is humbling and heartwarming to reflect on all of the help and support that I received throughout my time at Georgia Tech. I was lucky to receive the support and direction from two advisors who helped guide me through the PhD process. First, I would like to thank Dr. Bellamkonda for his support, patience, and encouragement. He provided me with a truly unique laboratory experience, giving me incredible flexibility and freedom, which allowed me to learn first-hand how to approach challenges. I have taken away many life-long lessons and skills that would not have been possible under other circumstances.

Very importantly, Dr. Santangelo, my committee member who turned into an unofficial advisor, has been an incredible force in helping me shape this dissertation. I am extremely grateful that he incorporated me into his lab group. I have learned so much about RNA biology, how to design experiments, ask questions, and solve problems through working with him.

I would also like to thank my committee members for advising me throughout my graduate work. They have asked insightful questions and have always steered me in a better direction and forced. They have all helped me to embrace the questions in research to gain a deeper understanding.

I had very little molecular biology experience when I began my PhD studies. I would like to thank Balakrishna Pai, Shannon Barker, Lohitash Karumbaiah, and Nalini Mehta for sharing their knowledge with me. Dr. Pai, especially, patiently taught me the basics of DNA cloning, Western blotting, and DNA gels, along with a few tricks and shortcuts along the way. He gave me the technical fundamentals in molecular biology that have enabled future experiments.

Both of the labs that I have been a part of have helped me grow. First, I would like to thank the Neurolab –past and present--for their help, inspiration, and support. The passion and excitement about science in the lab is contagious. I greatly appreciate the questions, support, and scientific conversations we have had over the years.

Every single member of the Santangelo lab has directly or indirectly impacted my thesis work in a major way. Many aspects of the work presented here have built upon previous studies in the lab. Daryll Vanover and Jonathan Kirschman have especially helped me with microscopy and general lab support. Sushma Bhosle assisted with experiments and provided company during so much of our time in the PRL.

I would also like to acknowledge the undergraduate students who have contributed to this work. Sarah Kutbay started working with me in the very beginning. She was extremely perseverant and cheerful as we struggled to establish protocols for making IVT mRNA and transfection cells. Shahmeer Mirza's enthusiastic questioning and excitement for the research helped me improve my understanding of our experiments. Lastly, Ravi Jindal showed extreme care in performing experiments, even when they were quite monotonous.

So many others helped me along the way. I want to thank Brani Vidakovic for his assistance with the statistical analysis of my PLA data. I also want to thank Laura O'Farrell for all of her advice and training. The core-facilities staff have also enabled my studies; Andrew Shaw's technical expertise guided me with some microscopy studies and Dalia Arafat Gulick helped me with the Fluidigm PCR studies. Ketki Patil, Claire McCauley, and Moliehi Mokoroane also provided so much support; they often went out of their way to assist with last minute orders and lab maintenance.

My PhD experience was so much richer because of the friends that I made along the way. Patricia Pacheco's support and friendship cannot be described. She helped me overcome setbacks, and balance my life outside of lab. I also want to thank my labmate

and classmate Akhil Srinivasan. We shared many late-nights doing homework, lab experiments, and exploring Atlanta. You have been an inspiration to watch navigate the PhD process. Last but far from least, I would like to thank Saujan Sivaram for his incredible love and support throughout my time at Georgia Tech. You have taught me so much about science and about life. I am grateful every day to have you in my life.

TABLE OF CONTENTS

LIST OF TABLES

LIST OF FIGURES

LIST OF SYMBOLS AND ABBREVIATIONS

5mc	5-methylcytosine
Ara h 2	Arachis hypogaea 2
BMDC	bone marrow-derived dendritic cell
cOVA	cytoplasmic ovalbumin
DNA	deoxyribonucleic acid
dsRNA	double-stranded ribonucleic acid
FBS	fetal bovine serum
HIV	human immunodeficiency virus
i.m.	intramuscular
Ifnβ1	interferon-beta 1
Il1β	interleukin-1 beta
IPS-1	interferon-beta promoter stimulator 1
IRAK4	interleukin-1 receptor-associated kinase protein 4
IRFs	interferon -regulatory factor
IVT mRNA	in vitro transcribed messenger ribonucleic acid
L2K	Lipofectamine-2000
LYVE-1	lymphatic vessel endothelial hyaluronan
M1Y	N^1-Methylpseudouridine
MDA5	melanoma differentiation-associated protein 5
MTRIP	multiply-labeled tetravalent ribonucleic acid imaging probes
MYD88	myeloid differentiation primary response gene 88
NF-κB	nuclear factor-κB
OAS-L	2'-5'-oligoadenylate synthetase-like

PAMP	pathogen-associated molecular pattern
PBS	Phosphate-buffered saline
PKR	protein kinase RNA-activated
PLA	proximity ligation assay
PRR	pathogen recognition receptor
qRT-PCR	quantitative reverse transcription polymerase chain reaction
RIG-I	retinoic acid-inducible gene 1
RiLA	ringer's lactacte solution
RNA	ribonucleic acid
RNP	ribonucleoprotein
SEAP	secreted alkaline phosphatase
siRNA	silencing ribonucleic acid
ssRNA	single-stranded RNA
TLR	toll-like receptor
UTR	untranslated region
Ψ	pseudouridine

SUMMARY

Synthetic messenger RNA (mRNA) produced via in vitro transcription (IVT mRNA) has emerged as an appealing tool for the transient introduction of genes, particularly for vaccination applications. The interaction that IVT mRNA has with the innate immune system is centrally important to its performance as a vaccine. These innate immune responses can both interfere with the expression of the encoded antigenic protein and direct development of adaptive immunity. The objective of this thesis is to investigate the innate immune responses to IVT mRNA and to identify strategies to modulate these immune responses.

We first demonstrated that substitution of the modified bases 5-methylcytosine and pseudouridine in IVT mRNA consistently reduces antiviral cytokine responses but affects transgene expression in a gene-specific manner. To assess the pathogen recognition receptors involved in detection of IVT mRNA, we developed proximity ligation assays, which allowed histological identification of PRR signaling complexes. We used these assays to identify that nanoparticle-mediated delivery modified PRR-activation following intramuscular delivery compared to delivery of the naked IVT mRNA molecule. Lastly, we developed a strategy to program the immunostimulatory properties of IVT mRNA by tethering adjuvants directly to the molecule. We show that upon intramuscular injection, the combination delivery of a TLR7 adjuvant and IVT mRNA lead to heightened local antiviral responses when delivered tethered, rather than as a cocktail. This work provides a foundation for the modulation and systematic study of IVT mRNA's interaction with the innate immune system. Insights gained from this work may help direct and advance the design of IVT mRNA sequences for vaccination applications.

CHAPTER 1

INTRODUCTION

The work presented here contains excerpts from the publication:

Loomis, K.H., Kirschman J.L., Bhosle S., Bellamkonda, R.V., and Santangelo PJ. Strategies for modulating innate immune activation and protein production of *in vitro* transcribed mRNAs. J. Mater. Chem. B, DOI:10.1039/C5TB01753J. (2015).

1.1 Principles of vaccination

Vaccines have prevented a countless number of deaths since their widespread adoption. Yet, infectious diseases are still responsible for one-third of all deaths and are the leading cause of childhood death in developing countries (1). Many of these diseases lack any preventative treatment. In addition, vaccination could potentially prevent or treat autoimmune diseases, cancers, and allergies.

The ultimate goal of vaccine design is to generate protective immunity against a pathogen. Successful protection may require specific types of adaptive immune responses for a pathogen. For example, vaccines targeting respiratory infections such as influenza mainly protect through immunoglobulin G serum antibodies, while vaccines targeting intestinal diseases such as cholera largely protect through immunoglobulin A gut antibodies (2).

Innate immune responses to a vaccine inform adaptive immune responses (3). Pathogen-recognition receptors (PRRs) recognize pathogen-associated molecular patterns (PAMPs), such as viral nucleic acids, to direct the formation of adaptive immune responses.

1.2 Current vaccine classifications

Several broad categories for vaccines are clinically used. These include live-attenuated, inactivated, and sub-unit vaccines.

1.2.1 Live attenuated vaccines

Live-attenuated vaccines generally elicit strong cellular and humoral immune responses to generate robust protective immunity. This class of vaccine is generated by weakening a pathogen, typically through repeated culture passage. However, as the pathogen is still active, it can pose safety risks. For example, live-attenuated vaccines for highly virulent diseases such as the human immunodeficiency virus (HIV) are difficult to declare sufficiently safe. Additionally, as temperature-controlled storage may be required, transport, delivery, and storage of these vaccines can impede their implementation. Examples of this approach include typhoid, mumps, and rubella vaccines (4).

1.2.2 Inactivated vaccines

Inactivated vaccines are a safer and more stable alternative to live-attenuated vaccines since the pathogens are killed. Inactivation is accomplished through heat, radiation, or chemical exposure. One limitation is that inactivated pathogens generally lead to a weaker immune response than live-attenuated vaccines, such that repeated boosters of the vaccine are often necessary. This class of vaccine tends to function through development of humoral immunity and is associated with lower cell-mediated immune responses. Inactivated pathogens have been used in vaccines to prevent polio, hepatitis A, and diphtheria (4).

1.2.3 Subunit vaccines

Subunit vaccines offer a further reduced risk of adverse reactions to inactivated vaccines. Antigenic subunits of pathogens (antigenic proteins or polysaccharides) are isolated and conjugated to other proteins or immune stimulating toxins. These vaccine components can be grown in recombinant systems or isolated from cultured pathogens. Similar to inactivated vaccines, subunit vaccines often require repeated boosts to develop protective immunity. Moreover, they lead to generally weak cellular immune responses. Subunit vaccines are currently used for hepatitis B and *Haemophilus influenza* type B (4).

1.3 Challenges facing future development of vaccines

Are current strategies for vaccine design appropriate for preventing the remaining diseases that lack a preventative measure? Previous vaccine strategies primarily rely upon humoral rather than cellular immunity to instill immunological protection (5). While these strategies have succeeded in preventing many infectious diseases, they have met limited success against infections such as malaria, HIV, and tuberculosis (6, 7). Indeed, a multitude of other infectious diseases, autoimmune diseases, and cancers remain potential targets for vaccine research and development.

There are several challenges facing vaccine development given our current toolbox:

- pathogens are difficult to grow *in vitro*
- pathogens are dangerous to grow *in vitro*
- pathogens or diseases have extensive antigen variability (e.g., cancer or HIV)

- pathogens have an intracellular phase in the host, and thus require developing cellular immune responses in addition to, or instead of, antibody-mediated responses
- vaccine development is not rapid enough to properly respond to quickly mutating diseases (e.g., influenza) (4, 8)

1.4 Nucleic acids as next generation vaccines

Nucleic acid vaccines present a safe, non-live approach for vaccination. Primarily researched nucleic acid vaccines include plasmid DNA and IVT mRNA. These platforms address many of the present challenges associated vaccine design. Nucleic acid vaccines deliver the genetic form of antigenic protein(s), directing antigen production in the host. As nearly cell-free systems produce nucleic acid-based vaccines, their production is rapid and relatively easy compared to other vaccine classifications. The ease in production also enables this platform to address antigenic variability in pathogens, as multiple IVT mRNA sequences can be manufactured with relative ease. Nucleic acid vaccines are also associated with eliciting a balanced immune response, directing production of both humoral and cellular immunity.

1.4.1 Plasmid DNA as next generation vaccines

Plasmids DNA vaccines consist of a circular piece of DNA that encodes for antigenic protein(s). Upon administration to a host, plasmid DNA interacts with normal cellular functions to undergo transcription and translation, leading to the production of antigenic protein. During plasmid DNA entry into the nucleus PRRs, namely TLR9 and absent in melanoma 2 (AIM2), detect the nucleic acid and initiate immune responses (9, 10). While initial clinical trials using plasmid DNA vaccines failed to initiate strong immune responses, recent preclinical research has identified strategies to enhance their

immunogenicity. These strategies include co-delivery of a plasmid with adjuvant molecules (11, 12), encoding adjuvant proteins along with the antigenic protein (13), more effective delivery strategies (using nanoparticles or electroporation), and co-delivery with RNA interference molecules (14, 15). While DNA vaccines are not used in clinical practice, several clinical trials are ongoing. They are also used in veterinary vaccination (16, 17).

1.4.2 IVT mRNA as next generation vaccines

Synthetic messenger RNA *(*mRNA) produced by *in vitro* transcription (IVT mRNA) has more recently gained interest as a vaccine platform. PRRs detect IVT mRNA and initiate immune responses. IVT mRNA's utility as a vaccine has been demonstrated in preclinical settings for cancer immunotherapy (18), allergy prevention (19), and infectious disease vaccines (20). It is now in clinical trials as a vaccine for several types of cancers including prostate (21) melanoma (22) and renal cell carcinoma (23).

There are some important distinctions between plasmid DNA and IVT mRNA that merit discussion: The more transient nature of IVT mRNA likely offers improved control over protein expression kinetics and nucleic acid dosing. For some cell types, particularly non-dividing cells, IVT mRNA leads to more effective protein production (24, 25) as plasmid DNA often relies on cell division to enter the nucleus and IVT mRNA only needs to enter the cytoplasm (26). IVT mRNA is touted as being more immunogenic than plasmid DNA. While this claim has not been tested, the field is hopeful that IVT mRNA's immunogenicity will translate to improved performance in clinical trials.

1.5 Multifunctionality of IVT mRNA

IVT mRNA is a multifunctional molecule, enabling transgene protein production and stimulating the innate immune system. It is important to recognize that PRR recognition affects transgene expression. Activation of antiviral PRRs initiate cellular protection mechanisms that inhibit protein production and degrade RNAs. This section discusses the ability of IVT mRNA to drive transgene protein production and its interactions with innate immunity.

1.5.1 Protein production by IVT mRNA

Protein translation requires host factors to interact with mRNA, forming ribonucleoproteins (RNPs). RNP formation not only regulate translation but also regulate localization and degradation of mRNAs. Despite the importance of RNP formation for mRNA performance, our understanding regarding the quality and formation of RNPs with IVT mRNA is limited. This section compares the regulation of endogenous mRNAs with exogenously delivered IVT mRNA to highlight some of the challenges facing protein production by IVT mRNA.

1.5.1.1 Transcription and translation of endogenous mRNAs

Localization, half-life, and protein expression of endogenous mRNAs are tightly regulated. Regulation of endogenous mRNAs is dynamic and complex: at least several hundred different proteins are involved (27, 28). Endogenous mRNAs are transcribed in the nucleus, where they concurrently bind to a variety of trans-acting factors. In the nucleus, there is evidence that mRNAs undergo a process termed *mRNA imprinting*. This process is believed to assist the cell in differentiating host mRNAs from foreign mRNAs. The process of mRNA imprinting includes the addition of a 5' cap, binding of the cap binding complex, the addition of a poly(A) tail, binding of a poly(A) binding

protein, splicing, and the binding of a variety of other trans-acting factors. Many mRNAs undergo splicing, where introns are removed from the mRNA. As introns are removed, exon junction complexes (EJCs) are deposited upstream of adjoined exon-exon junctions and serine and arginine-rich proteins bind to the mRNA. These factors, along with other cis and trans-acting factors ultimately direct a variety of regulatory processes (29-31).

Once in the cytoplasm, mRNAs undergo a pioneering round of translation. During this time, the nuclear cap-binding complex supports ribosome binding to the mRNA. The initiation factor eIF4e replaces the cap-binding complex as the mRNA enters steady state translation. At this time, mRNA circularization facilitates ribosome recycling- ribosomes that recently terminated translation are near the start codon to begin with the translation of a new protein (32).

1.5.1.2 Transcription and translation of exogenously delivered mRNAs

One stark contrast between IVT and endogenous mRNAs is that endogenous mRNAs are almost entirely in RNPs, where IVT mRNA formulations typically are protein-free. IVT mRNA often enters the cell via the endolysosomal system (33, 34). Throughout its extracellular, endosomal, and cytosolic presence, IVT mRNA likely interacts with PRRs, inducing antiviral immune responses. To undergo translation, IVT mRNA needs to interact with translation initiation factors and ribosomes.

1.5.1.3 Engineered untranslated regions for enhancing transgene protein production

Engineering 5' and 3' UTRs (untranslated regions) into IVT mRNA is an easy strategy for exerting control over transgene expression. UTRs in endogenous mRNAs interact with trans-factors to influence half-life and translation rates. Most IVT mRNAs

described in the literature include 3' UTRs from endogenous mRNAs that have long half-lives such as those from the α-globin (35), albumin (36), or β-globin (37, 38). Internal ribosome entry site (IRES) sequences are best known as elements in viruses, which function to recruit ribosomes and facilitate cap-independent translation. Thess et al. show that a viral IRES sequence allows for cap-independent translation in IVT mRNA (36). As exogenously delivered IVT mRNA likely encounter trans-acting factors in the same way that endogenously produced mRNA does, engineered UTRs will likely function differently in exogenously delivered mRNAs.

1.5.2 Innate immune stimulation by IVT mRNA

The immune stimulatory characteristics of IVT mRNA are often touted as an advantage in vaccination applications. Innate immune stimulation drives the development of adaptive immune responses (39-41). While many aspects of innate immune stimulation by IVT mRNA may be beneficial, certain aspects may be disadvantageous. Innate immune responses to IVT mRNA inhibits transgene protein production and leads to cell death, potentially stymieing development of adaptive immune responses. Thus, there needs to be a balance between innate immune stimulation and transgene protein production.

Pollard et al. demonstrated how an overactive innate immune response could have deleterious effects. The group showed that an IVT mRNA vaccine for HIV could generate potent T cell immunity against the HIV gag protein. However, they were curious regarding the high interferon responses initiated following IVT mRNA injection. To explore this, they vaccinated either interferon alpha receptor-deficient or wild type mice with their vaccine and showed that mice interferon alpha receptor had significantly increased gag-specific T cell responses (42). This finding clearly demonstrates that certain aspects of IVT mRNA's adjuvant effect can be disadvantageous for vaccination.

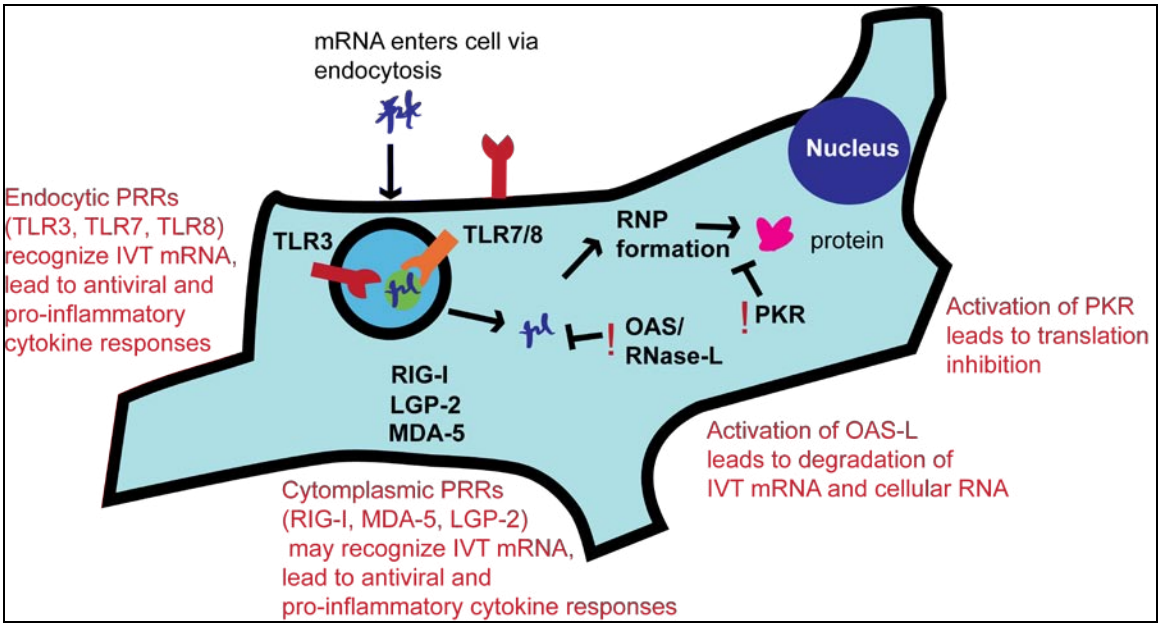

Figure 1.1. IVT mRNA interaction with PRRs. IVT mRNA may interact with PRRs in the extracellular space (TLR3) or in the endosomal system (TLR3, TLR7, or TLR8). Once escaped, cytosolic IVT mRNA is available for interaction with additional PRRs, including RIG-I, MDA-5, LGP-2, PKR, and OAS-L. Activation of the OAS pathway and PKR lead to degradation of RNA and inhibition of protein production, possibly causing cell death. Activation of other PRRs leads to generation of type I interferon as well as inflammatory cytokines. This triggers a positive feedback loop where PRR expression is upregulated.

Table 1.1 lists PRRs that potentially interact with IVT mRNA. Figure 1.1 describes how IVT mRNA's entry into the cell influences interactions with PRRs. Most commonly, IVT mRNA enters the cell via the endolysosomal system (34). Here, it can interact with TLR3 (43), TLR7 (44), or TLR8 (37) in the endolysosomal compartment. If IVT mRNA escapes into the cytoplasm, it may then activate OAS-L, PKR, and/or RIGI-I (45). Activation of these PRRs leads to upregulation of type I interferon and NF-κB related genes. As a result, the dsRNA-dependent protein kinase (PKR) and 2'-5'-Oligoadenylate Synthetase-Like (OAS-L), along with other PRR genes, are upregulated (35). Both PKR and OAS-L recognize unmodified IVT mRNA (46, 47). Thus, a positive feedback loop is generated for further response to IVT mRNA transfection (48).

PKR and OAS-L pathways are likely the most detrimental antiviral pathways to IVT mRNA delivery, as they both inhibit protein expression (of endogenous mRNA and IVT mRNA). When PKR is activated, it phosphorylates the initiation factor eIF2α, arresting initiation of protein translation, both from delivered and host mRNA. OAS-L response to IVT mRNA by activating the latent RNAs-L, which degrades ribosomal RNA and mRNA-- reducing transgene protein expression, cell proliferation, and potentially causing cell death (49).

Activation of some of these PRRs is centrally important in the efficacy of different vaccines (19, 50-52). For example, Mleczek et al. showed that when an anti-cancer IVT mRNA vaccine was complexed to protamine, TLR7 activation was enhanced, which also corresponded with tumor regression (44). The ability to reduce certain PRR activation (such as PKR and OAS-L) while potentially enhancing activation of other PRRs (such as TLRs and RLRs) could prove beneficial for IVT mRNA vaccines.

It may be surprising how antiviral receptors recognize IVT mRNAs but not endogenous mRNAs. Both the abnormal extracellular and endosomal location of IVT mRNA facilitates its detection by PRRs. However, IVT mRNA is also recognized by

cytoplasmic PRRs such as RIG-I and PKR. These PRRs recognize signatures of viral nucleic acids such as double stranded-RNA and 5' triphosphates. It is possible that PRRs detect secondary structure in IVT mRNAs. Secondary structure formation in endogenous RNAs may be hampered by RNP formation.

Table 1.1. PRRs known or suspected to respond to exogenous mRNA delivery

PRR	**Ligand**	**Commentary**		**Key References**
PKR*	Uncapped mRNA, RNA with complex secondary structure such as a pseudoknot	Phosphorylation of EIF-2α (inhibition of translation)		(46, 53, 54)
OAS-L*	dsRNA	Leads to activation of RNase-L, mRNA and rRNA degradation, possibly apoptosis, and activation of RIG-I		(47, 49, 55, 56)
MDA-5	Long dsRNA	Interferon, inflammatory cytokine production		(59)
RIGI-I*	5' triphosphate with dsRNA; complex secondary structure in RNA; RNase-L digestion products	Consistently expressed across cell types (57, 58)		(37, 60-62)
LGP2	dsRNA	Assists and modulates MDA-5 interaction with RNA		(63)
TLR3*	dsRNA	Active in the plasma membrane and endosomes	Expressed differentially across cell types	(37, 43, 64)
mTLR7*/ hTLR8*	ssRNA (GU rich RNA)	Active in endosomes		(37, 65-67)
hTLR7*	Possibly ssRNA (G rich ssRNA)			(37, 57, 67, 68)

*exogenously delivered IVT mRNA has been experimentally demonstrated to activate or interact with the receptor.

1.6 Strategies to modulate IVT mRNA's interaction with innate immunity

There are several strategies to alter protein production and innate immune activation by IVT mRNA. Figure 1.2 shows a diagram of IVT mRNA and outlines the various regions available for modulating its properties.

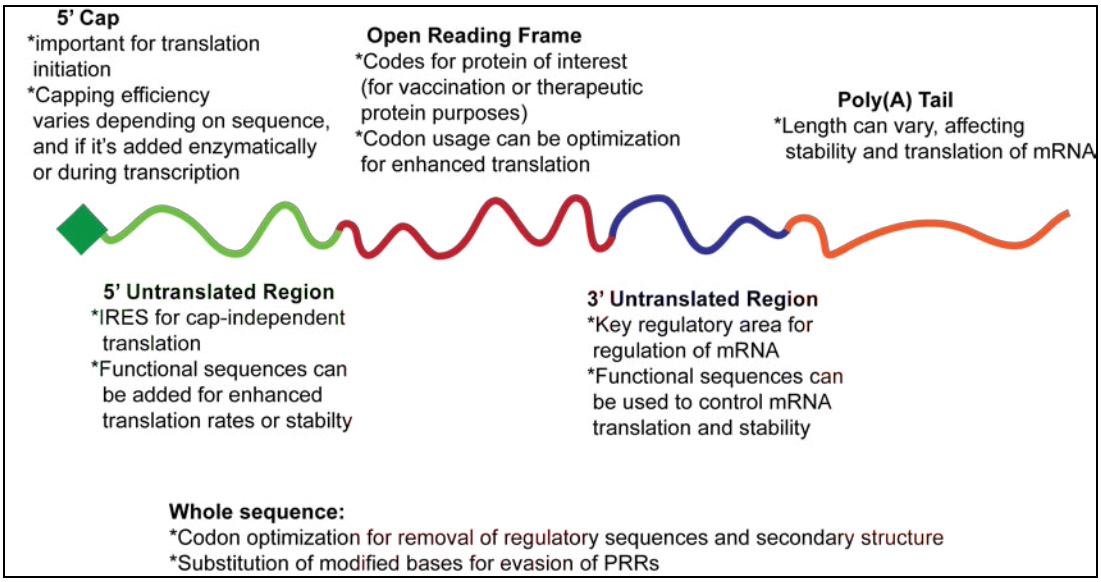

Figure 1.2. Diagram of IVT mRNA and opportunities for engineering its function. IVT mRNA consists of a 5' cap, 5' untranslated region, open reading frame, 3' untranslated region, and a poly(A) tail. Each of these areas can be engineered to affect IVT mRNA regulation and function.

1.6.1 Substitution of modified bases

One way to modulate IVT mRNA interaction with innate immunity is by substituting modified bases into the mRNA strand for their unmodified counterpart. Endogenous and viral RNAs are modified in over a hundred different ways (such as by addition of a methyl or thiol group to nucleobases) (69). These modifications can influence RNA secondary structure (70-73), regulate gene expression (74-77), and

influence RNA detection by PRRs (78-80). Thus, the inclusion of modified bases in IVT mRNA has also been explored. IVT mRNAs have been investigated that contain a variety of modified bases: 5-methylcytosine (35, 37), 2-thiouridine (37, 81), 5-methyluridine (46), 6-methyladenosine (45, 46), and most notably, pseudouridine (45-47, 82). Each modified base has been shown to impact IVT mRNA performance in a different way. Pioneering work by Kariko identified that that substitution of uridine with pseudouridine diminishes PKR activation (46), reduce RNase-L activity (47), and ultimately produce enhanced levels of protein (45, 46). Further work has shown that incorporation of pseudouridine and 5-methylcytosine, an analog of cytosine, further increases protein production (35). However, IVT mRNA transgene protein production doesn't always seem to increase upon substitution of these modified bases; benefits associated with incorporation of modified bases are likely gene- and sequence-specific, as shown in (36).

While pseudouridine can markedly increase transgene protein, it also influences IVT mRNA in ways that may be disadvantageous. Pseudouridine presence in the stop codon allows non-canonical base pairing and suppression of translation termination (83-85). As synthesis of IVT mRNA, to date, includes incubation of a DNA template, RNA polymerase, and the ribonucleotides of interest in a single reaction, there is no current method to control pseudouridine location in the IVT mRNA strand, and it is always included in the stop codon. The inclusion of modified bases in IVT mRNA has also been shown to reduce the functionality of UTR sequences (36).

1.6.2 Codon optimization

Degeneracy of the genetic code allows multiple gene sequences to encode for the same protein. Codon choice is an important determinant in transgene expression and has been studied extensively for decades. In some cases, codon usage is so

powerful that optimization in DNA plasmids improved protein yield over 1,000 fold (86). Codon choice influences protein expression in a variety of ways, including mRNA export from the nucleus, rate of mRNA translation, the error rate in the protein sequence, mRNA half-life (87), and even protein folding and function (88-90). Most commonly, algorithms for codon optimization focus on matching the codon usage bias of a species and avoiding regulatory sequences in the mRNA (91, 92). Algorithms are also used to reduce mRNA secondary structure (93-95) and enhance GC content.

A few studies researched how codon optimization specifically affects IVT mRNA, opposed to plasmid DNA. Kariko et al. used a codon-optimized sequence for IVT mRNA encoding the hormone erythropoietin, and showed that it performed better than the wild type sequence. Interestingly, the benefit of codon optimization only held true when pseudouridine was substituted for uridine in the transcript; when unmodified bases were used, codon optimization did not enhance protein production (82). Another study showed that GC enrichment of an IVT mRNA sequence encoding for either luciferase or erythropoietin could produce markedly increased levels of protein. This study also explored how incorporation of pseudouridine influenced transgene expression. However, the authors found a reverse trend from Kariko's paper: for both luciferase and erythropoietin encoding mRNA, pseudouridine substitution enhanced protein production in the non-optimized sequences, but reduced protein production in the codon optimized sequences (36). These disparate influence pseudouridine incorporation and codon optimization has on IVT mRNA sequences, suggests there remains much more to learn regarding how codon optimization and pseudouridine substitution influence expression of exogenously delivered mRNA.

1.6.3 Delivery strategies

Choosing an appropriate delivery strategy for IVT mRNA involves several considerations. The route (intradermal, subcutaneous, etc), mechanism (electroporation, injection, gene gun, etc), and formulation (lipid nanoparticle, polymer nanoparticle, etc) may all significantly affect IVT mRNA's performance. Many strategies for delivery of plasmid DNA or siRNA are applicable to IVT mRNA.

Surprisingly, naked IVT mRNA injected *in vivo* leads to noticeable transgene protein expression (96). However, the use of a delivery vehicle may improve protein levels and affect other characteristics of IVT mRNA. Several studies show that delivery vehicles can enhance transgene protein production *in vitro* (74, 97-99) and *in vivo* (26, 36, 97, 99-101). Efforts to design delivery vehicles focus on facilitating mRNA uptake (through receptor-mediated endocytosis or the use of a cationic particle) and endosomal escape (through the incorporation of pH-sensitive elements, (101), altering mRNA interaction with PRRs (through complexation of mRNA with protamine) (44, 102), and conferring protection from nucleases (26, 100). Figure 1.3 describes these strategies. Table 1.2 provides a list of relevant studies that use these strategies.

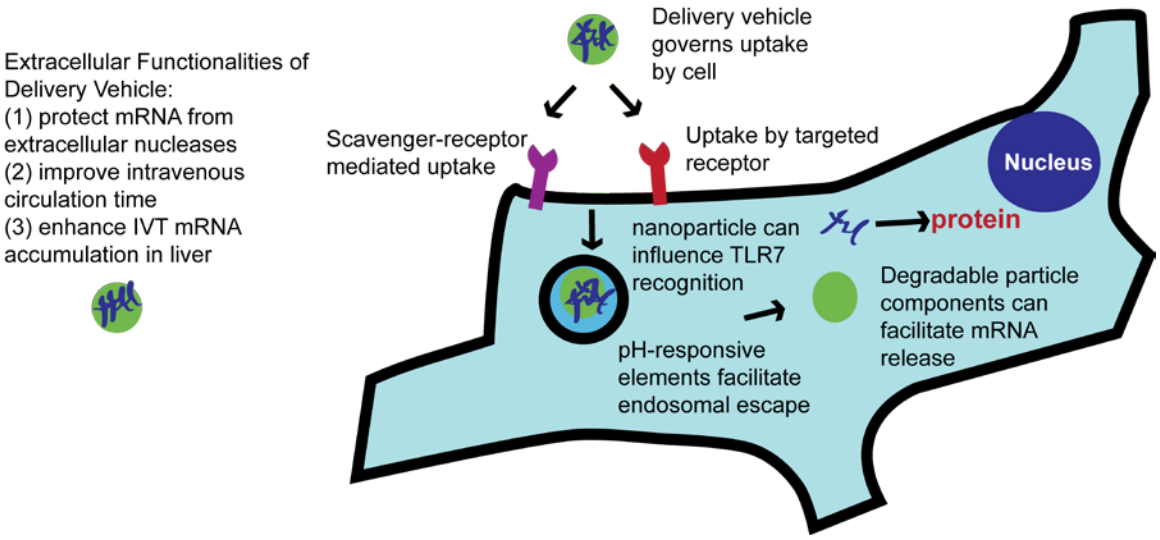

Figure 1.3. Strategies for effective delivery of IVT mRNA. Delivery vehicle may enhance *in vivo* circulation and distribution of mRNA, target certain cellular receptors for selective uptake, allow for endosomal disruption and IVT mRNA escape, and facilitate IVT mRNA release from the particle.

1.6.3.1 Differences in delivery strategies between IVT mRNA, siRNA, and plasmid DNA

Many concepts surrounding delivery of siRNA and plasmid DNA also apply to IVT mRNA; however, there are distinct differences that should be considered. Where IVT mRNA applications aim to introduce exogenous proteins into a host, siRNA applications aim to *reduce* endogenous proteins levels. This key difference may greatly affect delivery parameters. For siRNA to be most effective, applications may require its introduction into as many cells as possible. Further, a controlled, steady release of siRNA into the cytoplasm of cells may be required. For IVT mRNA, achieving transfection in a wide variety of cells may not be as crucial, especially if the protein is secreted extracellularly and then dispersed throughout the body. Instead, the goal of IVT mRNA delivery may be the generation of high levels of transgene protein in an appropriate area of the body. Also, while siRNA stimulates the immune system through

TLR7 recognition (103), the concern of immunostimulation by IVT mRNA may be greater as it is recognized by a more diverse array of PRRs (104).

Although the clinical applications of IVT mRNA overlap more with plasmid DNA compared to siRNA, there are still key differences in the design requirements for delivery of each nucleic acid. Plasmid DNA needs to enter the nucleus to be functional and thus targeted delivery to mitotic cells is important. IVT mRNA; however, does not have this limitation, as it is functional in the cytoplasm. Targeted delivery of IVT mRNA to the cytoplasm of potentially any cell type is more important. In addition, plasmid DNA is immensely less susceptible to nuclease degradation and thus more stable than IVT mRNA. Thus, nuclease protection may be more important for IVT mRNA than for plasmid DNA. As the lifetime of IVT mRNA is more transient than that of plasmid DNA, delivery vehicles may also aim to impart quicker uptake of IVT mRNA.

1.6.3.2 Influence of delivery strategy on innate immune stimulation

Delivery vehicles have the power to affect IVT mRNA interaction with PRRs. For example, complexing IVT mRNA to protamine leads to heightened TLR7-dependent immune responses compared to naked IVT mRNA delivery (105). This has also been observed with siRNA: Nguyen et al. screened a library of lipid-like materials for delivery of siRNA with enhanced immune-stimulatory properties. The authors show that lipid nanoparticle characteristics could have a dramatic effect on siRNA's stimulation of the immune system. The effects were shown to be both TLR7 independent and dependent (106). In both cases, it is unclear if delivery vehicles enhance immune responses by improving IVT mRNA's cellular uptake, enhancing its endosomal retention, affecting its recognition by PRRs, or simply by leading to a more inflammatory environment.

Table 1.2. Delivery vehicles tested for IVT mRNA

Vehicle Composition	**Injection Route**	**Application/Comments**	**Reference**
Lipoplex formulation consisting of the cationic lipids MLRI, TransFast and DOTMA	Intra-ventricular	Conferred protection of mRNA from RNases	(100)
Positively charged triblock polymer (DMAEMA, PEGMA, DEAEMA, and BMA)	studied *in vitro*	pH responsive segment for endosomal release, cationic segment for mRNA complexation, and a hydrophilic segment for *in vivo* stability	(107)
Poly(β-amino ester) core enveloped by a phospholipid bilayer	intranasal	pH responsiveness of poly(β-amino ester) allowed for endosomal disruption	(101)
mRNA-protamine associated with cationic liposome	intravenous	Conferred protection of mRNA from RNases and, prolonged circulation time, enhanced uptake by cancerous cells	(26)
mRNA-protamine complexed with poly(ε-caprolactone)	studied *in vitro*	pH responsiveness facilitates endosomal release	(74)
Ionizable cationic lipid/phosphatidylcholine/cholesterol/ polyethylene glycol (PEG) lipid	Intravenous	pH responsiveness facilitates endosomal release	(36)
(PEG)-polyamino acid block copolymer, polyplex nanomicelle	intrathecal injection	pH responsiveness facilitates endosomal release; PEG facilitates enhanced stability	(108)
Mannosylated and histidylated lipopolyplexes	intravenous	Mannose on nanoparticles enhanced dendritic cell uptake of mRNA	(109)
Protamine	intradermal	Conferred protection of mRNA from RNases, enhanced detection of mRNA by TLR7	(22, 44, 105)
Polyacridine-PEG-peptide	hydrodynamic tail vein injection	Peptide binds mRNA; poymers confer *in vivo* stability	(110)

Injection of IVT mRNA is currently under clinical evaluation for anti-cancer immunotherapy treatments. Clinical trials are ongoing using RNActive technology, where a portion of IVT mRNA is complexed to protamine (21, 22). Here, protamine complexation enhances IVT mRNA recognition by the PRR TLR7. Other clinical trials have tested IVT mRNA delivered in a free form, supplemented with granulocyte-macrophage colony stimulating factor as an adjuvant (111). It is notable that these studied employed efforts to enhance stimulation of innate immunity. The self-adjuvant properties of IVT mRNA may not be substantial enough to drive immunological protection.

The delivery route of IVT mRNA is another important factor to consider for both therapeutic and vaccination purposes. The use of IVT mRNA as a vaccination platform has predominated been studied by injection of IVT mRNA intradermally. While the exact rationale for why this route is so heavily explored is uncertain, this may be because intradermal injection exposes IVT mRNA to more $TLR7^+$ cells, allowing for enhanced stimulation of innate immune responses compared to other routes (112). Intranodal delivery for cancer applications has also been a focus of recent work. A study by Kreiter et al. explored how delivery route affected performance of an anti-cancer IVT mRNA vaccine. The authors compared subcutaneous, intradermal, near nodal, and intranodal injection routes, and found that intranodal delivery led to both the greatest amount of detectable protein expression as well as heightened T cell responses (113).

1.6.3.3 Challenges associated with delivery vehicle design

A significant hurdle for the development of delivery vehicles is the variability between *in vitro* and *in vivo* results. A study by Phua et al. illustrates these inconsistencies. Here, IVT mRNA nanoparticles transfected cells *in vitro,* but were ineffective upon subcutaneous administration to mice. Conversely, transfection was

unsuccessful when naked IVT mRNA was delivered to cells *in vitro*, but successful when delivered to mice subcutaneously. The study also showed that upon intranasal and intravenous delivery, naked IVT mRNA produced less protein than nanoparticle-mediated delivery (97). Others have also identified these inconsistencies and have shown that while cationic nanoparticles function well *in vitro*, they are less effective *in vivo* (114, 115). Interaction of nanoparticles with the extracellular matrix *in vivo* could explain this discrepancy. Cationic delivery vehicles may interact with negatively charged serum proteins or negatively charges within the extracellular matrix. Further, the extracellular matrix may also limit the diffusion of larger particles, inhibiting interaction with their cellular targets (116). Thus, delivery vehicles intended for *in vivo* use require either optimization and testing *in vivo* or the use of *in vitro* systems that appropriately mimic the specific route delivery.

1.7 Conclusion

IVT mRNA is a potential platform that addresses many of the current challenges in vaccine development. Similar to plasmid DNA, IVT mRNA does not require extensive culture of pathogens, addresses antigen hypervariability, generate cellular immunity, and undergoes rapid development. IVT mRNA stands out from other nucleic acid vaccines, as it could potentially lead to enhanced antigenic protein production and has unique immune stimulation characteristics. Moreover, a variety of strategies can modulate IVT mRNA characteristics.

These strategies include the incorporation of modified nucleotides, codon optimization, incorporation of untranslated regions, and engineered delivery systems. Previous works on these strategies have relied on overall levels of transgene protein expression and cytokine responses to assess performance. However, this metric leaves many cellular mechanisms of action unanswered. Further, the literature suggests that

the efficacies of these strategies have significant gene-to-gene variation. While IVT mRNA possesses many qualities that make it an appealing platform for next generation vaccines, a better understanding of its interaction with cellular machinery is likely required before it can become a platform technology.

1.8 Thesis outline

The goal of this thesis is to investigate the innate immune responses to IVT mRNA and to explore strategies to modulate these immune responses. *Chapter 2* focuses on the cytokine responses developed in response to IVT mRNA delivery transfection by bone marrow-derived dendritic cells and compares these responses to those elicited by plasmid DNA transfection. *Chapter 3* investigates the innate immune responses developed following vaccination with IVT mRNA intramuscularly, and how nanoparticle-mediated delivery can affect these immune responses. *Chapter 4* creates and describes a strategy for controlling the innate immune responses to IVT mRNA by conjugation of adjuvants to the IVT mRNA. *Chapter 5* discusses the conclusions made by this thesis work and discusses future recommendations for related research.

CHAPTER 2

RESPONSES OF BONE MARROW DERIVED DENDRITIC CELLS TO TRANSFECTION WITH PLASMID DNA AND IVT MRNA

2.1 Introduction

Non-viral nucleic acid-based vaccines, namely plasmid DNA and IVT mRNA, are appealing alternatives to traditional platforms for vaccine development. Traditional platforms include the use of killed or attenuated pathogens, where development can be time-consuming. Nucleic acids based vaccines; however, are produced rapidly and safely. Performance of plasmid DNA and IVT mRNA is dependent on their generation of antigenic protein as well as their activation of innate immunity.

Plasmid DNA has been heavily explored for a variety of vaccine applications (117, 118). However, early clinical trials using plasmid DNA have found that it yields a generally weak adaptive immune response against the encoded protein (119). IVT mRNA has more recently received attention for vaccine research. IVT mRNA boasts several potential advantages over plasmid DNA for vaccine applications. First, IVT mRNA has reportedly higher transfection efficiencies compared to plasmid DNA (120, 121). Second, where the antigenic protein may be toxic or dangerous, IVT mRNA transfection results in more transient protein production compared to plasmid DNA transfection. Protein production resulting from plasmid DNA transfection may persist over several months (122, 123). Lastly, IVT mRNA is supposed to elicit stronger innate immune responses upon transfection than plasmid DNA; however, there are limited studies providing direct comparisons of the two.

Innate immune responses elicited upon IVT mRNA transfection can be modified by substitution of bases with naturally occurring modified bases. These modifications are known to influence a variety of characteristics of RNA, including secondary structure (70-73), gene expression (74-77), and detection by PRRs (78-80). Warren et al. showed that two key modified bases 5methylcytosine (5mC) and pseudouridine (Ψ) could enhance protein production of green fluorescent protein IVT mRNA dramatically. Further, transfection with IVT mRNA bearing these modifications (5mC/Ψ IVT mRNA) led to reduced cytokine responses compared to unmodified IVT mRNA (35).

This study examines the immunostimulatory properties of IVT mRNA containing both modified and unmodified nucleobases in relationship to plasmid DNA. The objective of this study is to elucidate the differences between IVT mRNA, 5mC/Ψ IVT mRNA, and plasmid DNA. A potential vaccine application of nucleic acids is for prophylactic allergy prevention (124, 125). Therefore, nucleic acid vaccines were prepared for two model allergens - peanut allergen (Ara h 2) and egg allergen (ova) to study the use of these nucleic acids in this context.

2.2 Materials and Methods

2.2.1 Preparation of IVT mRNA

IVT mRNA was prepared according to the DNA templates provided in the Appendix. For ovalbumin, the DNA template was prepared from the PCL-neo-cOVA plasmid from Addgene (Plasmid #25097). The DNA sequence for the peanut allergen Ara h 2 was generated by GeneArt based on the Arah2.01 protein sequence (Accession# AAK96887), optimizing for GC content and murine expression. Prior to transcription, DNA template were amplified using the Q5 high-fidelity DNA polymerase (New England Biolabs). The PCR product was purified, digested with the restriction

enzyme NOTI to create a 5' overhang, and then re-purified. The QIAquick PCR purification spin column (QIAGEN) was for all purifications of the linear DNA template. The T7 mScript Standard mRNA Production System was used to generate IVT mRNA (Cellscript), enzymatically add a Cap-1 structure, and enzymatically add a poly(A) tail. The manufacturer's instructions were followed, however. the RNeasy mini kit (QIAGEN) was used to purify IVT mRNA when necessary. To incorporate modified bases, ribonucleotide cocktails were prepared to consist of 25 mM of each base. pseudouridine-5'-Triphosphate (ψ) and 5-methylcytidine-5'-triphosphate (5mC) were purchased from TriLink Biotechnologies; adenosine triphosphate and guanosine triphosphate were purchased from USB. Following, IVT mRNA was treated with Antarctic phosphatase (New England Biolabs) for 30 min to remove residual 5′-triphosphates, and then cleaned up and quantified using the Nanodrop 2000 (Thermo Scientific). RNA integrity was verified by denaturing gel electrophoresis.

2.2.2 Plasmid DNA constructs

For ovalbumin, the plasmid PCL-neo-cOVA was used (Addgene Plasmid #25097), which contained the sequence for cytoplasmic ovalbumin under the control of the cytomegalovirus (CMV) promoter. For Ara h 2, GeneArt gene synthesis (Thermo Fisher) was used to custom design a DNA template that was codon optimized for expression in mouse cells. This template, as well as the template for G39C were cloned into the plasmid eGFP-C1 under the control of the CMV promoter using the restriction digest sites NheI and XbaI (blunt end ligation). Plasmids were amplified in E. coli (DH5α), and isolated using an endotoxin-free maxiprep kit (QIAGEN).

2.2.3 Cell line culture and IVT mRNA transfection

The human embryonic kidney cell line 293T was maintained in High Glucose Dulbecco's Modified Eagle's Medium (DMEM) (Lonza) with 10% FBS (Hyclone) and 100 U/ml penicillin and streptomycin (Invitrogen). Approximately 60,000 cells were seeded in a 24 well plate the evening prior to stimulation. Cells were transfected with the indicated treatment using Lipofectamine 2000 (Invitrogen) or the Mirus transfection reagent as indicated, according to each manufacturer's instructions. NIH 3T3 cells were cultured in DMEM supplemented with 10% bovine calf serum and 100U/ml penicillin and streptomycin.

2.2.4 Bone marrow derived dendritic cell culture and transfection

Bone marrow was collected from 6-8 week old BALB/c mice and homogenized by agitation with the rubber plunger of a 1 ml syringe. Red blood cells were lysed with red blood cell lysis buffer (eBioscience), washed with PBS in 2% FBS, sequentially passed through 100 µm and 70 µm cell strainers, and then cultured for six days in DMEM in the presence of 4 ng/ml interleukin 4 (IL-4) (Sigma) and 20 ng/ml Granulocyte-macrophage colony-stimulating factor (GM-CSF) (Peprotech) at 10^6 cells/ml. Every two days, half of the cell culture media was replaced with fresh media containing IL-4 and GM-CSF. On day six, cells in suspension were plated in 24 well plates (10^6 cells in 1 ml/ well) and transfected in triplicate using Lipofectamine 2000 with 0.5 µg of nucleic acid.

2.2.5 Hek Blue TLR7 cell culture and assay for TLR7 activation

Hek Blue TLR7 and wild type (TLR7 negative) cells were purchased from Invivogen. The cells were engineered to contain a gene for secreted embryonic alkaline phosphatase (SEAP) under control of the nuclear factor kappa-light-chain-enhancer of activated B cells (NF-KB) promoter. Cells were cultured in DMEM with 10% FBS and 100 U/ml

penicillin and streptomycin and 100 µg/ml Normocin (Invivogen). Plasmid expression was maintained by culturing cells in blasticidin at 10mg/ml (for TLR7 expression) and Zeocin at 100mg/ml (for SEAP expression). To assess SEAP production, cells were seeded in a 96 well plate (40,000 cells/well) in Hek Blue detection media (Invivogen). Cells were transfected with nucleic acid using Lipofectamine 2000 in Opti-MEM (Invitrogen). Color absorbance was measured with a 96 well plate reader at 635 nm 6-16 hours following transfection.

2.2.6 Quantitative RT-PCR

Cells were transfected as mentioned in Section 2.2.4. At the indicated time point, total RNA was collected with QIAGEN's RNeasy kit, which used an on-column DNAse treatment. RNA was quantified by absorbance at 260nm and converted to cDNA using the RT^2 First Strand kit (SA Biosciences). qRT-PCR was performed using the StepOnePlus real-time PCR system (Applied Biosciences) using 15 ng of cDNA and SYBR green master mix (SA Biosciences), which was used according to manufacturer's directions. For measuring intracellular IVT mRNA levels, fold changes were calculated using the ddCT method on StepOne software in reference to GAPDH. For gene expression studies, qPCR was conducted in technical triplicates using the FLUIDIGM Biomark system on a 48 by 48 chip. Indicated PCR primer assays were designed by and purchased from FLUIDIGM. Samples were used from four independent biological experiments. QIAGEN's online data analysis center was used for data analysis. Statistical significance was based on a Student's t-test of the replicate $2^{-\Delta CT}$ values for each gene in the control group and treatment groups. The reference genes ActB and RBP13a were used to normalize expression relative to untreated cells. Sequences for gene-specific primers are listed in the Appendix.

2.2.7 Secondary structure modeling of IVT mRNA using Mfold

The first 100 bases of IVT mRNA sequences were input into Mfold (126). IVT mRNA was modeled as linear DNA polymer under approximately intracellular conditions (10mM NaCl, 1mM MgCl, 37C).

2.2.8 Western blots

At the indicated time point following transfection, cell lysates were harvested with RIPA buffer containing a protease inhibitor cocktail (Roche) on ice. The protein content of lysates was determined using the bicinchoninic acid (BCA) assay (Pierce), and an equivalent quantity of cellular protein were run on NuPAGE Novex 4-20% tris-glycine gels (Thermo Fisher Scientific). Protein was transferred to a polyvinylidene fluoride membrane overnight. The membrane was washed in tris buffered saline with 0.1% triton X 100 (TBST), blocked with 5% BSA in TBST, stained with primary antibodies overnight at 4C, washed with TBST, stained with secondary antibodies (LI-COR) for 30 minutes at room temperature and then washed with TBST and PBS. Chicken anti-Ara h 2 antibody (a gift from Soheila Maleki, United States Department of Agriculture, New Orleans, USA) and rabbit anti-ovalbumin (Abcam) and mouse anti GAPDH (Abcam) were used as primary antibodies. Anti-rabbit DyLight 680, anti-mouse DyLight 680, and anti-chicken DyLight 800 were used as secondary antibodies. Blots were imaged using the LI-COR infrared imager.

2.2.9 Flow cytometry

BMDCs were kept on ice throughout the flow cytometry staining procedure. Cells were lifted from cell culture plates with cell dissociation buffer (Sigma), washed with PBS+2% FBS, stained for cell surface expression of CD80, CD86, CD11c, MHCII, or OX-40L, which were diluted 1:100 in PBS supplemented with calcium and magnesium

and 2% human serum. Cells were then washed two times in PBS+2% FBS and then analyzed using the Accuri flow cytometer. Data was analyzed using FlowJo after gating for viable single cell populations. For each experiment, treatment response ratios were calculated by dividing the median staining fluorescence of the treatment group over the Lipofectamine 2000 only control. Data was analyzed by a one-way ANOVA in JMP followed by a Dunnett's post-analysis test.

2.2.10 Proximity ligation assay

NIH 3T3 cells were electroporated with the pUNO1-mTLR7-HA3x plasmid (Invivogen) using the Neon electroporation system (Thermo Fisher Scientific) according to the manufacturer's instructions and plated on glass coverslips in 24 well plates (approximately 40,000 cells/well). Approximately 48 hours later, cells were transfected with 400ng of IVT mRNA using Lipofectamine 2000. After five hours, cells were fixed with 2% paraformaldehyde in PBS, permeabilized with PBS supplemented with 0.2% tween 20, and then blocked for 1 hour with a solution containing 0.5% Tween-20, 0.1% Triton X-100, 0.1% gelatin (Aurion), 2% donkey serum (VWR) and 1% bovine serum albumin (EMD) in PBS. Samples were stained with the primary antibodies rabbit anti-HA, (Abcam) and mouse anti IRAK4 (LSBio) diluted 1:500 in a solution of 0.25% gelatin, 0.5% donkey serum, and 1% BSA in PBS. Proximity ligation assay was then performed in accordance with manufacturer's instructions (Olink Bioscience). Following PLA, cells were imaged using an UltraVIEW spinning disk confocal microscope, Zeiss LSM 510 Meta, a Hamamatsu Flash 4.0v2 CMOS camera and an 89000 Sedat Quad-ET filter set. A 40x, NA 1.3 Zeiss EC Plan-Neofluar oil objective was used for all tiled images and a 63×, NA 1.4 Zeiss Plan-Apochromat oil objective was used for all other images. Imaging was controlled by Volocity acquisition software (PerkinElmer). Image stacks were

recorded at 350 nm intervals. The number of PLA signals per cell were counted using Volocity software.

2.3 Results

2.3.1 Ara h 2 IVT mRNA translation is dependent on 5' secondary structure

To assess IVT mRNA functionality, we first transfected human embryonic kidney 293T cells. Cell lysates were collected after 6, 12, or 24 hours, and analyzed by Western blot for presence of the Ara h 2 or ovalbumin protein. Initially, while ovalbumin protein was detected, Ara h 2 protein was not. To investigate this discrepancy, Ara h 2 and ovalbumin IVT mRNA were transfected again, and qRT-PCR was performed on cellular RNA to determine if Ara h 2 IVT mRNA was found intracellularly in a comparably amount to ovalbumin IVT mRNA (Figure 2.1A). Intracellular IVT mRNA levels were found to be comparable.

Next, IVT mRNA secondary structure was examined at the 5' end to see if the secondary structure was possibly interfering with protein translation. We hypothesized that reducing the secondary structure near the 5’ end would enhance translation, either by enhancing enzymatic capping of the IVT mRNA or by better allowing ribosome binding. The 39^{th} base in the mRNA sequence for Ara h 2 was modified from a guanosine to a cytosine to reduce secondary structure, which maintained the protein sequence (Figure 2.1B). The modified mRNA strand was produced (OAH2 G39C) and 293T cells were again transfected, using the modified and original construct (OAH2). Cell lysates were analyzed by Western blot for the Ara h 2 protein. Figure 2.1C shows that this mutation enabled translation of the Ara h 2 protein.

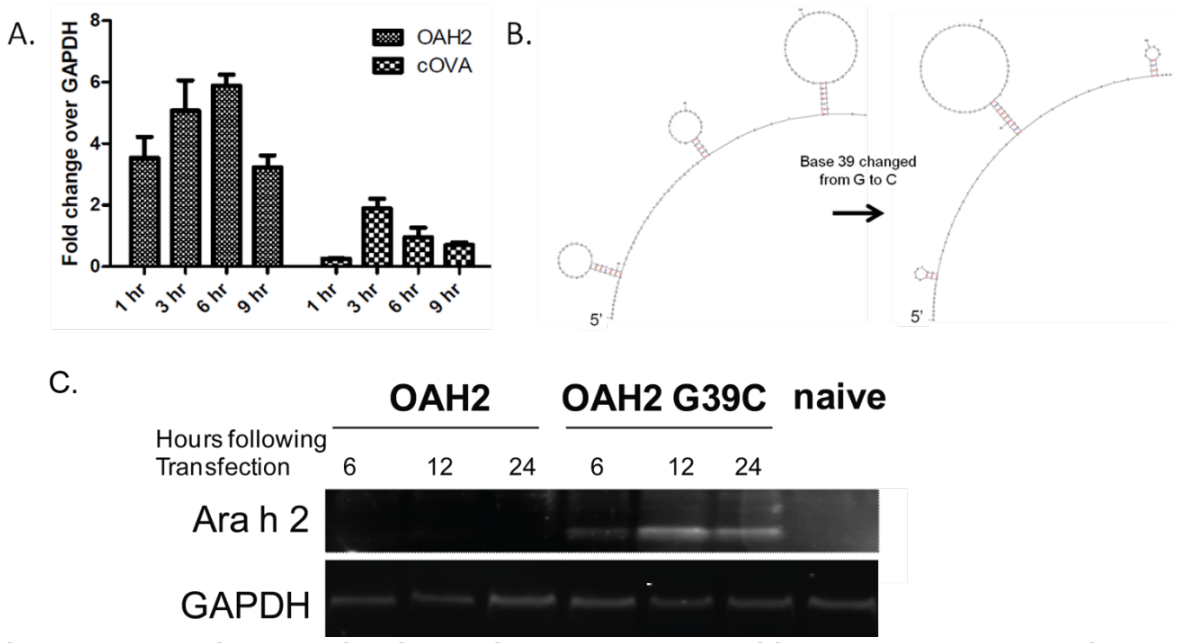

Figure 2.1. A point mutation in Ara h 2 IVT mRNA enables transgene expression. A.) 293T cells were transfected with 0.25µg of either ovalbumin or Ara h2 encoding mRNA with the Mirus Trans-it kit. Intracellular presence of the transfected mRNA was analyzed over time with qRT-PCR (data representative of three experimental repeats). B.) IVT mRNA secondary structure was modeled using the Mfold program. Modification of the 39th base from G to C altered the secondary structure without modifying the protein sequence. C.) This modification allows for detection of the Ara h 2 protein.

2.3.2 Transfection of BMDCs with plasmid, IVT mRNA, and 5mC/Ψ IVT mRNA

We next wanted to assess if incorporation of 5methylcytosine and pseudouridine would also lead to increased protein expression for the IVT mRNAs used in this study. Bone marrow-derived dendritic cells (BMDCs) were used, as they are potent antigen presenting cells. IVT mRNA and 5mc/ψ IVT mRNA were prepared to encode for either ovalbumin or Ara h 2. IVT mRNAs or plasmid DNAs were transfected into BMDCs using Lipofectamine 2000. Sixteen hours later, cell lysates were collected and analyzed by Western blot for protein expression. Interestingly, we see that 5mc/ψ IVT mRNA leads to increased protein expression for ovalbumin. However, the reverse is true for Ara h 2

IVT mRNA. We were not able to detect protein expression of the genes when they were delivered in plasmids (Figure 2.2).

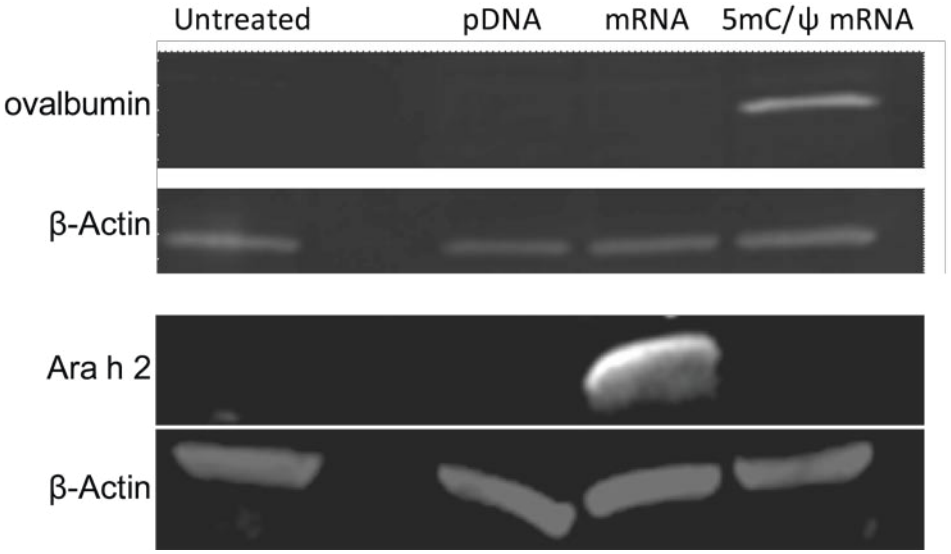

Figure 2.2 Transgene expression of mRNA, 5mC/Ψ mRNA, and plasmid DNA. Cell lysates were analyzed by Western blot 18 hours following transfection for presence of the genetically delivered protein.

2.3.3 Transfection with plasmid DNA, not IVT mRNA, leads to increased expression of dendritic cell maturation markers

Dendritic cell maturation is an important event in the development of adaptive immune responses. It is associated with enhanced antigen presentation, migration to the lymph nodes, and T cell priming. We wanted to determine if transfection with plasmid DNA, IVT mRNA, or 5mc/Ψ IVT mRNA were associated with BMDC maturation. BMDCs were again transfected with plasmid DNA or IVT mRNA encoding for either ovalbumin or Ara h 2. To isolate any effect that the peanut allergen protein may have on the cellular response, we also used the OAH2 sequence, which did not produce detectable Ara h 2 protein as well the plasmid vector that held Ara h 2 with the open reading frame

removed. Eighteen hours following transfection, cells were analyzed for expression of maturation markers as well as gene expression of antiviral and inflammatory cytokines.

BMDCs were transfected with 0.5 μg of mRNA, 5mc/Ψ mRNA, plasmid DNA, or a blank water control using Lipofectamine 2000. Eighteen hours following transfection, cell surface expression of CD80, CD86, CD11c, and MHCII were analyzed by flow cytometry. Surface staining is shown in Figure 2.3 and is represented by the "treatment response ratio." The treatment response ratio indicates the median fluorescence intensity for each transfection group divided by the median fluorescence intensity for the untreated control. Values plotted represent the average of 6 to 11 experiments. We see that plasmid DNA transfection led to increased cell surface expression of CD80, CD86, and MHCII; while IVT mRNA transfection did not. We do see that CD11c cell surface expression is reduced in response to transfection across all treatment groups, a response that is indicative of PRR activation (Figure 2.4).

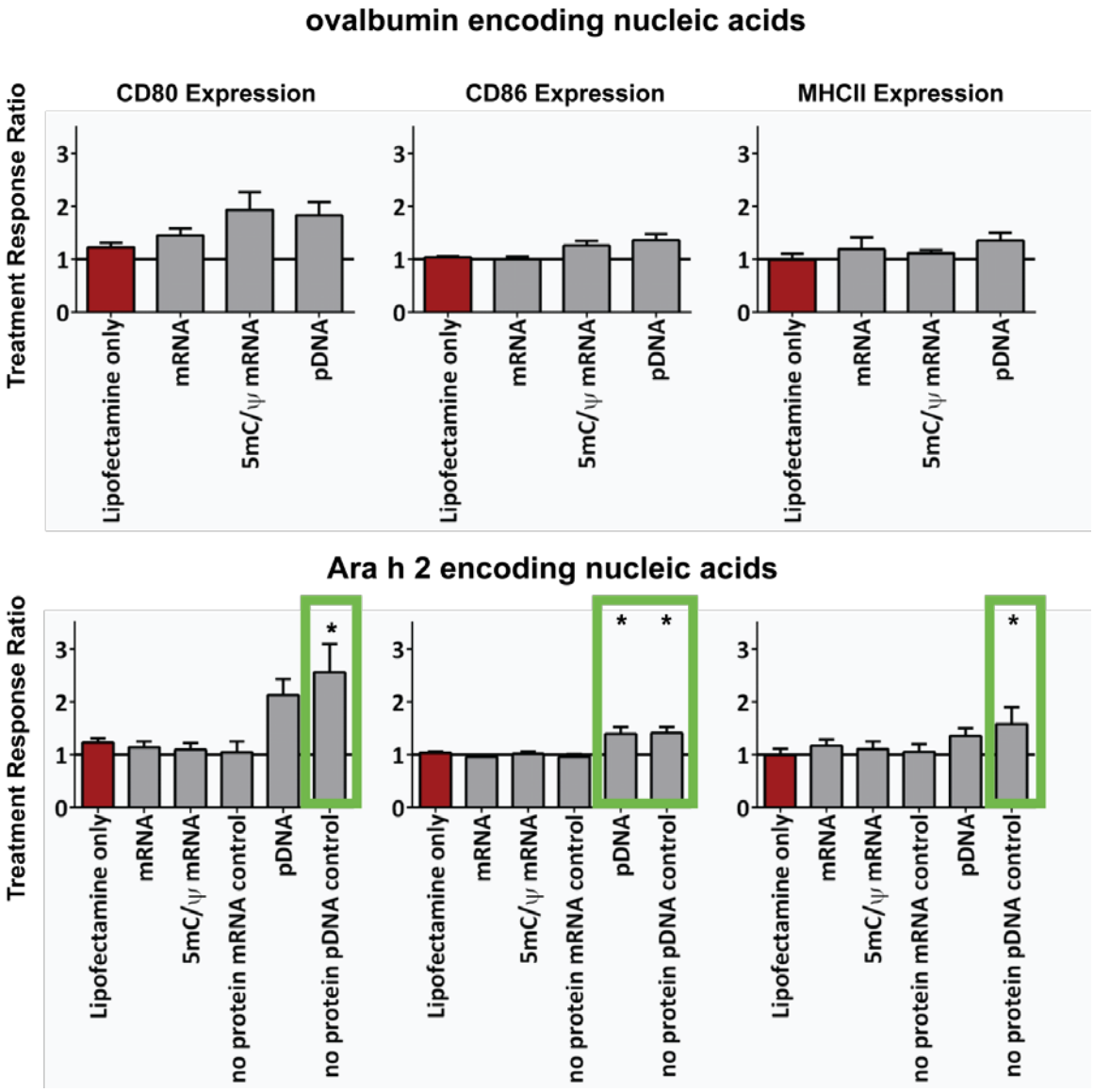

Figure 2.3. Transfection of plasmid DNA, but not mRNA, upregulates BMDC maturation markers. BMDCs were transfected with IVT mRNA or plasmid DNA encoding the peanut allergen Ara h 2 or the egg allergen ovalbumin. Eighteen hours following transfection, cells were analyzed with flow cytometry for cell surface staining of CD80, CD86, and MHCII. Cell staining is represented as treatment response ratio, which is median cell staining intensity divided by the cell staining intensity of untreated controls. Plotted values represent an average of 6 to 11 experiments. Significance was tested by a one-way ANOVA followed by a Dunnett's test ($p<0.05$).

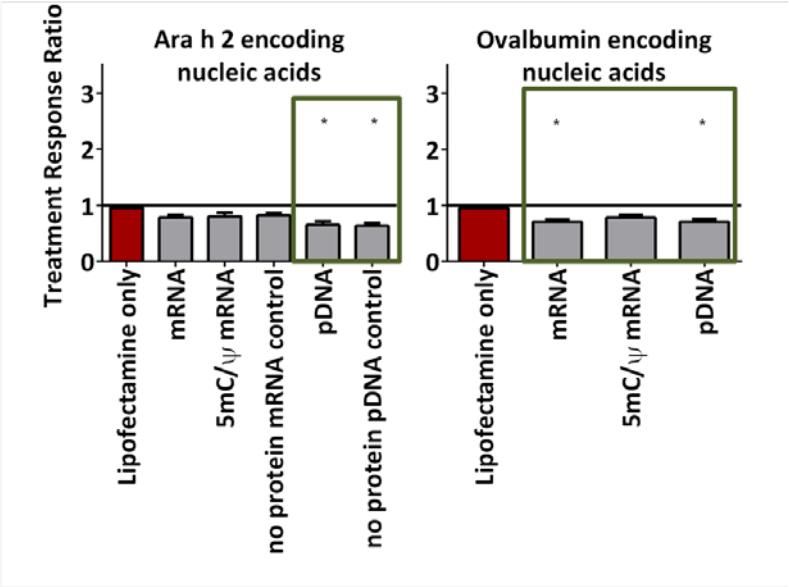

Figure 2.4. Transfection of plasmid DNA and IVT mRNA downregulate CD11c cell surface expression. BMDCs were transfected with the indicated nucleic acid encoding for Ara h 2 or ovalbumin. Eighteen hours following transfection, cells were analyzed with flow cytometry for cell surface staining of CD11c. Cell staining is represented as treatment response ratio, which is median cell staining intensity divided by the cell staining intensity of untreated controls. Plotted values represent an average of 6 to 11 experiments. Significance was tested by a one-way ANOVA followed by a Dunnett's test ($p<0.05$).

2.3.4 IVT mRNA and plasmid DNA transfection do not lead to appreciable cell death

Next, we wanted to determine if mRNA or plasmid DNA transfection led to cell death or apoptosis. To test this, cells were transfected with mRNA or plasmid DNA as described earlier. Twenty-four hours following treatment, cells were stained for apoptosis using the Annexin-V-FITC apoptosis kit (Millipore). Cell staining for Annexin-V and propidium iodide were analyzed with flow cytometry, and the treatment response ratios are shown in Figure 2.5. Analysis of cells in early and late stages of apoptosis, indicated by Annexin only staining and Annexin and propidium iodide staining was also performed, but no significance was detected.

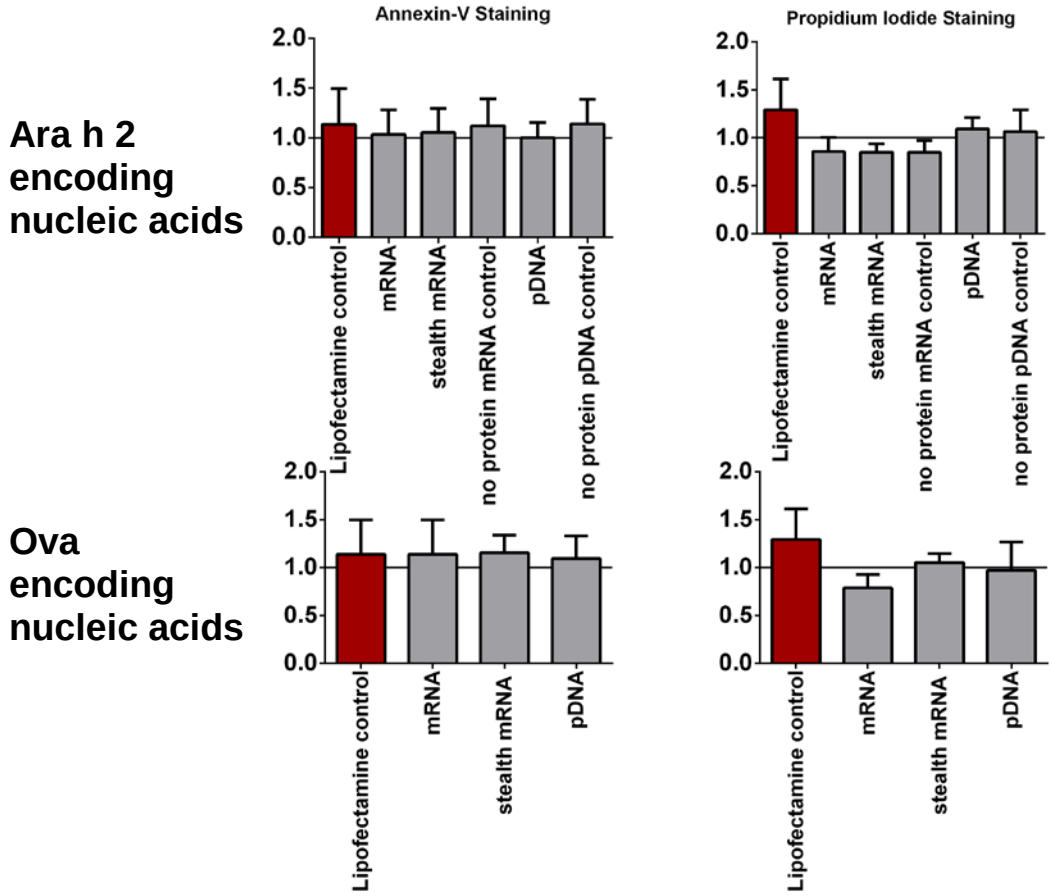

Figure 2.5. IVT mRNA and plasmid DNA transfection do not lead to appreciable cell death. BMDCs transfected with mRNA or plasmid DNA encoding either the peanut allergen Ara h 2 or the egg allergen ovalbumin. Twenty-four hours following transfection, cells were analyzed for apoptosis by staining with Annexin-V and propidium iodide. Difference between groups was tested with a one-way ANOVA followed by a Dunnett's test, n= 5.

2.3.5 IVT mRNA transfection leads to upregulation of antiviral associated cytokines

Cellular antiviral defenses sense foreign nucleic acids to initiate a variety of protective innate immune responses, which both reduce protein expression and initiate development of adaptive immune responses. We conducted a qRT-PCR analysis to assay for gene expression in response to nucleic acid transfection. We transfected

BMDCs as described earlier and extracted RNA from the cells 18 hours later (Figure 2.6).

It is clear that IVT mRNA transfection elicits strong antiviral responses, characterized by IFN-α and TNF-α upregulation, and that this response can be downregulated by substitution of modified bases. This trend occurs for both Ara h 2 and ovalbumin-encoding nucleic acids, suggesting that it is not responsible for the variation in transgene protein expression. In fact, we see that ovalbumin-encoding mRNA elicited an almost four-fold higher upregulation of IFN-α and TNF-α compared to Ara h 2 mRNA.

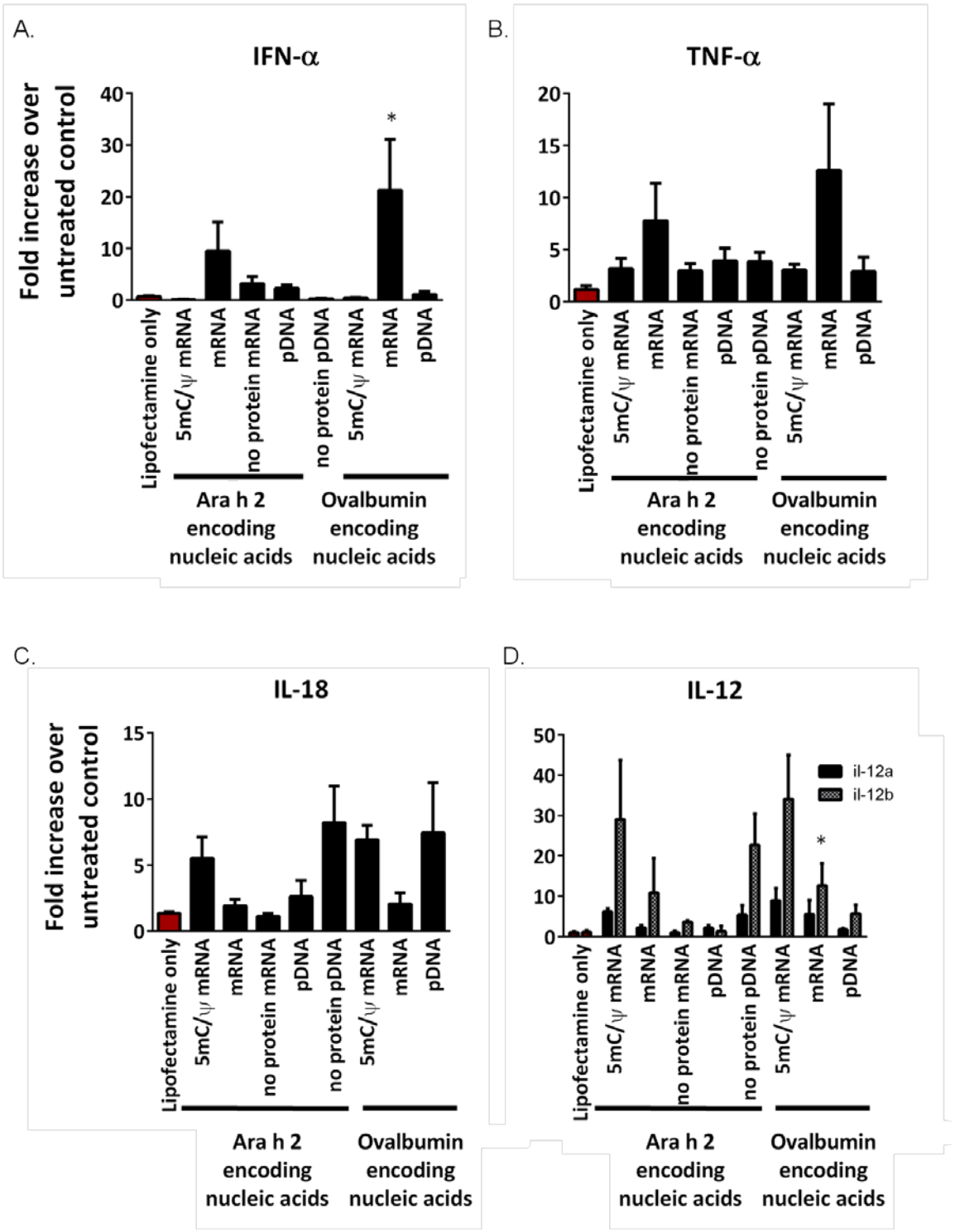

Figure 2.6. Expression of antiviral cytokines in response to nucleic acid transfection. BMDCs were transfected with the indicated nucleic acid, and then gene regulation was assessed. n=4. ANOVA followed by Tukey's Post Analysis test (* indicates $p<0.05$)

2.3.6 TLR7 activation by IVT mRNA

We hypothesized that incorporation of modified bases 5mC/Ψ may influence detection of IVT mRNA by the TLR7. TLR7 detects endosomal single-stranded RNAs, and delivery of IVT mRNA by some have shown to activate TLR7 (127). To test this hypothesis, we used Hek293t cells that were stably transfected with a plasmid encoding murine TLR7. $TLR7^{+}$ cells or wild-type $TLR7^{-}$ cells were transfected with indicated amounts of ovalbumin IVT mRNA using Lipofectamine 2000. Sixteen hours following transfection, NF-κB expression was assayed as assayed by measuring SEAP activity, which was genetically engineered under the control of NF-κB (Figure 2.7). SEAP activity is plotted relative to SEAP activity from the untreated control cells. The small molecule imiquimod is used as a positive control for TLR7 activation. There are no significant differences between TLR7 positive and negative cells. Interestingly, we see increased SEAP activity for 5mC/Ψ IVT mRNA compared to unmodified mRNA.

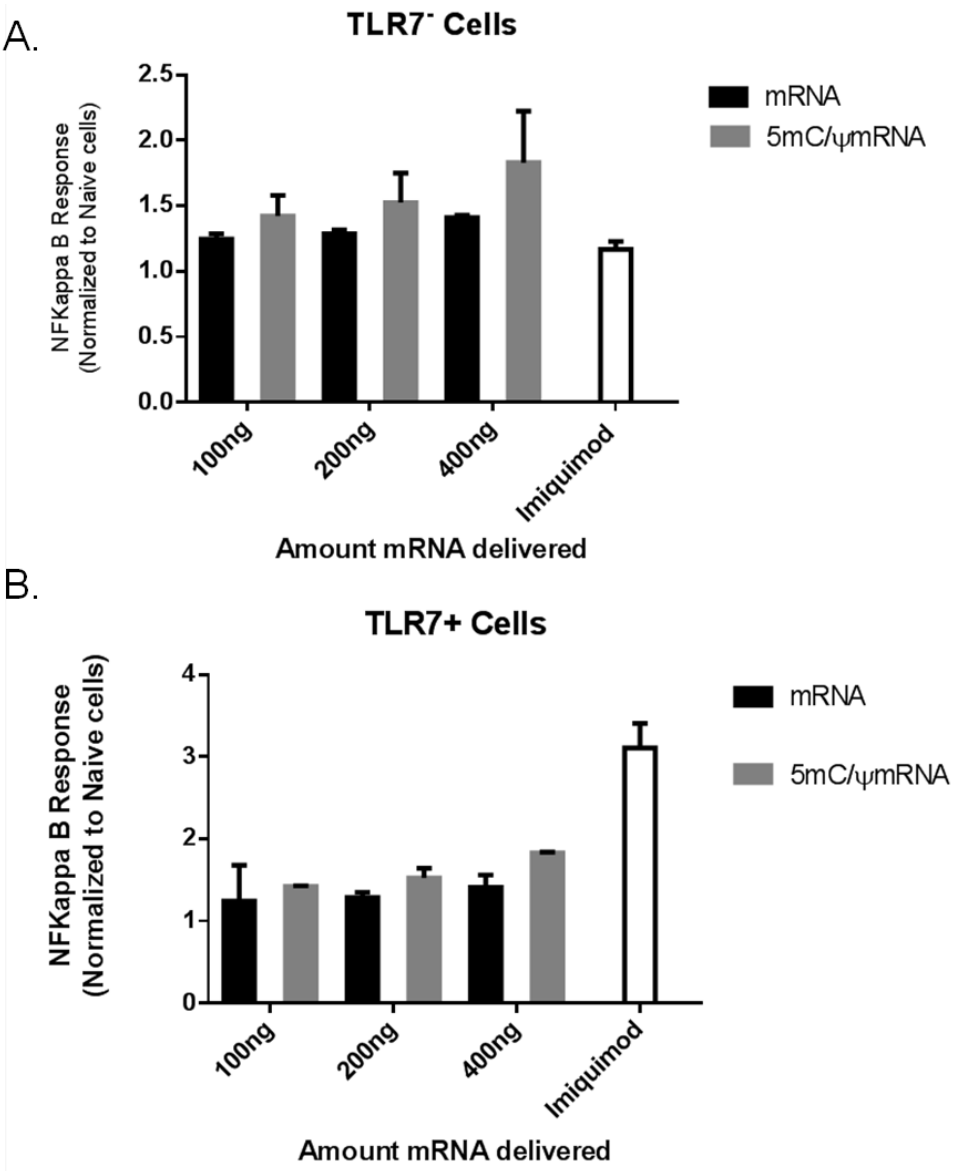

Figure 2.7 NF-ΚB responses by TLR7-positive and TLR7-negative cells in response to transfection with IVT mRNA. Cells were transfected with indicated amounts of IVT mRNA using Lipofectamine 2000. Sixteen hours later, NF-ΚB activation was assayed by measuring SEAP production. The TLR7 agonist imiquimod was used as a positive control.

The results found in Figure 2.7 were surprising, as there is significant literature showing that delivery of ssRNA composed of unmodified bases should activate TLR7 (128-130), where our experiment showed that NF-ΚB upregulation was not TLR7 dependent. We hypothesized that perhaps while TLR7 is activated, other antiviral responses are shielding its detection via NF-ΚB mediated protein responses. Upon activation, TLR7

forms a complex with IRAK4 and other proteins to initiate signaling. To further investigate if IVT mRNA activates TLR7, a proximity ligation assay was designed to assay for TLR7 activation. NIH3T3 cells were electroporated with a plasmid encoding for the TLR7 gene with a human influenza hemagglutinin (HA) tag. Forty-eight hours later, cells were transfected with ovalbumin IVT mRNA. Five hours after transfection, a proximity ligation assay was performed to detect complex formation of TLR7 and IRAK4, which resulted in fluorescent puncta. The number of PLA puncta were imaged using fluorescent microscopy and counted per cell. Figure 2.8 indicates the number of PLA signals per cell. Cells transfected with IVT mRNA composed of unmodified bases showed increased TLR7 activation compared to 5mC/Ψ IVT mRNA.

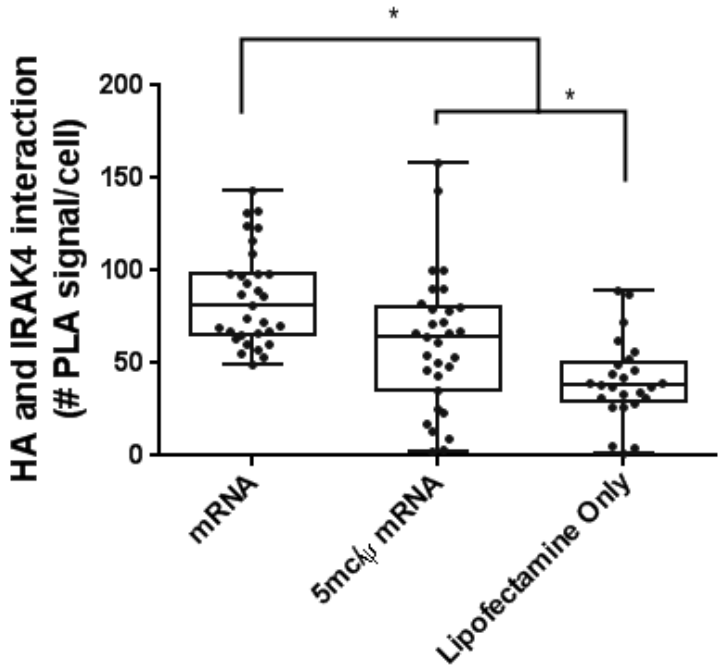

Figure 2.8 TLR7 signaling complex formation in response to IVT mRNA. A proximity ligation assay between TLR7 tagged HA and IRAK4 was performed to detect TLR7 activation. NIH3T3 cells were transfected with a plasmid that encoded a TLR7-influenza hemagglutinin fusion protein. A proximity ligation assay was performed to detect interaction between HA and IRAK4. The number of PLA signals were counted per cell. * indicates $p<0.05$, Mann-Whitney test.

2.4 Conclusion

In this study, we compared the innate immune responses to transfection with plasmid DNA, IVT mRNA, and 5mc/Ψ IVT mRNA. We identified that inclusion of modified bases in IVT mRNA leads to disparate effects on protein expression for different gene constructs- where ovalbumin IVT mRNA produced more protein with modified bases were included, Ara h 2 IVT mRNA produced more protein when all unmodified bases were used. This study also found that transfection with plasmid DNA lead to indicators of BMDC maturation (MHCII, CD80, and CD86 cell surface expression) while transfection with IVT mRNA and 5mc/Ψ IVT mRNA did not.

In accordance with previous literature, this we found that transfection with IVT mRNA upregulated the antiviral cytokines interferon-α and tumor necrosis factor-α. We also found that 5mC/Ψ substitution reduced this effect. This effect was consistent for both ovalbumin and Ara h 2 IVT mRNA. However, we also identified that 5mC/Ψ substitution upregulated: interleukin 18 and interleukin 12. This may indicate that 5mc/Ψ IVT mRNA activates PRRs differently than unmodified IVT mRNA.

While substitution of modified bases in IVT mRNA has disparate effects on protein expression, differences between the two constructs were not identified in BMDC maturation, Annexin/propidium iodide or gene expression studies. This suggests that there may be a physical reason why the two constructs may behave differently upon substitution of modified bases. It would be interesting to see if the disparate protein expression would persist upon altering the codon usage in each construct. We also found that while IVT mRNA transfection activated TLR7, incorporation of modified bases reduced this activation.

CHAPTER 3

IN SITU ANALYSIS SHOWS NANOPARTICLE DELIVERY OF MRNA VACCINE AFFECTS INNATE IMMUNE RESPONSES

The work presented here contains excerpts from the publication: In situ analysis shows nanoparticle-mediated delivery of mRNA vaccine affects innate immune responses. Loomis, Bellamkonda RV Santangelo PJ et al.. *Manuscript in preparation*

3.1 Introduction

Synthetically produced IVT mRNA is currently being pursued as a flexible platform technology that would allow for the safe, rapid, and potentially rational development of future vaccines. IVT mRNA's interaction with the innate immune system is a central factor in its performance as a vaccine vector. Injection of IVT mRNA elicits strong innate immune responses, characterized by type I interferon and inflammatory cytokines, which are released in response to PRR activation (131, 132). Upon recognition of IVT mRNA, PRRs initiate paracrine and autocrine signaling that prime a multitude of responses against pathogenic stimuli. This signaling can lead to the up or down regulation of other PRRs and infiltration of immune cells to the injection site. The quality, magnitude, and nature of innate immune responses are large factors in determining vaccine performance (40, 41, 133-135).

Despite the importance of these early events, we have a limited understanding of how IVT mRNA interacts with the innate immune system and what opportunities exist to modulate the interaction. While it is established that IVT mRNA elicits strong cytokine responses upon injection, the PRRs responsible are unclear. Previous studies have shown that IVT mRNA has the capability to interact with retinoic acid-inducible gene 1

(RIG-I) (37, 45), protein kinase RNA-activated (PKR) (46), Toll-like receptor 7 (TLR7) (44, 127), Toll-like receptor 8 (TLR8) (37), and Toll-like receptor 3 (TLR3) (37). TLR7 detects endosomal single-stranded RNA (ssRNA), particularly ssRNAs that are guanosine and uridine-rich (65, 136). RIG-I, along with Melanoma Differentiation-Associated Protein 5 (MDA5) are both cytoplasmic anti-viral PRRs that detect double-stranded RNAs (dsRNAs): RIG-I detects shorter dsRNA bearing 5' phosphates, an intermediate structure found during viral replication (137); MDA5 detects longer double-stranded RNA, another structure found during viral replication. To the best of our knowledge, MDA-5 has not yet been studied as a receptor for IVT mRNA (138, 139).

Previous work has relied on overexpression or knockout systems of target PRRs to study their activation. However, both of these strategies hamper paracrine and autocrine signaling and, therefore, may hide the importance of certain PRRs while over-crediting the contribution of others. Further, many PRRs are heterogeneously expressed across cell types (64, 140). Cell type choice used for *in vitro* experiments may significantly bias the assayed importance of a PRR using these methods.

To gain a more comprehensive understanding of the innate immune reactions to vaccination with IVT mRNA, we developed proximity ligation assays (PLAs) (141) to detect PRR activation. Figure 3.1 provides a schematic illustrating the central concept of PLA. PLAs detected the formation of essential protein complexes involved in PRR signaling pathways. Upon activation, TLR7, RIG-I, and MDA5 each form protein complexes that initiate signaling cascades, and that can be detected using a PLA. TLR7 forms a protein complex termed the myddosome, which includes myeloid differentiation primary response gene 88 (MYD88), and interleukin-1 receptor-associated kinase proteins (IRAK1, IRAK2, IRAK3, and IRAK4) (142, 143). RIG-I and MDA5 each interact with interferon-beta promoter stimulator 1 (IPS-1), also known as MAVS, to form protein complexes that are referred to as signalosomes (144, 145). PLAs used in this study

detected the formation of these protein complexes histologically by assaying for the proximity of either TLR7 with IRAK4, RIG-I with IPS-1, or MDA5 with IPS-1. This methodology is advantageous, as it allows observation of PRR activation *in situ* without perturbation of the host's antiviral responses. TLR7, RIG-I, and MDA5 signaling can all lead to upregulation of inflammatory and interferon cytokines through the activation of nuclear factor-κB (NF-κB) and interferon (IFN)-regulatory factors (IRFs) (138, 143).

Strategies to modulate innate immune responses to IVT mRNA will likely be needed for vaccine development. We examined how IVT mRNA delivery in a nanoparticle formulation with a cholesterol-derived lipid (cholk) affected innate immune responses. We found that nanoparticle-mediated delivered altered PRR signaling, the infiltration of immune cells to the injection site, and the presence of the injected mRNA in the draining lymph nodes. Additionally, IVT mRNA was fluorescently labeled prior to intramuscular (i.m.) injection. This enabled histological visualization of mRNA distribution, its uptake by different cell types, and its presence in the lymph nodes over time.

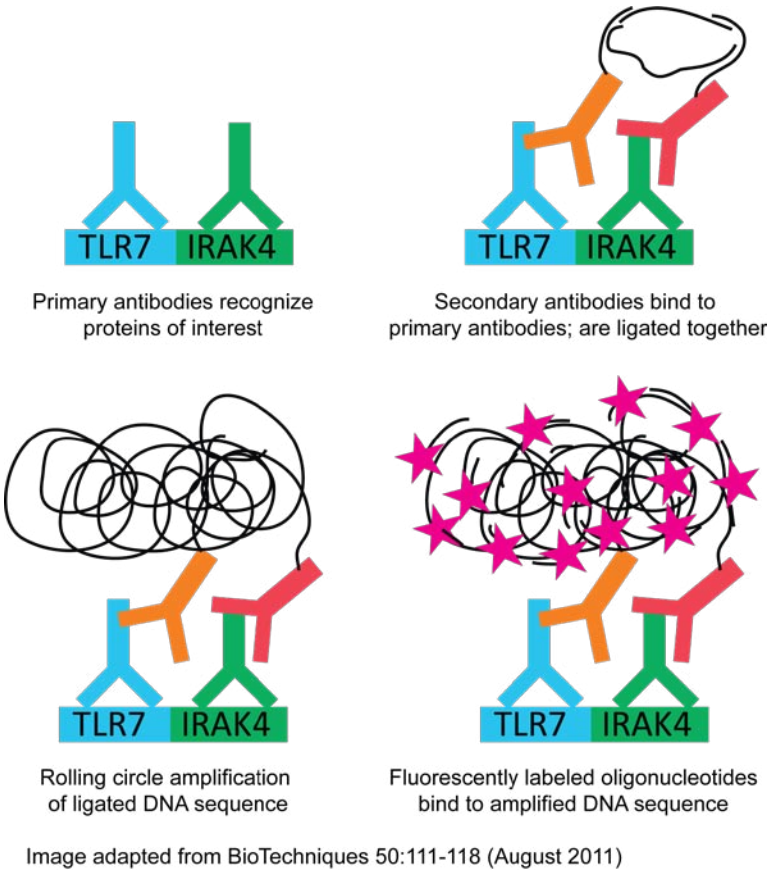

Figure 3.1. Schematic illustrating mechanism of PLA. Primary antibodies detect the proteins of interest (top left panel). Secondary antibodies bearing oligonucleotide sequences bind to primary antibodies, and then are ligated together (top right panel). Rolling circle amplification expands the ligated DNA sequence (lower left panel). Fluorescent molecules bind to the amplified sequence (lower right panel), allowing visualization of the proximity event with microscopy. PLA settings used for this study detected proteins that were less than 40 nm apart.

3.2 Materials and Methods

3.2.1 IVT mRNA and MTRIP labeling

IVT mRNA that coded for firefly luciferase was provided by CureVac GmbH (Tübingen, Germany). The mRNA had a 5’ cap, included the 3' untranslated region (UTR) from human albumin as well as a poly(A) tail. IVT mRNA was labeled with multiply-labeled tetravalent RNA imaging probes (MTRIPS) for detection by histology and flow cytometry. MTRIPs were synthesized in the Santangelo laboratory, and the procedure is described in full detail here (146). Briefly, 2'O-methyl RNA/DNA chimeras complementary to three different regions of the 3' UTR of the luciferase mRNA were purchased from Biosearch Technologies (Petaluma, CA). Each oligo contained a 5' biotin and multiple dT-C6-NH2 modifications. Free amine groups in the oligos were labeled with either Cy3B NHS ester (GE healthcare) or DyLight 680 NHS ester (Pierce) according to the manufacturers' protocols; unbound dye was removed by centrifugal filtration (3 kDa MWCO, Millipore). To assemble MTRIPS, each fluorescently labeled biotinylated oligo was incubated with Neutravidin at a 5:1 molar ratio for 1 hour at room temperature. Unbound oligos were removed by centrifugal filtration (30 kDa MWCO, Millipore). To bind label IVT mRNA with MTRIPS, IVT mRNA was first incubated at 70C for 10 minutes and then immediately placed on ice to remove secondary structure. IVT mRNA was then incubated with each MTRIP at a 1:1 molar ratio overnight at 37C. Unlabeled probes were removed by filtration (200 kDa MWCO, Advantec), and IVT mRNA was buffer exchanged into Ringer’s lactate (RiLa). IVT mRNA content was then determined by 260nm absorbance using the Nanodrop 2000 (Thermo Scientific).

3.2.2 Preparation and sizing of mRNA nanoparticles

Cholk was provided by In-Cell-Art (Nantes, France). To prepare nanoparticles, mRNA and cholk were individually diluted in RiLa to obtain final volumes of 20µl each (10 µg of mRNA, and a 1:10 charge ratio of mRNA:cholk). The cholk solution was then added to the mRNA, mixed well, and allowed to incubate for 15 minutes prior to injection. Size and zeta potential of particles were measured with Malvern Instruments Zetasizer Nano ZS. Particles were diluted in either PBS to measure size or in deionized water to measure zeta potential.

3.2.3 Mouse intramuscular injection and luciferase assay

Female BALB/c mice (Charles River, Wilmington, MA) were anesthetized with 2.5% isoflurane and then injected in the anterior tibialis with 10µg (40µl) of IVT mRNA diluted in RiLa using a 29G needle. The alternate leg served as a sham injection control. Mice were housed and manipulated under specific-pathogen-free conditions in the animal care facilities of Georgia Institute of Technology. All experiments were in accordance with the Institutional Animal Care and Use Committee. For the luciferase assay, anterior tibialis muscle was removed and snap frozen in liquid nitrogen 16 hours following IVT mRNA injection. Tissue was homogenized according to (117) with a mortar and pestle cooled with liquid nitrogen, suspended in 0.5ml of passive lysis buffer (Promega), subjected to 4 freeze-thaw cycles (between liquid nitrogen and a 37C water bath), and centrifuged at 10,000 RCF for 3 minutes to remove debris. The process was then repeated with the debris, and the supernatants were pooled together. Protein content was determined using the BCA assay (Pierce). Luciferase activity was assayed using the luciferase assay system (Promega) by measuring light output on the Biotek Synergy H4 plate reader over a 10 second integration period. The surrounding muscles

were also processed and assayed for luciferase activity, but no luciferase activity was detected.

3.2.4 Immunohistochemistry and antibodies

Extracted tissue was fixed using 4% paraformaldehyde in PBS overnight, embedded in paraffin, and sectioned to 5 µm thick. To stain tissue, sections were deparaffinized, antigen retrieval was performed in citrate buffer (Dako, Carpinteria, CA) for 20 minutes under steam, and then tissue was permeabilized in PBS with 0.1% tween-20 (CalBioChem) (PBST) for 10 minutes. Tissue was blocked with 5% donkey serum in PBST, incubated with primary antibodies (at a 1:200 dilution) overnight at 4C in PBST, washed three times in PBST, incubated with the secondary antibody for one hour in PBST, stained with DAPI, and then mounted with prolong gold (Life Technologies). Primary antibodies used were rat anti-MHCII (eBioscience), rabbit anti-CD11b (Abcam), rabbit anti-lyve-1 (Pierce), goat anti-RIG-I (Santa-Cruz cat# sc-48929), goat anti-MDA5 (ProSci, cat# 4037), rabbit anti-MAVS (Bethyl Laboratories cat# IHC-00477), rabbit anti-TLR7 (Novus, cat# NBP2-24906), and mouse anti-IRAK4 (LS Bio, cat# LS BIO452). Secondary antibodies were purchased pre-conjugated to either Alexa Fluor 488 (Life Technologies), Cy3 (Jackson Immuno), or Alexa Fluor 647 (Life Technologies). Primary and secondary antibodies were used at a dilution of 1:200.

3.2.5 Proximity ligation assay

Following deparaffinization, antigen retrieval, and permeabilization as described above, tissue was blocked for 1 h with a solution containing 0.5% Tween-20, 0.1% Triton X-100, 0.1% gelatin (Aurion), 2% donkey serum (VWR) and 1% bovine serum albumin (EMD) in PBS. Tissue was then stained with primary antibodies as specified above overnight at 4C diluted 1:500 in a solution of 0.25% gelatin, 0.5% donkey serum, and 1%

BSA in PBS. All remaining steps were in accordance with manufacturer's instructions (Olink Bioscience).

3.2.6 Proximity ligation assay image quantification and statistics

All samples for PLA were imaged and quantified by a researcher blind to the sample identity. Six images were taken of each tissue section and a total of four animals were used per group per time point. The PLA frequency/imaging frame was quantified using Volocity software (Perkin Elmer). The PLA signal was identified as objects by the overall fluorescence intensity, using a minimum size of 0.2 µm. Touching punctae were separated into individual signals using Volocity's 'separate touching objects' tool. Statistical analysis on the data was conducted using MATLAB and Statistics Toolbox R2015a (The Mathworks, Inc., Natick, Massachusetts). The data were transformed to better approximate normality using variance-stabilizing and symmetrizing power transformation with exponent 1/3. The cube-roots of observations also minimized the Jarque-Bera statistic measuring discrepancy from the normality. A hierarchical ANOVA was performed on the cube-root transformed data followed by Tukey's multiple comparison battery of tests. MATLAB code and additional figures regarding statistical analyses are included in Appendix A.

3.2.7 Fluorescence imaging

Images were taken using an UltraVIEW spinning disk confocal microscope, Zeiss LSM 510 Meta, a Hamamatsu Flash 4.0v2 CMOS camera and an 89000 Sedat Quad-ET filter set. A 40x, NA 1.3 Zeiss EC Plan-Neofluar oil objective was used for all tiled images and a 63×, NA 1.4 Zeiss Plan-Apochromat oil objective was used for all other images. Imaging was controlled by Volocity acquisition software (PerkinElmer). Image

stacks were recorded at 350 nm intervals. Tiled images of the lymph node and muscle were stitched using Volocity.

3.2.8 Flow cytometry and statistics

Lymph nodes and muscle were removed with the assistance of the Fluobeam NIR imaging system (Fluoptics) at indicated time points. Muscle tissue was dissociated with Type IV collagenase (Worthington Biochemical) for 1.5 hours at 37C with gentle agitation. Lymph node and muscle samples were then dissociated by straining through a 40 µm cell strainer with gentle agitation from a syringe plunger. Cells were washed in PBS + 2% FBS, blocked with Fc block (BD Biosciences) according to the manufacturer's directions, and then stained with a panel of antibodies diluted 1:100 in PBS with Fc block for 30 minutes on ice. Cells were washed with PBS + 2% FBS, fixed with 4% paraformaldehyde in PBS for 10 minutes, washed with PBS+2% FBS and stored at 4C until analysis on the flow cytometer. Flow cytometry was performed with a BD LSRII and analyzed with FlowJo software. Samples were stained using two different antibody panels, either anti-F4/80 BV421, anti-LYVE1 Alexa 488 (eBioscience), I-Ad PE, anti CD11c APC-Cy7, and anti CD11b Alexa 647, or anti CD3 BV421; anti CD45R Alexa 488 (Biolegend), anti CD335 PE, anti CD11b Alexa 647, and anti CD19 APC-Cy7. IVT mRNA was labeled with DyLight 680. All antibodies were purchased from BD Biosciences unless otherwise noted. ANOVA followed by Hsu's multiple comparisons with best post analysis was performed to determine significance using JMP Pro software (SAS, Cary, NC).

3.2.9 Cell lines

Sol8 mouse myoblast cells (ATCC CRL-2174) and HeLa human epithelial cells (ATCC CCL-2) were maintained in High Glucose Dulbecco’s Modified Eagle’s Medium

(DMEM) (Lonza) with 20% FBS (Hyclone) for Sol8 cells and 10% FBS for HeLa cells, and 100 U/ml penicillin and streptomycin (Invitrogen).

3.2.10 siRNA transfection and quantitative reverse transcriptase polymerase chain reaction

Cells were electroporated using the Neon transfection system (ThermoFisher Scientific) (10^6 cells in 100ul) using 200μM indicated siRNA (Dharmacon, On-TARGETplus Smartpool), and then plated in 24 well plates. After 48 hours, cells were transfected with the mRNA vaccine (400ng) using Lipofectamine 2000 (Invitrogen) according to the manufacturer's protocol. Six hours later, total RNA was collected with the QIAGEN RNeasy, which used an on-column DNAse treatment. RNA was quantified by absorbance at 260nm and converted to cDNA using the RT2 First Strand kit (SA Biosciences). qRT-PCR was performed using the StepOnePlus real-time PCR system (Applied Biosciences) using 15 ng of cDNA and SYBR green mastermix (SA Biosciences), which was used according to manufacturer's directions. Gene-specific primers for GAPDH, ACTB, IFNβ-1, IL-6, and IL-8 were designed by and purchased from Fluidigm. Primers for DDX58 (RIG-I), IFIH1 (MDA5), and TLR7 were designed by and purchased from SA Biosciences. Fold changes were calculated using the ddCT method on StepOne software in reference to the genes GAPDH and ACTB. For cytokine responses, average fold change over at least three experiments is reported in reference to individual control samples treated with Lipofectamine only. For reporting PRR transcript levels, results from independent experiments are shown. Fold changes are reported in reference to samples treated with control siRNA and Lipofectamine only treatment. The standard error of the mean is shown. Each experiment was repeated at least three times. ANOVA followed by Tukey-Kramer's post analysis was performed on

data from at least three independent experiments to determine significance using JMP Pro software.

3.3 Results

IVT mRNA was labeled with MTRIPS that targeted the 3' UTR as shown in Figure 3.2 prior to injection. Previous work in our lab has not found MTRIP labeling to affect the behavior or trafficking of target mRNA molecules, nor have we found MTRIP labeling to elicit cellular immune responses (147-150). IVT mRNA was then incubated with a cholesterol-derived lipid (cholk) at a 1:10 charge ratio to form nanoparticles. Dynamic light scattering measured nanoparticles to be approximately 300 nm in diameter and to have a zeta potential of approximately -15.3 mV. To test for IVT mRNA functionality, the entire muscle was removed and assayed for luciferase activity (Figure 3.3). IVT mRNA delivered with or without cholk leads to luciferase activity. Interestingly, we see a higher variability in luciferase activity when IVT mRNA is injected alone compared to when it is delivered along with cholk.

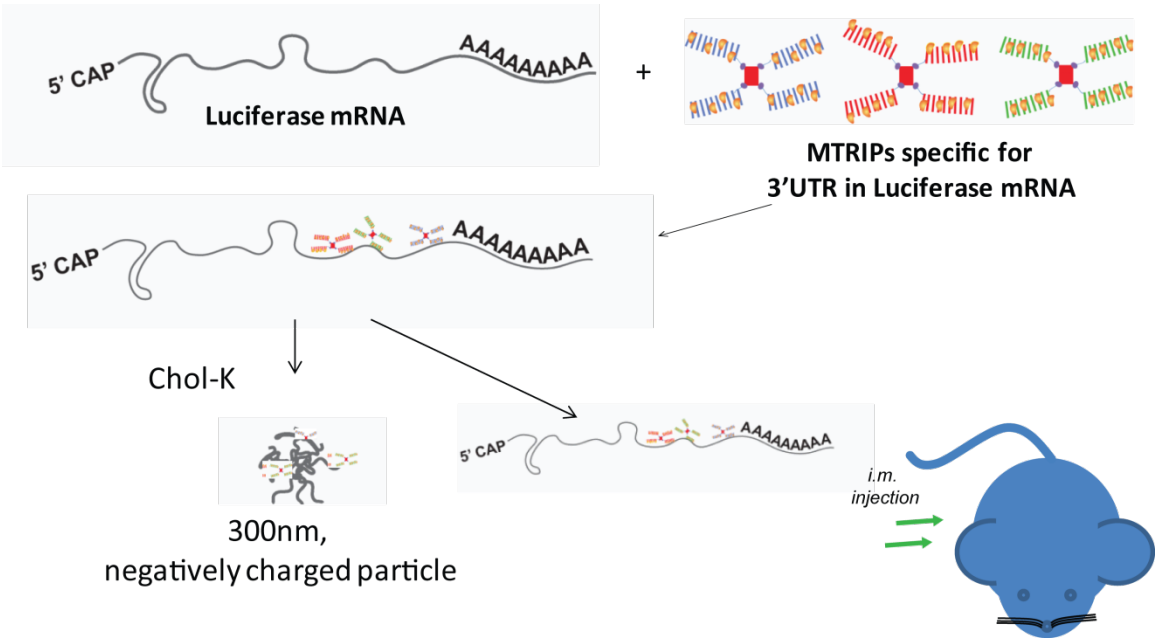

Figure 3.2. Experimental overview. Luciferase encoding IVT mRNA was labeled in the 3' UTR with MTRIPS. IVT mRNA was then complexed with cholk to form a nanoparticle. IVT mRNA alone, or complexed to cholk was injected i.m. into BALB/c mice.

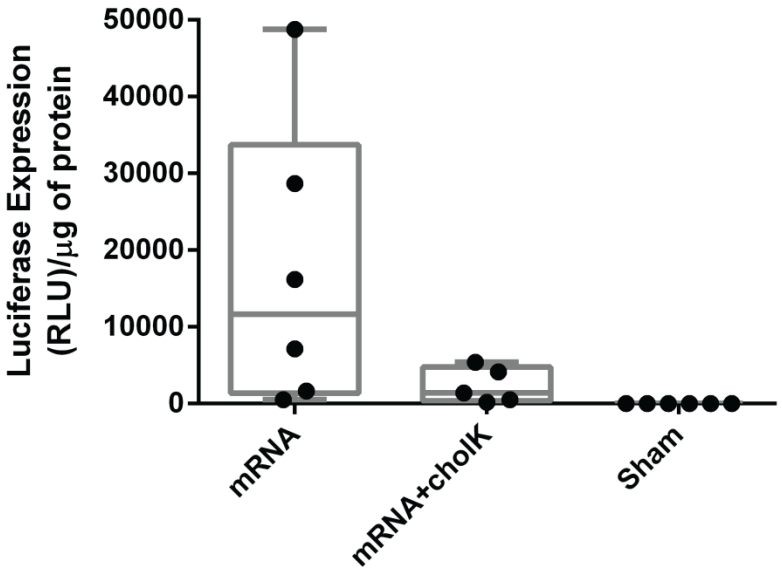

Figure 3.3. Luciferase expression in the anterior tibialis 16 hours following IVT mRNA injection. The entire muscle was removed and homogenized prior to performing a luciferase assay. Luciferase activity is expressed relative to total protein content in homogenized muscle.

3.3.1 Spatial distribution of IVT mRNA within muscle and cell infiltration to site of injection

We next wanted to assess how nanoparticle-mediated delivery of IVT mRNA affected its distribution in the muscle. To do this, IVT mRNA was fluorescently labeled with MTRIPs in the 3' untranslated region, if needed, complexed to cholk, and then injected i.m. IVT mRNA distributions were then visualized with microscopy 1.5 and 16 hours after i.m. injection (Figure 3.4). At 1.5 hours following injection, IVT mRNA (red) is evenly distributed throughout the muscle and primarily in areas between skeletal muscle fibers for IVT mRNA delivered alone or as a nanoparticle with cholk. Sixteen hours following injection, the free IVT mRNA appears to be somewhat cleared from the muscle compared to nanoparticle-mediated delivery. Infiltration of $CD11b^+$ cells (green) and $MHCII^+$ cells (white) is also evident at 16 hours following injection, and more pronounced in muscles injected with mRNA+cholk. To quantify these observations, we used flow cytometry to assess uptake of mRNA 16 hours following injection. As shown in Figure 3.5, IVT mRNA injection leads to increased presence of $CD11b^+$ cells in the muscle. A fraction of the $CD11b^+$ cells also costained for IVT mRNA. We also saw increased levels of $MHCII^+$ cells as well as infiltration of natural killer cells, which were identified by dual staining of CD335 and CD11b. There was no increase in macrophages, as detected by dual staining of $F4/80^+$ $CD11b^+$.

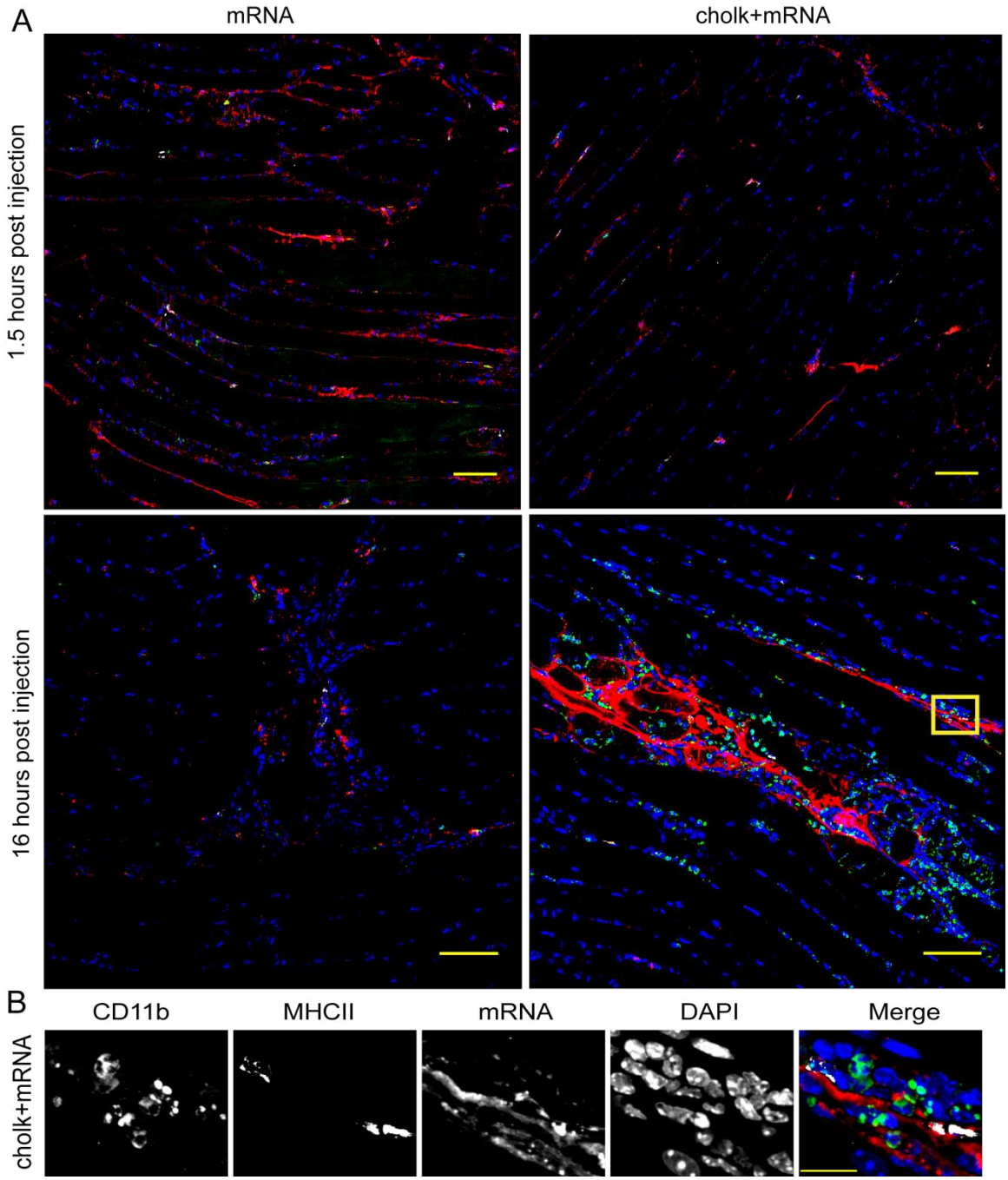

Figure 3.4. Distribution of IVT mRNA following injection and uptake by CD11b+ and MHCII+ cells. A.) Histological section of skeletal muscle tissue 1.5 and 16 hours following intramuscular injection into the anterior tibialis of 10µg of luciferase mRNA with and without cholk. IVT mRNA is shown in red, CD11b staining is green, MHCII is white, and nuclei (DAPI) is blue. Scale bar is 100 µm. B.) Scale bar is 20 µm

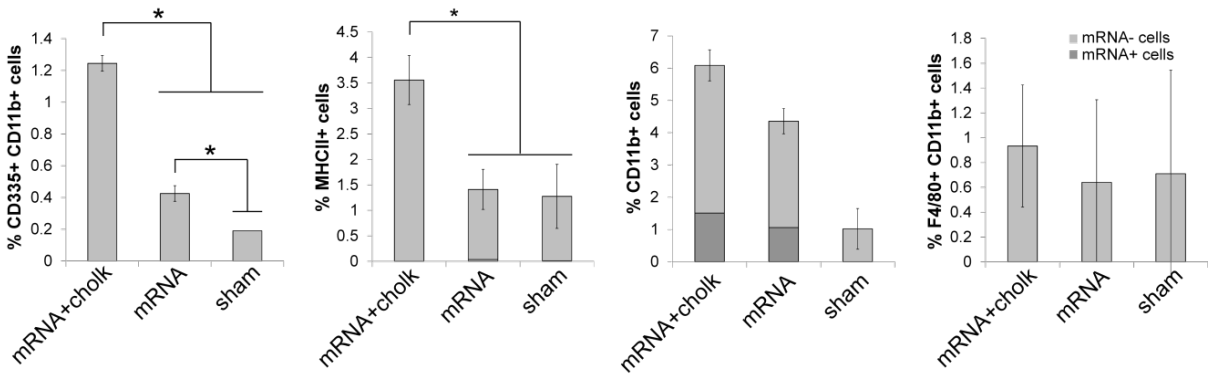

Figure 3.5. Cell types containing IVT mRNA 16 hours after i.m. injection. 16 hours following intramuscular injection, the whole anterior tibialis was dissociated into a single cell suspension and flow cytometry was performed to determine the indicated cell types in the area and if they had taken up labeled IVT mRNA. Mean values and the standard error of measurement are shown (n=3). *indicates $p<0.05$, ANOVA followed by Hsu's multiple comparison with best.

3.3.2 RNA uptake by TLR7$^+$, RIG-I$^+$ and MDA5$^+$ cells

We next wanted to assess expression of the PRRs TLR7, RIG-I, and MDA5 in skeletal muscle tissue following IVT mRNA injection. We first stained tissue from a sham injection control to understand the baseline expression levels of these PRRs (Figure 3.6). Figure 3.7 shows representative images of staining for these PRRs 16 hours following injection with IVT mRNA. We see that cells with elevated levels of these PRRs are distributed throughout the tissue and that these cell types are associated with IVT mRNA. To assess staining specificity of staining, control tissue samples were stained only with the secondary antibodies (Figure 3.8). The marked enhancement of PRR staining following IVT mRNA injection may be mediated by both upregulation of PRRs in the extant cell populations in response to PRR activation as well as infiltration of cell types that highly express certain PRRs. This is supported by Figure 3.9, which shows that TLR7, RIG-I, and MDA5 transcripts are upregulated in response to IVT mRNA transfection.

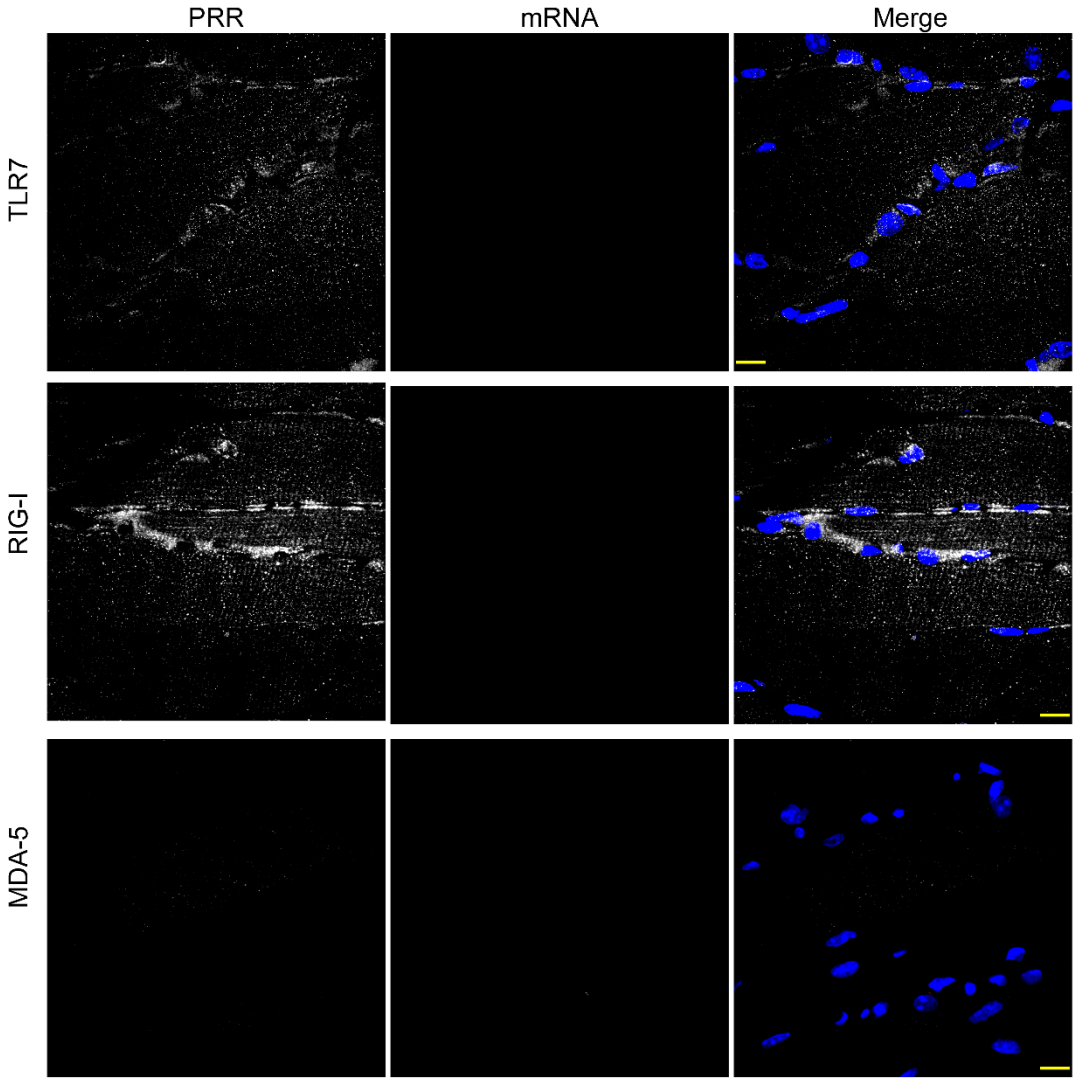

Figure 3.6. TLR7, RIG-I, and MDA5 staining in sham injected skeletal muscle tissue. Histological sections of skeletal muscle tissue 16 hours following intramuscular injection into the anterior tibialis with RiLa. In the merged image, the indicated PRR is shown in white, the channel used for IVT mRNA imaging would be shown in red, and DAPI staining for nuclei is shown in blue**.** Scale bars are 12 µm.

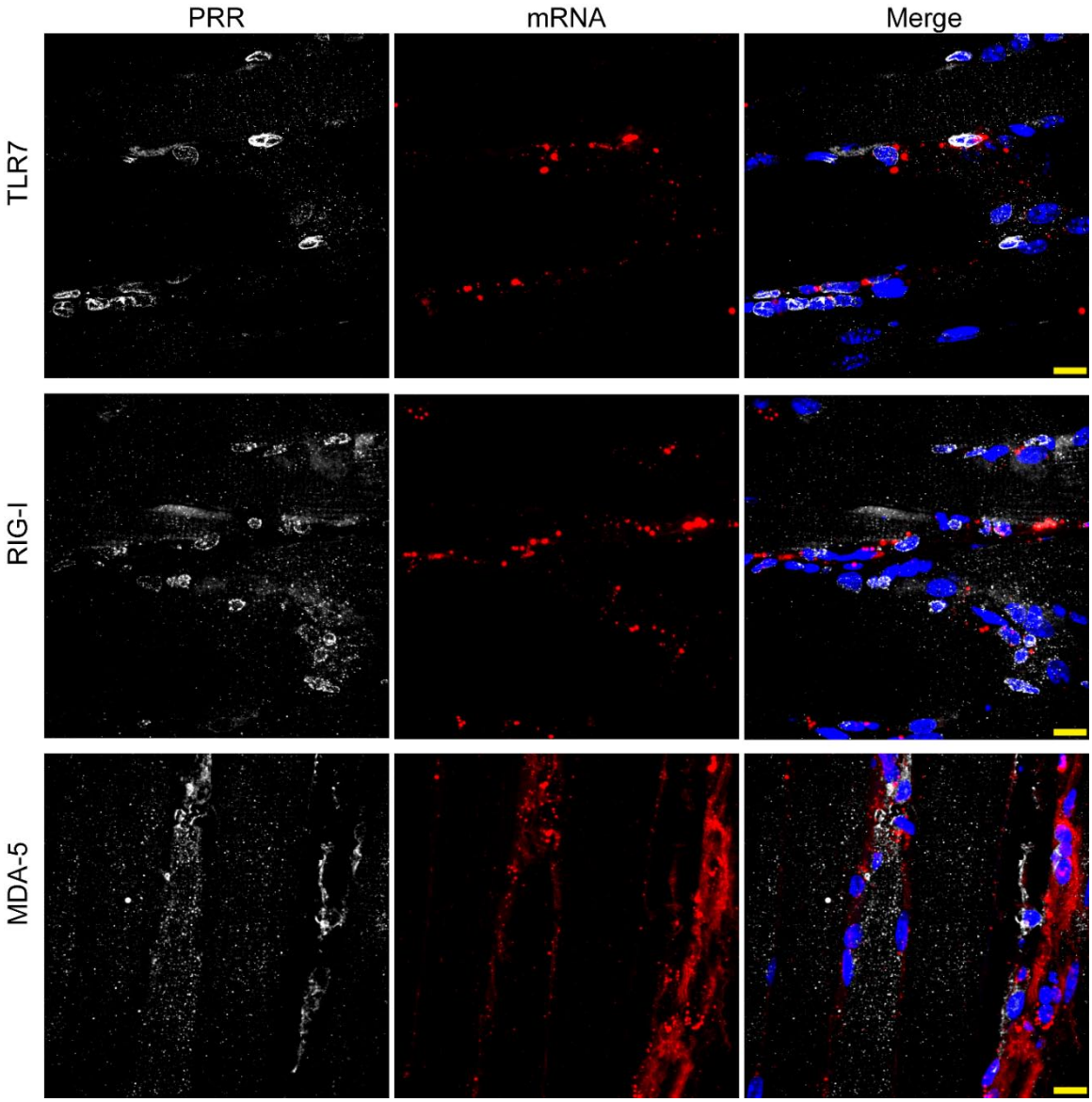

Figure 3.7. IVT mRNA uptake by TLR7+, RIG-I+, and MDA5+ cells. Histological section of skeletal muscle tissue 16 hours following i.m. injection into the anterior tibialis of 10 µg of MTRIP-labeled luciferase mRNA. In the merged image, the indicated PRR is shown in white, IVT mRNA is shown in red, and the merged image includes nuclei (DAPI) is blue**.** Scale bars are 12 µm.

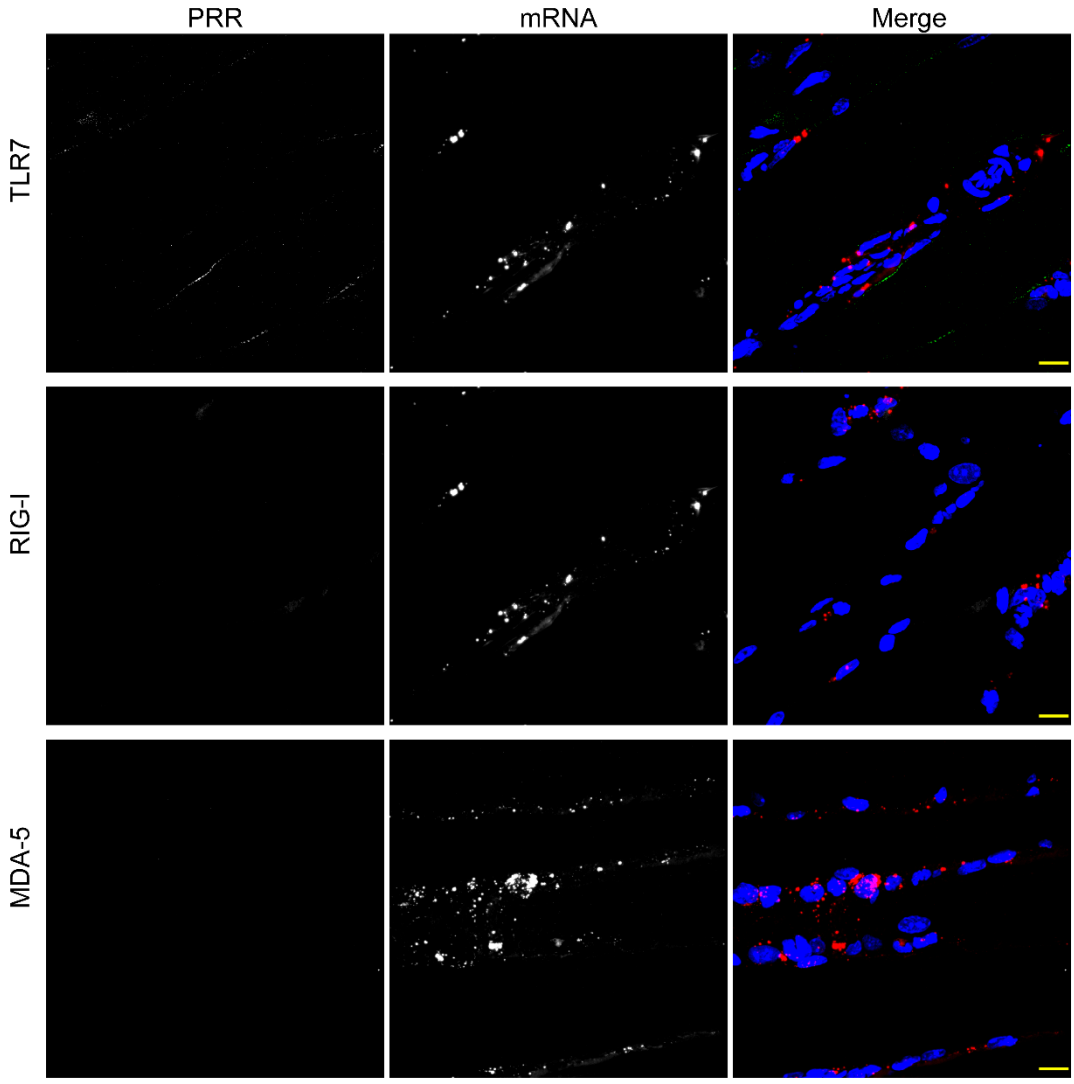

Figure 3.8. Immunohistochemistry staining controls for TLR7, RIG-I, and MDA5 detection. Histological sections of skeletal muscle tissue 16 hours following i.m. injection into the anterior tibialis with RiLa. As a negative control, tissue was stained with the appropriate secondary antibody for the indicated PRRs and imaged with the same acquisition settings used in Figures 3.6 and 3.7. In the merged image, the indicated PRR is shown in white, IVT mRNA is shown in red, and nuclei (DAPI) is blue**.** Scale bars are 11 µm.

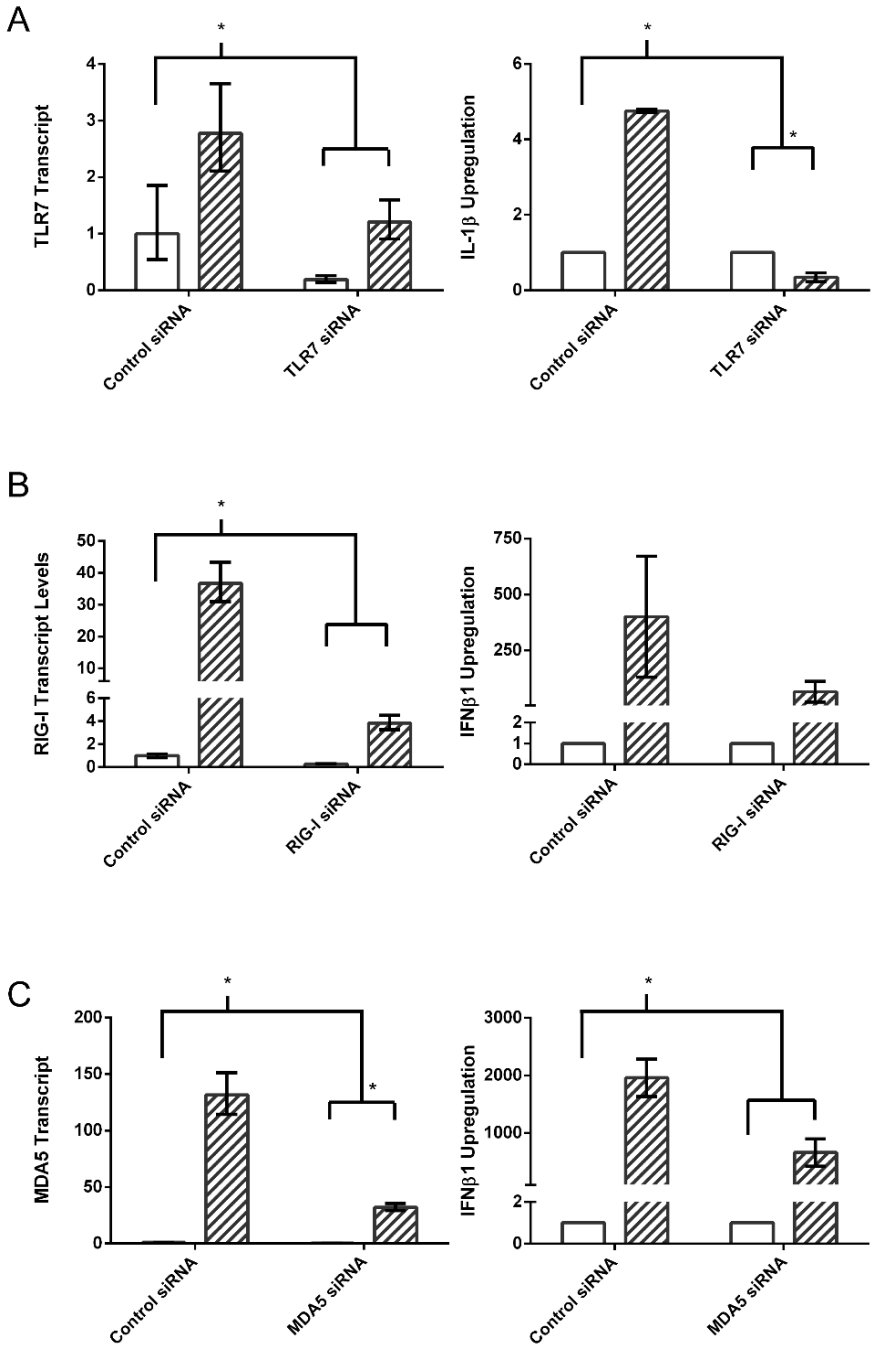

Figure 3.9. Effect of PRR knockdown on cell responses to IVT mRNA transfection. Clear bars are Lipofectamine 2000 only, dashed is Lipofectamine+ RNA. A.) Sol8 mouse myoblasts were electroporated with siRNA targeting murine TLR7. Two days later, cells were transfected with luciferase IVT mRNA and then analyzed with qRT-PCR six hours later. HeLA human epithelial cells were electroporated with siRNA targeting murine RIG-I. B.) or MDA5. C.) Two days later, cells were transfected with luciferase IVT mRNA and then analyzed with qRT-PCR six hours later for RIG-I and 9 hours later for MDA5 siRNA studies. * Indicates $p<0.05$, ANOVA followed by Tukey's post analysis.

We next assessed how cholk nanoparticle-mediated delivery affects TLR7 activation. To visualize TLR7 activation, we developed a PLA that detects formation of the myddosome signaling complex. The myddosome complex consists of a variety of proteins including TLR7, MYD88, and IRAK4 that come together when TLR7 is activated (142, 151). To detect this complex, we assayed for the proximity of IRAK4 and TLR7 on muscle tissue sections 1.5, 6, and 16 hours following IVT mRNA injection. The PLA allows visualization of this interaction via fluorescent puncta, which we imaged with confocal microscopy (Figure 3.10A). To account for false-positive PLA signals that could occur as a result of TLR7 or IRAK4 protein levels being upregulated in response to immune stimulation, we also ran two controls where an isotype control antibody was substituted for either primary antibody involved in the assay. PLA signals were quantified for each condition, and aggregated data is shown in Figure 3.10B. IVT mRNA causes TLR7 myddosome formation as early as 1.5 hours and lasting until 16 hours following injection. Analyzing the data across all time points (Figure 3.10C) shows that IVT mRNA + cholk also leads to TR7 activation, but to a lesser degree than IVT mRNA alone.

We also wanted to assess RIG-I and MDA5 detection of IVT mRNA. Upon activation, both RIG-I and MDA5 form a protein complex, known as signalosomes, with the adaptor protein IPS-1 (138, 152). To detect their activation, we developed PLA assays to identify RIG-I and MDA5 signalosome formation. Figure 3.11 and Figure 3.12 show RIG-I and MDA5 activation, respectively. In both cases, PLA signals are evident beginning 6 hours after injection. However, there is more pronounced activation at 16 hours. Microscopy shows that cells with strong PLA signals for RIG-I and MDA5 show diffuse IVT RNA signal, suggesting that the RNA is cytoplasmic and available to interact with RIG-I or MDA5. Analysis of the data across all time points for RIG-I and MDA5 (Figures 3.11C and 3.12C, respectively) shows that mRNA+cholk leads to activation of both of these PRRs.

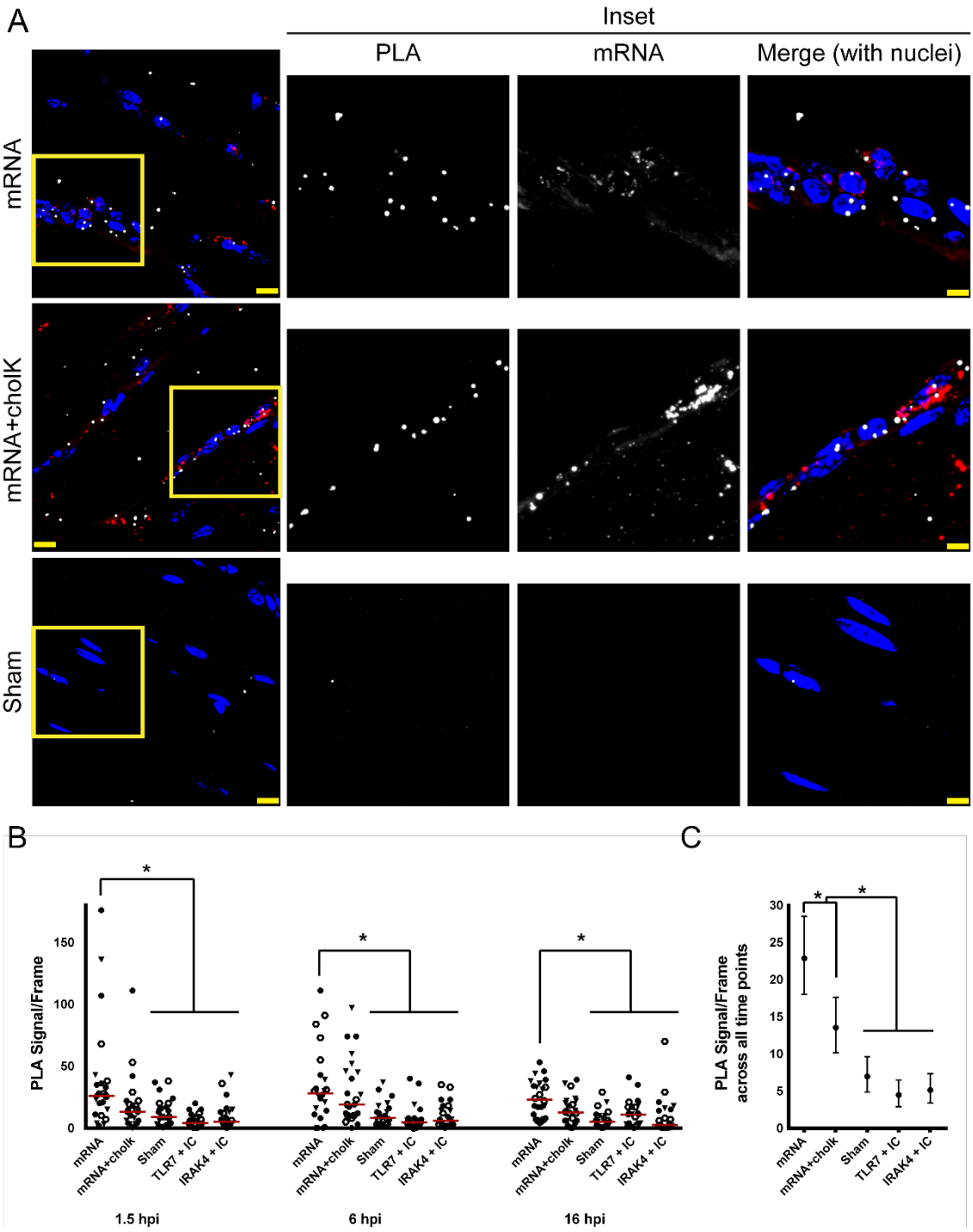

Figure 3.10. PLA detection of TLR7-IRAK4 signaling complex following IVT mRNA injection. (A) Representative images of PLA: IVT mRNA (red), PLA signals (white), and nuclei (blue). Scale bar is 11 µm (leftmost panel) and 7 µm (right most panel). (B) Quantified PLA data. Each data point represents the number of PLA signals quantified in one confocal image; red bar indicates the median PLA counts per condition. Each symbol represents a unique animal. IC indicates antibody isotype control. (C) Means and approximate 95% confidence intervals of transformed PLA counts for each condition across all time points. Significant differences were tested by a hierarchical ANOVA followed by Tukey's multiple comparisons, * indicates $p<0.05$.

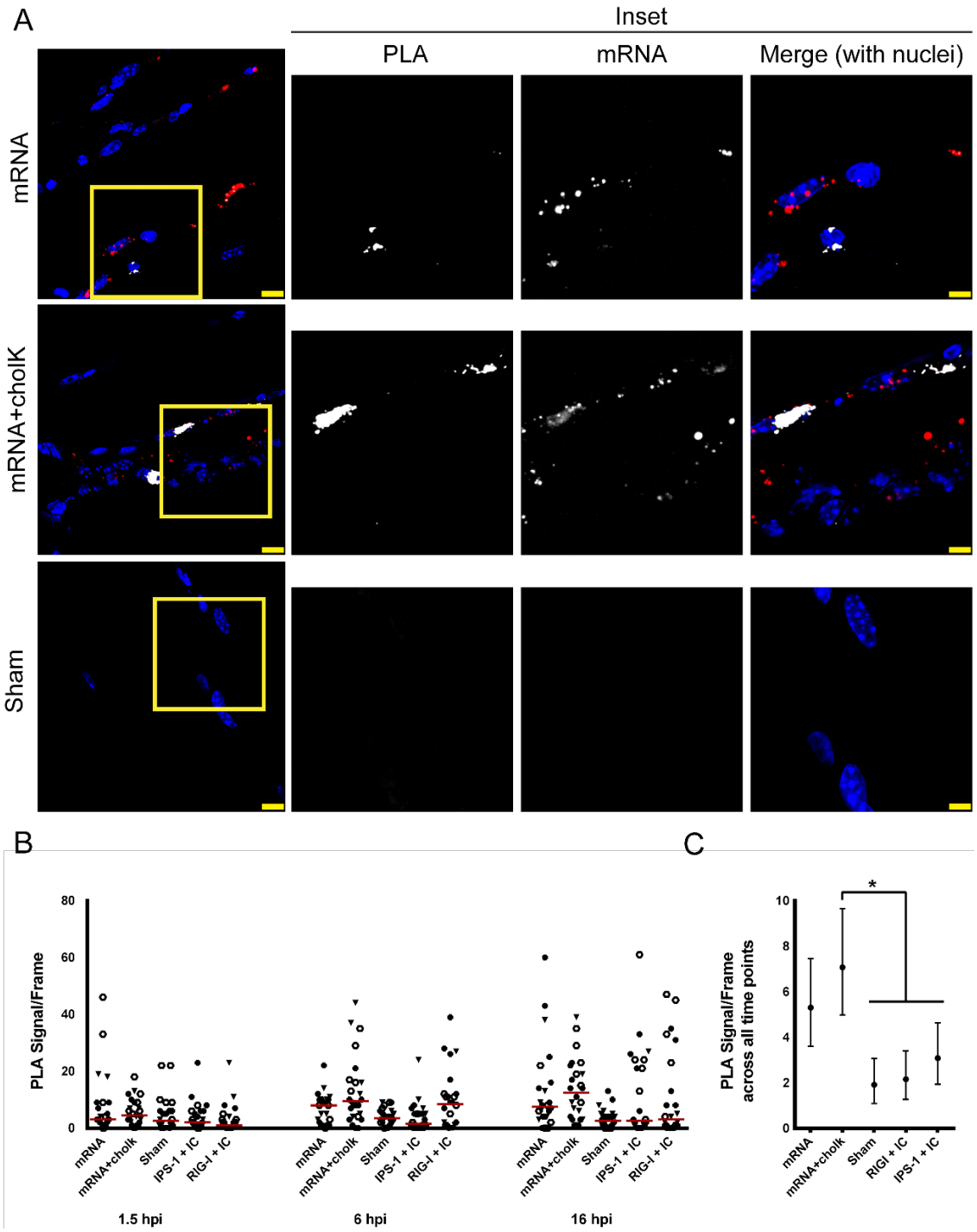

Figure 3.11. PLA detection of RIG-I-IPS-1 signaling complex following IVT mRNA injection. (A) Representative images of PLA: IVT mRNA (red), PLA signals (white), and nuclei (blue). Scale bar is 11 µm (leftmost panel) and 7 µm (right most panel). (B) Quantified PLA data. Each data point represents the number of PLA signals quantified in one confocal image; red bar indicates the median PLA counts per condition. Each symbol represents a unique animal. IC indicates antibody isotype control. (C) Means and approximate 95% confidence intervals of transformed PLA counts for each condition across all time points. Significant differences were tested by a hierarchical ANOVA followed by Tukey's multiple comparisons, * indicates $p<0.05$.

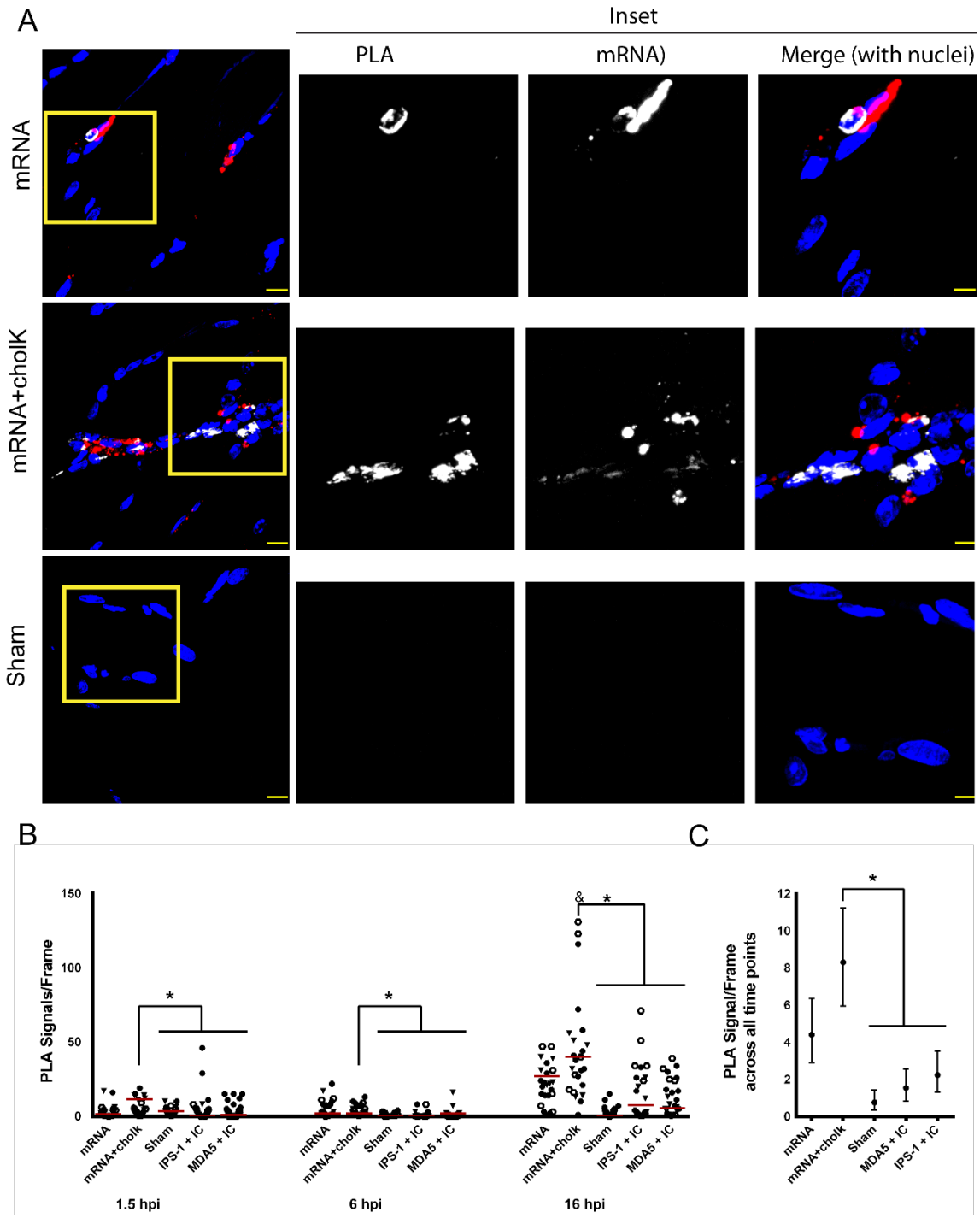

Figure 3.12. PLA detection of MDA5-IPS-1 signaling complex following IVT mRNA injection. (A) Representative images of PLA: IVT mRNA (red), PLA signals (white), and nuclei (blue). Scale bar is 11 µm (leftmost panel) and 7 µm (right most panel). (B) Quantified PLA data. Each data point represents the number of PLA signals quantified in one confocal image; red bar indicates the median PLA counts per condition. Each symbol represents a unique animal. IC indicates antibody isotype control. (C) Means and approximate 95% confidence intervals of transformed PLA counts for each condition across all time points. Significant differences were tested by a hierarchical ANOVA followed by Tukey's multiple comparisons, * indicates $p<0.05$.

3.3.3 IVT mRNA is detected in lymph nodes in a variety of cell types

We next assessed if mRNA was trafficked to lymph nodes following i.m. injections. Here, MTRIPS with DyLight 680 fluors were used to label IVT mRNA. Following injection, the Fluobeam imaging system (Fluoptics) was used on recently euthanized mice to determine if IVT mRNA was present in the draining lymph nodes (representative image shown in Figure 3.13). The Fluobeam system detected IVT mRNA in the lumbar aortic, inguinal, and popliteal lymph node. Figure 3.14C shows the number of lymph nodes where IVT mRNA was found using the Fluoptics system. Interestingly, cholk-mediated delivery allowed for more consistent uptake in all lymph nodes compared to mRNA delivered alone. To see if mRNA+cholk affected the level of IVT mRNA present in the lymph node we analyzed lymph nodes with flow cytometry. Figure 3.14A shows that IVT mRNA was present in lymph nodes at 1.5 hours following injection, and the amount of IVT mRNA in the lymph nodes modestly increases at 16 hours following injection. Lymph nodes were also histologically analyzed to determine IVT mRNA distribution, and a representative image is shown in Figure 3.13 with zoomed in regions shown in Figures 3.13B and 3.13C. Here, lymph nodes were stained for Lyve-1 to delineate sinuses. It is evident that IVT mRNA is closely associated with the sinuses. To better understand what cell types had taken up the IVT mRNA, we repeated the experiment and analyzed the lymph nodes with flow cytometry 16 hours following i.m. injection (Figure 3.14B). IVT mRNA was largely shown to be in antigen presenting cells. A significant portion of MHCII+, CD11b+, and $CD19^{+}CD3^{-}$ (B cells) lymph node cells were positive for IVT mRNA signal.

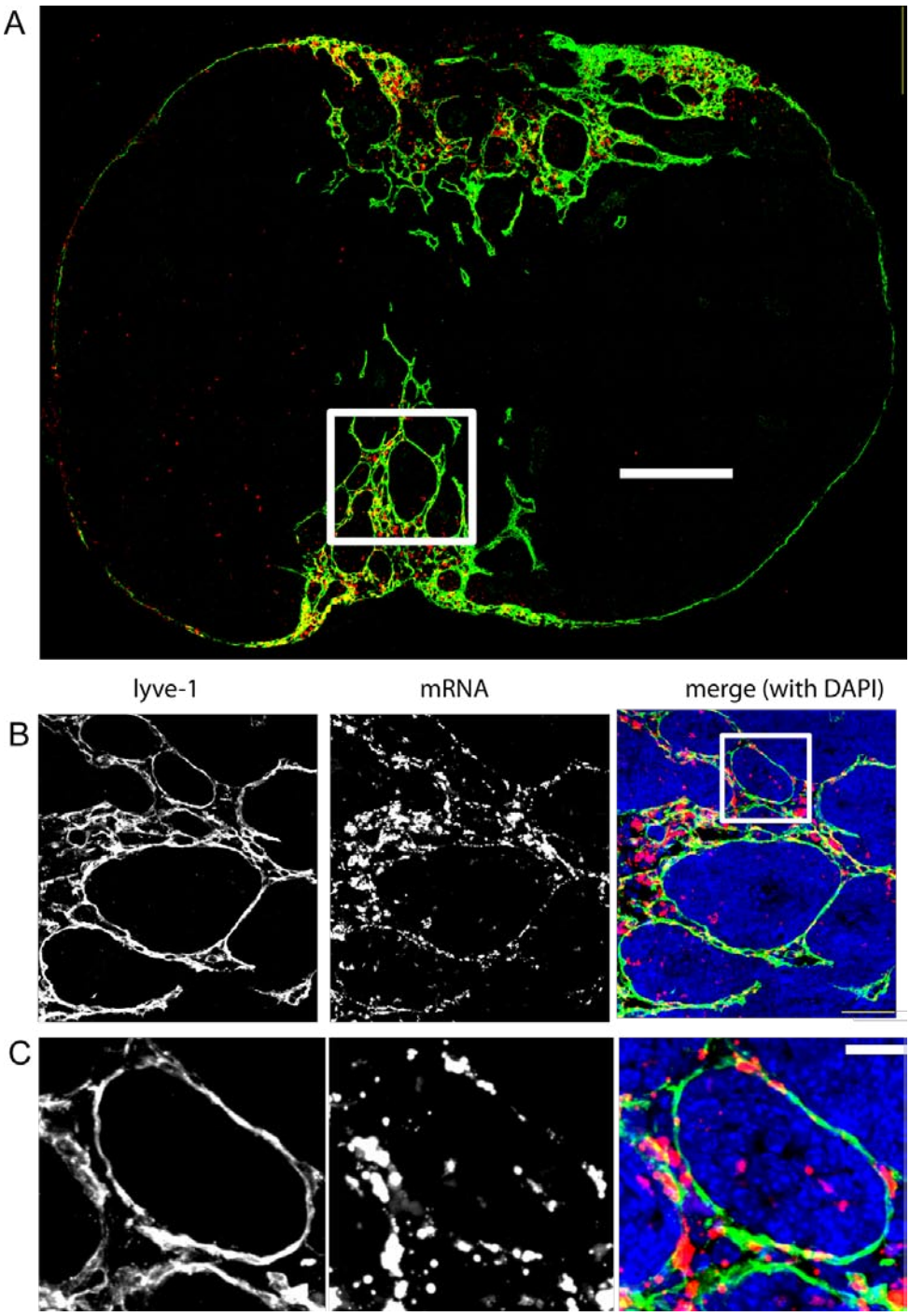

Figure 3.13. IVT mRNA distribution in draining lymph node. A.) Histological cross-section of the lumbar aortic lymph node 16hours after i.m. into the anterior tibialis of 10µg of luciferase mRNA. IVT mRNA is shown in red and lyve-1 staining is shown in green. IVT mRNA associates with lyve-1 staining, indicating presence in lymph node lymphatic vessels. Scale bar is 300 µm. B.) Blow-up image of the area indicated in (A) with scale bar of 50 µm and C.) Blow-up image of the area indicated in (B) with a scale bar of 18 µm. For both B and C, the merged image shows IVT mRNA in red, Lyve-1 in green and nuclei (DAPI) in blue. It is evident that mRNA is around lymphatic vessels, but does not always associate with lyve-1 positive cells.

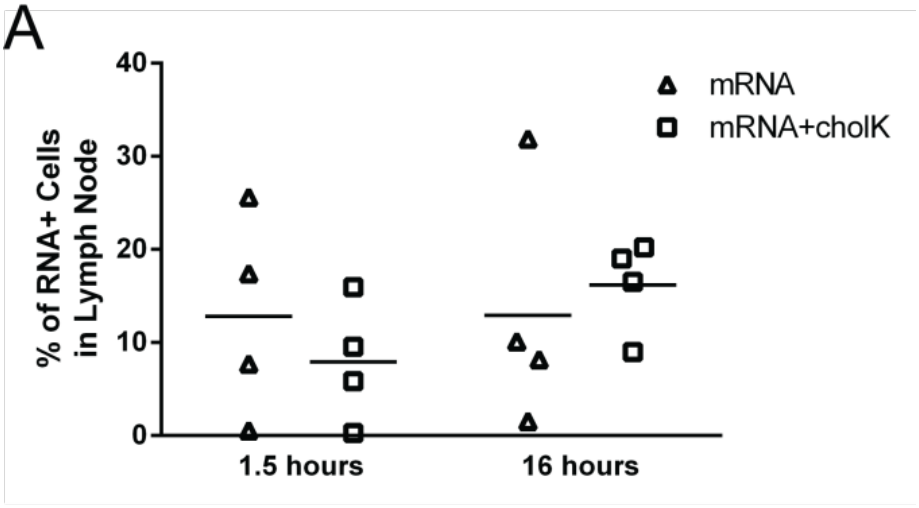

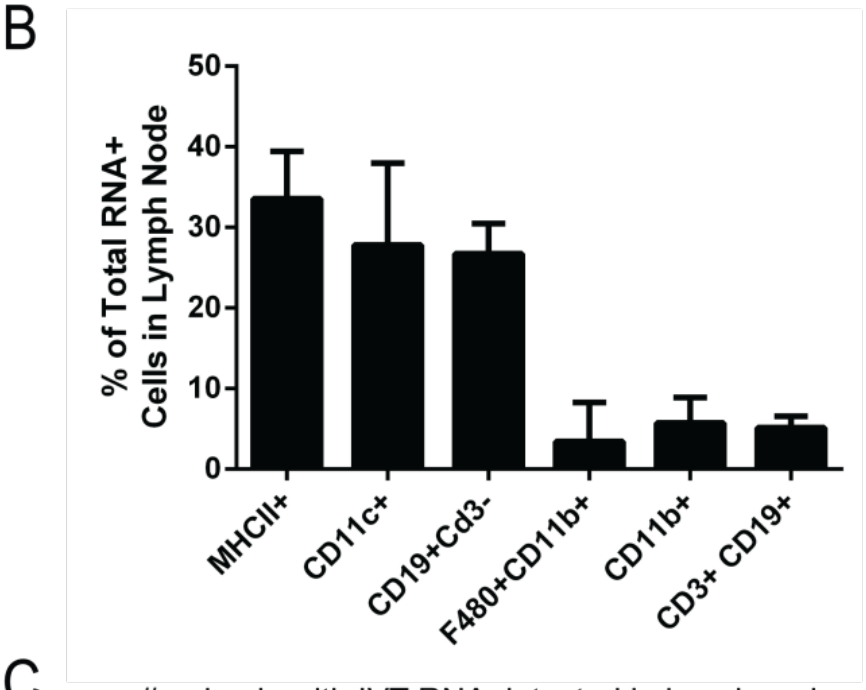

C

animals with IVT RNA detected in lymph node

	Popliteal	Inguinal	Lumbar aortic
mRNA	3/4	2/4	4/4
mRNA+cholK	4/4	4/4	4/4

Figure 3.14. IVT mRNA presence in draining lymph nodes. A.) Mice were injected with MTRIP-labeled IVT mRNA with and without complexation to cholk. 1.5 and 16 hours following injection, lumbar aortic lymph node were removed and analyzed with flow cytometry. The percent of cells positive for MTRIP label are shown as a fraction of all cells analyzed. B.) Flow cytometry analysis of the lymph nodes. Lymph node cells phenotypes and the percent of cells containing IVT mRNA are shown for mRNA+cholk (n=3). C.) Aggregate data of positive detection of IVT mRNA in lymph nodes 16 hours following injection.

3.3.4 Lymph node cells show TLR7, RIG-I, and MDA5 activation in response to IVT mRNA injection

Lastly, extracted lymph nodes were assessed for PRR activation. PLAs were performed as described earlier on lumbar aortic lymph nodes excised 16 hours post injection (Figure 3.15). It is apparent that cells in the lymph node show activation by TLR7, RIG-I, and MDA5. IVT mRNA delivered alone shows activation of TLR7 as also found in the muscle. We also see that mRNA+cholk activates RIG-I. Interestingly, we also see that mRNA delivered alone also shows significant activation of MDA5, where mRNA+cholk does not.

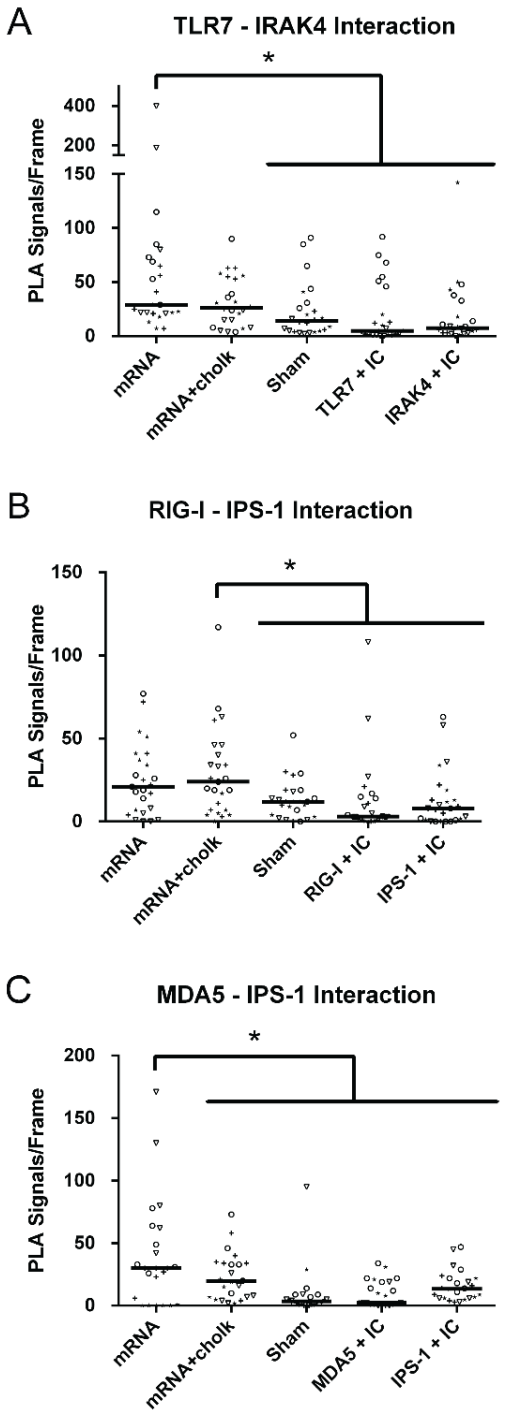

Figure 3.15. PLA assays showing activation of TLR7, RIG-I, and MDA5 signaling pathways. Quantified PLA data of A.) TLR7-IRAK4 interaction, B.) RIG-I-IPS-1 interaction and C.) MDA5-IPS-1 interaction in sections of the lumbar aortic lymph node. Mice were injected with MTRIP labeled IVT-mRNA and the lumbar aortic lymph nodes were collected 16 hours post injection. PLA was quantified from 6 images per mouse; 4 mice per condition. The bar indicates the median PLA count across all images for given conditions. IC indicates isotype control antibody. Significant differences were tested by a hierarchical ANOVA on collected data transformed to fit a normal distribution, * indicates $p<0.05$.

3.4 Conclusion

This study used PLAs to follow TLR7, RIG-I, and MDA5 activation by i.m. injection of IVT mRNA over time. This methodology allowed for PRR activation to be visualized *in situ* without perturbing paracrine and autocrine signaling events. The kinetics of observed PRR activation follows a predicted flow, as endosomal TLR7 is activated as early as 1.5 hours and the cytoplasmic PRR MDA5 shows most prominent activation 16 hours following injection. We see that cholk-mediated delivery of IVT mRNA reduces TLR7 activation and enhances RIG-I and MDA5 activation in the muscle. Cholk-mediated mRNA delivery may enhance the cytoplasmic presence of IVT mRNA, perhaps by facilitating endosomal escape, or altering the route of cellular entry. Another possibility is that cholk shields IVT mRNA from interacting with TLR7.

PLA detection of PRR signaling only offers visualization of PRR activation during a single snapshot in time. The length of time that each signaling complex lasts is unclear, and it is likely that each signaling complex has a unique stability. Additionally, the efficiency of antibody binding and ligation of the secondary antibodies is also unique for each signaling complex. Therefore, comparisons can only be made between different treatment groups and time points in the same PRR, and should not be made between two different PRR signaling complexes. Another limitation of this approach is that while we can detect the occurrence of activation through certain PRRs, the importance of each individual pathway for achieving functional outcomes is not identified.

To the best of our knowledge, this is the first time that MDA5 has been experimentally implicated as a PRR that detects IVT mRNA. This is somewhat surprising, as MDA5 is known to detect long double-stranded RNAs, and IVT mRNA is single stranded. We hypothesize that IVT mRNA develops secondary structures that are

detected by MDA5. While RNAs are well known to form secondary structures outside of a cellular environment, probing of RNA secondary structure *in vivo* has shown that native RNAs have dramatically reduced secondary structures (153). This is likely because cellular RNAs are always in ribonucleoprotein complexes, potentially shielding the development of secondary structures and interaction with MDA5. IVT mRNA; however, is delivered without any bound proteins, potentially allowing for the enhanced formation of secondary structures compared to native mRNAs, and thus activation of MDA5.

It is also surprising that IVT mRNA activates RIG-I, as natural ligands are RNAs with 5' triphosphates (uncapped RNAs). IVT mRNA should not have 5' triphosphates, as theoretically, the 5' cap substitute 5' triphosphates. However, current methodologies for synthesis of IVT mRNA enzymatically add a 5' cap and then treat IVT mRNA with Antarctic phosphatase to remove triphosphates from uncapped IVT mRNAs. It is difficult to purify out any uncapped RNAs from the final IVT mRNA cocktail, and some 5' triphosphates may contaminate the IVT mRNA solution. Another possibility to explain RIG-I activation is that 5' triphosphates are created by activation of the 2′-5′ oligoadenylate synthase (OAS) pathway. OAS proteins are antiviral receptors that detect dsRNA. Upon detection of dsRNA, OAS-L activates the latent endoribonuclease RNAs-L, which digests RNA into RIG-I activating pieces (154-156).

Direct observation of the PRRs that detect IVT mRNA allows for targeted adjustments to IVT mRNA vaccine formulation and more rational modulation of the innate immune responses. We now have evidence that double-stranded regions in IVT mRNA activate PRRs. Future efforts could focus on removing the secondary structure from IVT mRNA. Additionally, our findings highlight the fact that a delivery vehicle can influence IVT mRNA's interaction with the innate immune system. Future design of delivery vehicles may aim to either avoid or facilitate IVT mRNA interaction with PRRs.

As TLR7 stimulation is beneficial for some vaccine applications (157), but not for others (158); delivery vehicle design may be tailored to interact with the most appropriate PRRs for a given vaccine application.

This study also showed that cholk nanoparticle-mediated delivery of IVT mRNA enhanced infiltration of immune cells to the skeletal muscle. As shown in Figure 3.4, particle-mediated delivery appeared to enhance IVT mRNA retention at the site of injection. This may be simply due to how the increased size of the mRNA reduced its mobility out of the muscle. This also may have led to increased localization of the innate immune responses, which was more easily located by infiltrating immune cells. The enhanced infiltration of immune cells observed upon IVT mRNA+cholk injection may also be due to increased activation of cytoplasmic PRRs, particularly RIG-I and MDA5, which trigger strong type I interferon responses (159). Type I interferon has been shown to be required for natural killer cell accumulation at a site of infection (160) and is also known to promote the migration of antigen presenting cells to lymph nodes (160, 161). Thus, the increased infiltration of immune cells to the muscle following mRNA+cholk delivery may be responsible for the enhanced cell-mediated trafficking of IVT mRNA from the muscle to the lymph nodes.

CHAPTER 4

DEVELOPMENT OF IVT MRNA WITH PROGRAMMABLE INNATE IMMUNE STIMULATION

4.1 Introduction

This chapter presents a strategy to enhance immunogenicity of IVT mRNA without affecting transgene protein production. As described in Figure 4.2, we use a modular approach to build immunostimulatory IVT mRNA with programmable PRR activation. This approach may be used with modified or unmodified IVT mRNA to modulate the stimulatory responses. This strategy enables modulation of transgene production and immune stimulation of IVT mRNA on a broader spectrum than otherwise capable.

The success of a vaccine is likely dependent upon unique stimulation characteristics of innate immunity. For example, the co-delivery of an RSV vaccine with a TLR9 adjuvant improves immunological protection against the virus; however, the same vaccine with a TLR7 adjuvant results in no improvement over the vaccine alone (158). In the case of an HIV vaccine, co-delivery of either TLR7 or TLR9 adjuvants with the vaccine improved protective responses; this effect was not seen by co-delivery with a TLR8 adjuvant (162). Several studies show that more protective and longer lasting immune responses are developed when a vaccine activates multiple TLRs (134, 163).

Researchers currently seek to enhance the immunogenicity of IVT mRNA vaccines to enhance protective responses. For example, an anti-melanoma vaccine undergoing clinical trials is supplemented with granulocyte macrophage colony-stimulating factor (GM-CSF) as an adjuvant (23, 164). A complex of IVT mRNA and

protamine is also currently in clinical trials. This formulation is believed to enhance TLR7 recognition of the vaccine (20, 22).

There is evidence to suggest that vaccine performance is weakened due to the interferons produced in response to unmodified IVT mRNA. Pollard *et al*. demonstrate this using interferon receptor alpha knock out ($IFN\alpha R^{-/-}$) animals. Figure 4.1 shows that $IFN\alpha R^{-/-}$ mice have more interferon-gamma and IL-2 secreting splenocytes than those from the wild type when exposed to the antigenic protein. The study also demonstrates that interferon responses were detrimental to antigen protein production (42).

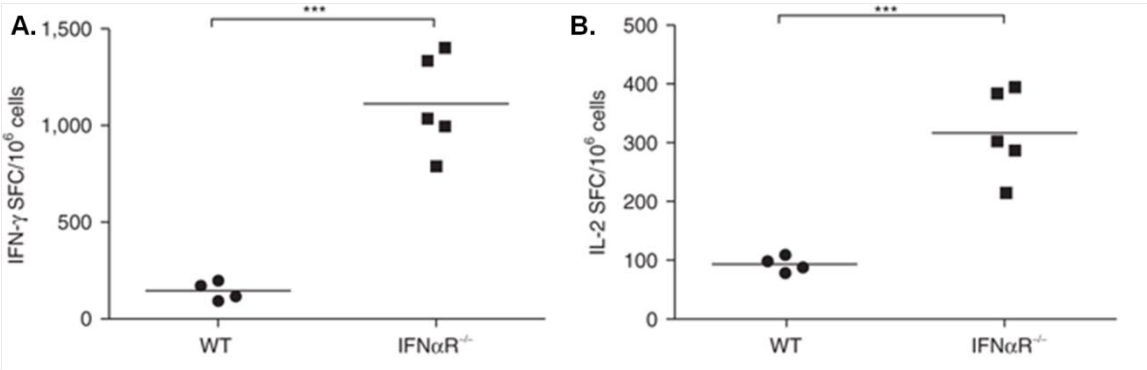

Figure 4.1. T cell responses by wild-type (WT) and interferon alpha-receptor knockout mice ($IFN\ \alpha R^{-/-}$) to an IVT mRNA vaccine. Antigen-specific IFN-γ (A) and interleukin-2 (B) secreting T cells were determined by enzyme-linked immunosorbent spot on isolated spleens. Figure adapted from Pollard et al (42).

Here, we show that IVT mRNA that incorporates the modified base M1Y in place of uridine elicits reduced interferon responses. M1Y substitution also enhances transgene protein production. We tethered adjuvants to M1Y IVT mRNA to enable activation of multiple TLRs. Programmable IVT mRNA enables future work that may explore how the amount and/or type of PRR adjuvants affect vaccine performance.

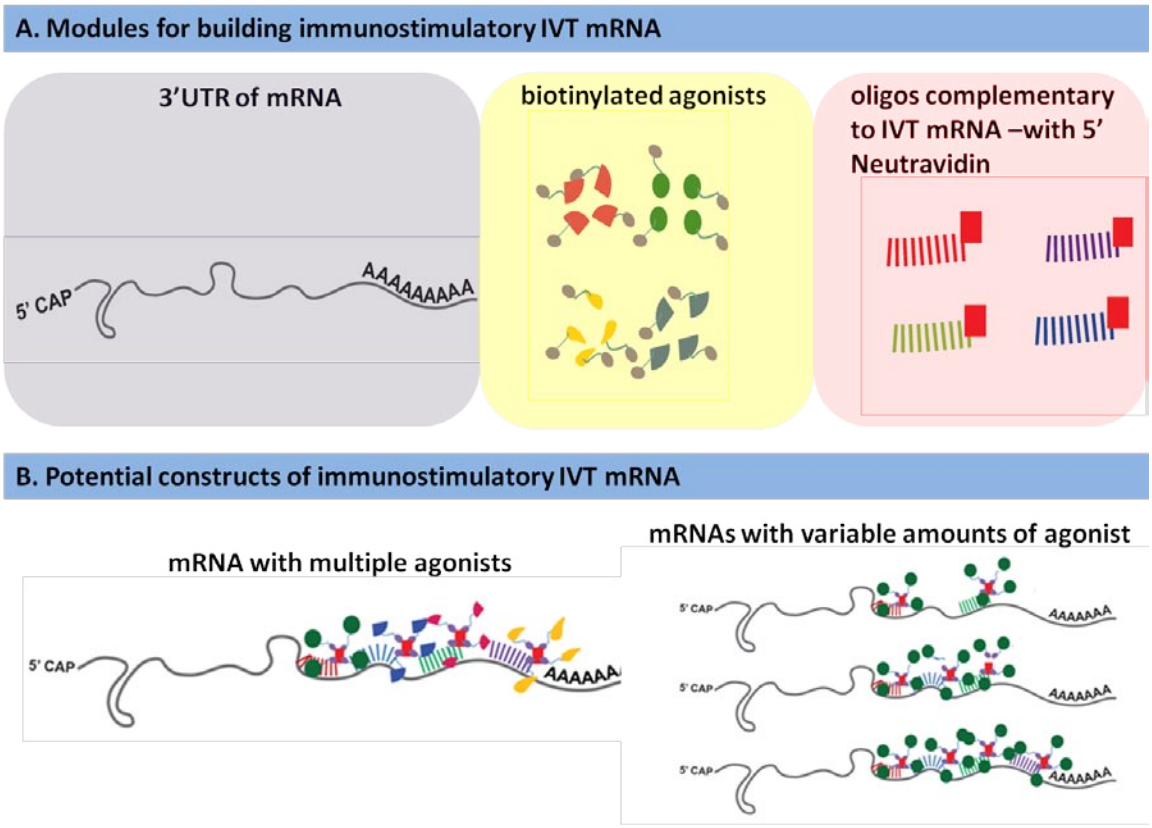

Figure 4.2 Approach for building programmable IVT mRNA. As shown in (A), a known 3'UTR is incorporated into the IVT mRNA. Oligonucleotides bearing a Neutravidin are designed to be complementary to the 3' UTR. Biotinylated agonists are incubated with the targeting oligonucleotides, which are annealed to the IVT mRNA. (B) Shows that immunostimulatory IVT mRNA can be constructed to contain multiple types of agonists, as well as to contain varying amounts of agonists.

4.2 Materials and Methods

4.2.1 Preparation of Neutravidin-labeled targeting oligonucleotides

Four 2'O-Methyl RNA/DNA chimeric oligonucleotides targeting the 3' UTR of the ovalbumin IVT mRNA were designed and purchased from Biosearch Technologies. The sequence of each oligonucleotide is:

1.) $TTTTTTT^{MO}G^{MO}C^{MO}A^{MO}A^{MO}G^{MO}C^{MO}C^{MO}C^{MO}C^{MO}G^{MO}C^{MO}A^{MO}G^{MO}A^{MO}A^{MO}G^{MO}G$

2.) $TTTATTT^{MO}A^{MO}G^{MO}A^{MO}G^{MO}A^{MO}A^{MO}G^{MO}A^{MO}A^{MO}G^{MO}G^{MO}G^{MO}C^{MO}A^{MO}U^{MO}G^{MO}G$

3.) TTTTTTA^{MO}C^{MO}C^{MO}A^{MO}A^{MO}G^{MO}A^{MO}G^{MO}G^{MO}U^{MO}A^{MO}C^{MO}A^{MO}G^{MO}G^{MO}U^{MO}G^{MO}C

4.) TTTTTTT^{MO}C^{MO}U^{MO}A^{MO}C^{MO}U^{MO}C^{MO}A^{MO}G^{MO}G^{MO}C^{MO}U^{MO}U^{MO}U^{MO}A^{MO}U^{MO}U^{MO}C

where ^{MO} indicates a 2'O-methyl RNA linkage

Each oligonucleotide contained a disulfide C6 5' modification. Neutravidin was bound to the 5' end of each using Solulink chemistry as follows. The disulfide was reduced by incubation with TCEP (5mM) (Thermo Fisher Scientific). Reducing agent was removed by repeated dilution in PBS and centrifugal filtration (3kDa MWCO, Millipore). Oligonucleotides were then incubated overnight with 20 µg of Maleimide HyNic (Solulink) along with 0.3 mM ethylenediaminetetraacetic acid (EDTA). The following day, Neutravidin was labeled with succinimidyl-4-formylbenzamide (S4-FB). 500 µg Neutravidin was incubated with 20 µg of SF-FB in Solulink's modification buffer for 2 hours at room temperature. Neutravidin was then buffer exchanged into Soulink's conjugation buffer with centrifugal filtration (30kDA MWCO, Millipore). The modified oligonucleotides were individually buffer exchanged into conjugation buffer with centrifugal filtration (3kDA MWCO). Neutravidin and each oligonucleotide were then allowed to react by incubation for two hours at room temperature in a 2:1 oligonucleotide:Neutravidin molar ratio in the presence of 1x Turbolink catalyst (Solulink). Any unconjugated oligonucleotides were removed by centrifugal filtration (30kDA MWCO). Protein content in the remaining solution was determined by bicinchoninic acid assay (Pierce) against a Neutravidin standard curve. Nucleic acid content was determined by measuring the absorbance at 260nm using the Nanodrop 2000 (Thermo Scientific). Approximately a 1:1 molar ratio of Neutravidin:oligonucleotide was found for each targeting sequence.

4.2.2 Preparation of IVT mRNA

IVT mRNA was prepared according to the DNA template provided in the appendix. For cytoplasmic ovalbumin, the DNA template was modified from the PCL-neo-cOVA plasmid from Addgene (Plasmid #25097). The Kozak consensus sequence was modified from AATTCATGG to the more common CCACCATGG. The 3' UTR from murine alpha globin was also inserted into the DNA template. Prior to transcription, the DNA template was amplified using the Q5 high-fidelity DNA polymerase (New England Biolabs). The PCR product was purified, digested with the restriction enzyme NOTI to create a 5' overhang, and then purified again. The QIAquick PCR Purification spin column (QIAGEN) was used to purify the DNA template. The T7 mScript Standard mRNA Production System was used to generate mRNA (Cellscript), add a Cap-1 structure, and enzymatically add a poly(A) tail. The manufacturer's instruction were followed; however, the RNeasy mini kit (QIAGEN) was used to purify IVT mRNA when necessary. To incorporate modified bases, ribonucleotide cocktails were prepared of 25mM of each base. Pseudouridine-5'-Triphosphate, 5-Methylcytidine-5'-Triphosphate, and N1-Methylpseudouridine-5'-Triphosphate were purchased from TriLink Biotechnologies; adenosine triphosphate, guanosine triphosphate were purchased from USB. Cytosine triphosphate was purchased from Affymetrix. Following, IVT mRNA was treated with Antarctic Phosphatase (New England Biolabs) for 30 min to remove residual 5′-triphosphates, and then cleaned up and quantified using the Nanodrop 2000 (Thermo Scientific).

4.2.3 Preparation of agonist tethered IVT mRNA

Biotin conjugated adjuvants were purchased: ODN 1826 Biotin, Pam2CSK4 Biotin, and CL264 Biotin were purchased from Invivogen. Biotinylated agonists were incubated with Neutravidin bound oligonucleotides individually at room temperature for 1

hour in PBS at a 1:5 molar ratio of Neutravidin to Biotinylated agonist. Unbound agonist was removed with centrifugal filtration (30kDA MWCO). To anneal the targeting sequence to IVT mRNA, IVT mRNA was first melted at 75C for 5 minutes to remove the secondary structure, and then immediately placed on ice. Each Neutravidin targeting probe was incubated with IVT mRNA at a 1:1 molar ratio for approximately 12 hours at 37C. To remove unbound targeting oligonucleotides, IVT mRNA was filtered through a 200 kDA filter (Advantec), concentrated using a 30 kDA centrifugal filter, and then quantified by measuring the absorbance at 260 nm. To confirm removal of unbound adjuvant, a mock reaction control was used where an equivalent amount of Neutravidin targeting probe-biotin-adjuvant complex was incubated overnight without IVT mRNA. The sample was purified using a 200 kDA filter. Cells were treated with the mock reaction mixed with an appropriate amount of IVT mRNA using Lipofectamine 2000.

4.2.4 Characterization of Binding Percentage

The amount of CL264 bound to IVT mRNA was approximated by substituting biotinylated Atto 565 for the adjuvant molecule as discussed in sections 4.2.2 and 4.2.3. Following purification, the fluorescence and 260 absorbance was measured of the fluorescently labeled IVT mRNA. IVT mRNA fluorescence was compared to a standard curve of Atto 565 dye to determine the ratio of dye bound to IVT mRNA.

4.2.5 Cell Lines and IVT mRNA transfection

The RAW264.7 mouse macrophage cell line (ATCC TIB-71) and HeLa human epithelial cells (ATCC CCL-2) were maintained in High Glucose Dulbecco's Modified Eagle's Medium (DMEM) (Lonza) with 10% FBS (Hyclone) and 100 U/ml penicillin and streptomycin (Invitrogen). Approximately 60,000 cells were seeded in a 24 well plate the

evening prior to stimulation. Cells were transfected with the indicated treatment using Lipofectamine 2000 (Invitrogen) according to the manufacturer's protocol.

4.2.6 *In vitro* stimulation and qRT-PCR

Cells were treated as mentioned in section 4.2.5. Six hours following transfection, total RNA was collected with the QIAGEN RNeasy, which used an on-column DNAse treatment. RNA was quantified by absorbance at 260 nm and converted to cDNA using the RT2 First Strand kit (SA Biosciences). qRT-PCR was performed using the StepOnePlus real-time PCR system (Applied Biosciences) using 15ng of cDNA and SYBR green master mix (SA Biosciences), which was used according to manufacturer's directions. Gene-specific primers for ACTB, IFNβ-1, and IL-1β and IL-6 were designed by and purchased from Fluidigm. Fold changes and 95% confidence intervals were calculated using the ddCT method on StepOne software in reference to ACTB. Significant differences were determined by an ANOVA followed by Tukey-Kramer's post analysis. Each experiment was independently repeated at least two times.

4.2.7 Flow cytometry of protein expression

Cells were treated as mentioned in section 4.2.5. At the indicated time point, cells were lifted from cell culture plastic using Versene solution (Thermo Fisher Scientific) and then washed in PBS + 2% FBS, fixed with 4% paraformaldehyde for 10 minutes, washed two times with PBS + 2% FBS, and then permeabilized with 0.2% triton X 100 in PBS. Cells were then stained for transgene expression using an anti-ovalbumin FITC (Abcam) diluted 1:50 in PBS with 2% FBS and 0.1% triton X 100 for 30 minutes at 4C. Cells were then washed two times with PBS + 2% FBS and 0.1% triton X 100 and then analyzed using the BD Accuri C6 Cytometer. Samples were gated to remove debris and doublets and then gated to demarcate the $FITC^+$ population.

4.2.8 Mouse Injection

Female BALB/c mice (Charles River, Wilmington, MA) were anesthetized with 2.5% isoflurane and then injected in the anterior tibialis with 40µl of indicated treatment (10 µg of IVT mRNA and/or 3.14 ng CL264) diluted in RiLa using a 29-gauge needle. Mice were housed and manipulated under specific-pathogen-free conditions in the animal care facilities of Georgia Institute of Technology. All experiments were in accordance with the Institutional Animal Care and Use Committee.

4.2.9 RT-qPCR on mouse muscle tissue

IVT mRNA was injected into the anterior tibialis muscle. Five hours later, the muscle was removed and stored in RNAlater (Thermo Fisher Scientific) overnight at 4C. The following day, tissue was homogenized using the Bullet Blender and Navy RNAse free Stainless Steel Beads (Next Advance) in the presence of 1ml of Trizol (Thermo Fisher Scientific). The samples were extracted with chloroform and then bound to an RNEasy column (QIAGEN) following the addition of an equivalent volume of ethanol. The samples were further purified according to the RNEasy kit's instructions, which included an on-column DNAse digestion. RNA content was determined by A260 absorbance using the Nanodrop 2000, (Thermo Fisher) and quality was checked using RNA gel electrophoresis. Extracted RNA (1 µg) was converted to cDNA using the RT^2 PreAMP pathway primer mix (QIAGEN) according to the manufacturer's directions. qPCR was conducted using the Fluidigm system and the mouse antiviral response PCR primer array (QIAGEN) according to the manufacturer's directions with technical duplicates. Five mice were analyzed per treatment condition. QIAGEN's online data analysis center was used for data analysis. Statistical significance was based on a Student's t-test of the replicate $2^{-\Delta CT}$ values for each gene in the control group and treatment groups. The reference genes Gusb, Gapdh, Hsp90ab1, and ActB were used

to normalize expression. Heat maps for gene expression were generated in JMP using the multivariate clustering tool.

4.3 Results

4.3.1 Effects of modified base substitution in IVT mRNA

It was established in Chapter 2 of the thesis that incorporation of modified bases can reduce the self-adjuvant properties of IVT mRNA. Pseudouridine (Ψ) and N1-Methylpseudouridine (M1Y) have both been identified as modified bases that reduce the interferon responses to IVT mRNA. We compared how incorporation of each of these bases in ovalbumin-encoding IVT mRNA affected immunostimulation as well as ovalbumin protein levels.

To do this, RAW 264.7 macrophages were transfected using Lipofectamine 2000 with ovalbumin mRNA either composed of unmodified bases or substituting Ψ or M1Y for uridine. Five hours after transfection, total RNA was collected from the cells, and gene expression was analyzed using a mouse antiviral PCR array, as shown in Figure 4.3. The greatest amount of antiviral responses were detected in response to IVT mRNA composed of unmodified bases followed by IVT mRNA substituting pseudouridine, and then IVT mRNA substituting M1Y. Flow cytometry was used to assess ovalbumin protein expression following transfection. As shown in Figure 4.4, substitution of M1Y leads to an increased percentage of transfected cells, as well as an increased intensity of ovalbumin staining for the cells that were transfected.

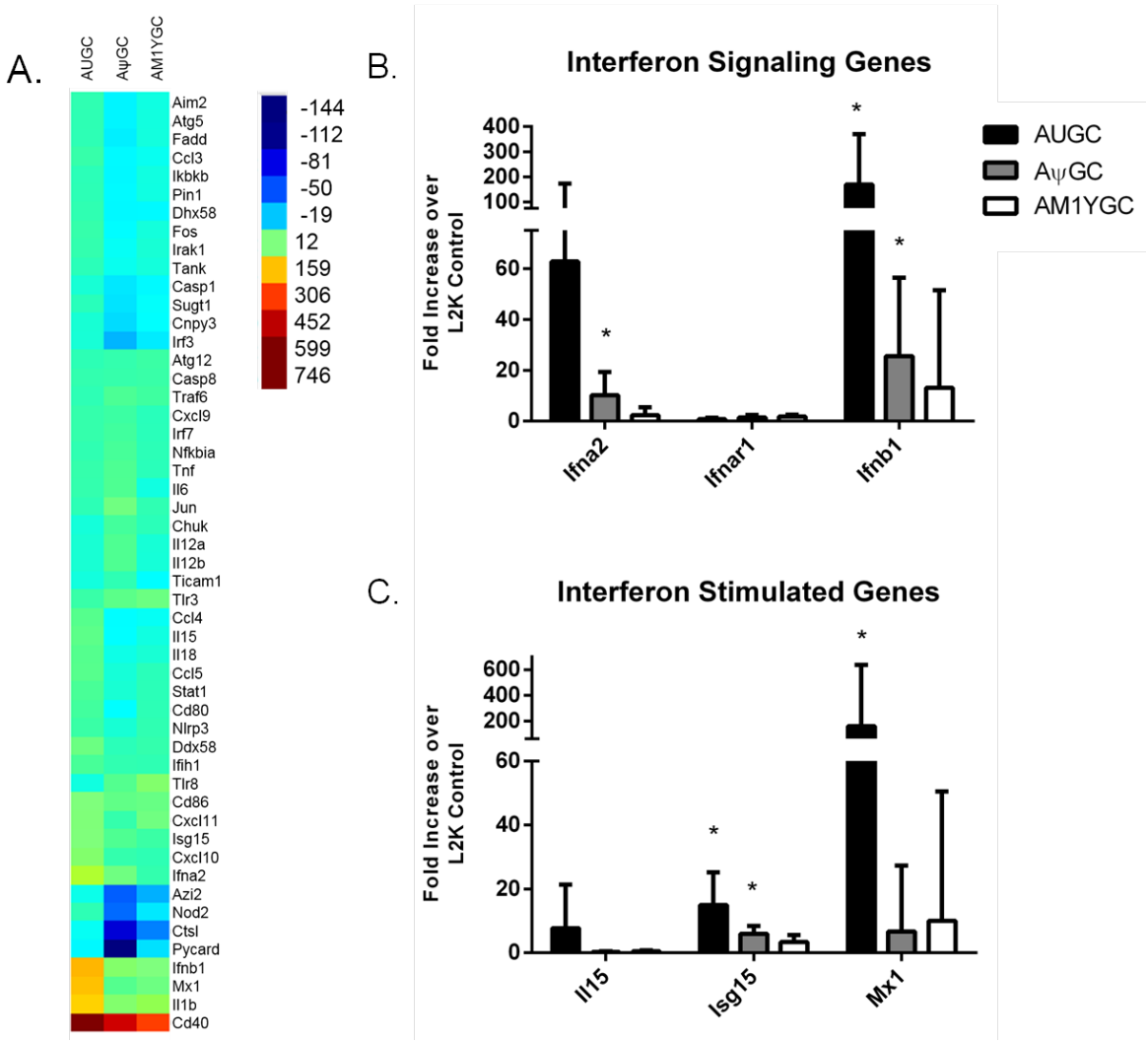

Figure 4.3 Gene expression of RAW264.7 cells following transfection with ovalbumin IVT mRNA incorporation the modified base pseudouridine or M1Y. (A) Heat map of gene expression relative to cells treated with Lipofectamine only (L2K control). (B). Fold increase of interferon alpha 2 (Ifna2), interferon alpha receptor 1 (Ifnar1), and interferon-beta 1 (Ifnb1) in response to transfection with IVT mRNA composed of the indicated nucleobases. (C) Fold increase of inerleukin-15 (Il15), Ubiquitin-Like Modifier (Isg15), and MX Dynamin-Like GTPase 1 (Mx1). 95% confidence intervals are shown. * indicates significantly different from L2K control.

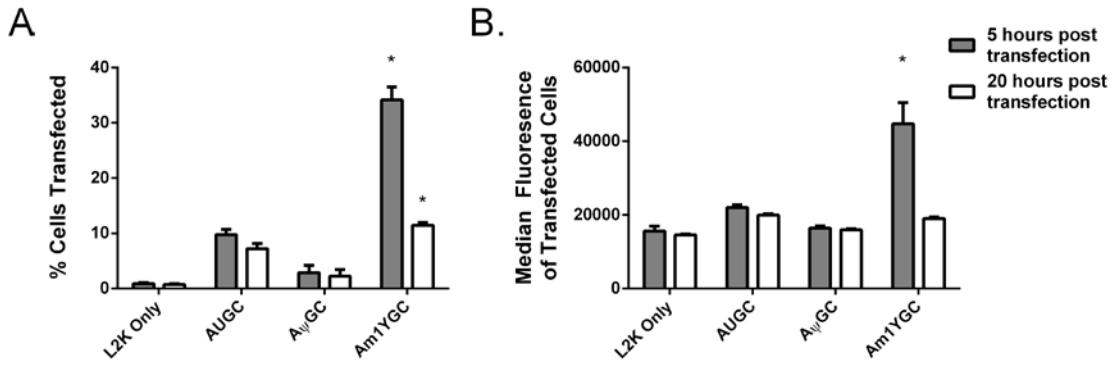

Figure 4.4 Effect of modified base incorporation on IVT mRNA protein expression. RAW 264.7 cells were transfected with mRNA composed of the indicated bases. Five or 20 hours following transfection, cells were stained for ovalbumin protein content and analyzed with flow cytometry. As shown in (A), M1Y incorporation into IVT mRNA leads to a higher percentage of cells transfected. (B) Shows that M1Y incorporation also lead to an increased intensity of ovalbumin staining compared to other IVT mRNA constructs. Error bars show standard deviation across three groups. * Indicated significantly different from all other groups for the given time condition ($p<0.05$, Tukey's test).

4.3.2 Adjuvants tethered to IVT mRNA affect innate immune stimulation

We next investigated the efficiency of biotinylated molecules to be tethered to IVT mRNA of different chemistries. Neutravidin bound oligonucleotides targeting the 3' UTR of the IVT mRNA were prepared. Following, a biotinylated fluorescent dye was incubated with the oligonucleotides in place of an immunostimulatory molecule. The now fluorescently labeled oligonucleotides were allowed to anneal to the IVT mRNA overnight. The sample was purified using filtration (200,000 MWCO), and then the overall fluorescence and 260 absorbance of the sample were determined. We found that approximately 3-4 fluorescent molecules were bound to an IVT mRNA on average and that RNA chemistry did not significantly affect binding.

IVT bearing the TLR7 adjuvant CL264 was then prepared. RAW264.7 macrophages were transfected with IVT mRNA with CL264 delivered tethered to the IVT

mRNA or as a cocktail solution. As a control for any error in purification techniques, a mock reaction control was also prepared. Here, the procedure for preparing CL264 tethered IVT mRNA was followed; however, IVT mRNA was omitted from the preparation. The resulting solution was then mixed with IVT mRNA prior to cell transfection. We also prepared a cocktail solution of IVT mRNA and CL264 adjuvant, which were also delivered with Lipofectamine-2000. Five hours following transfection, cellular mRNA was collected and analyzed using RT-qPCR. Figure 4.5 shows IFNβ1 and IL-1β cytokine levels following transfection. Tethering CL264 agonist to IVT mRNA yields increased cellular immune responses.

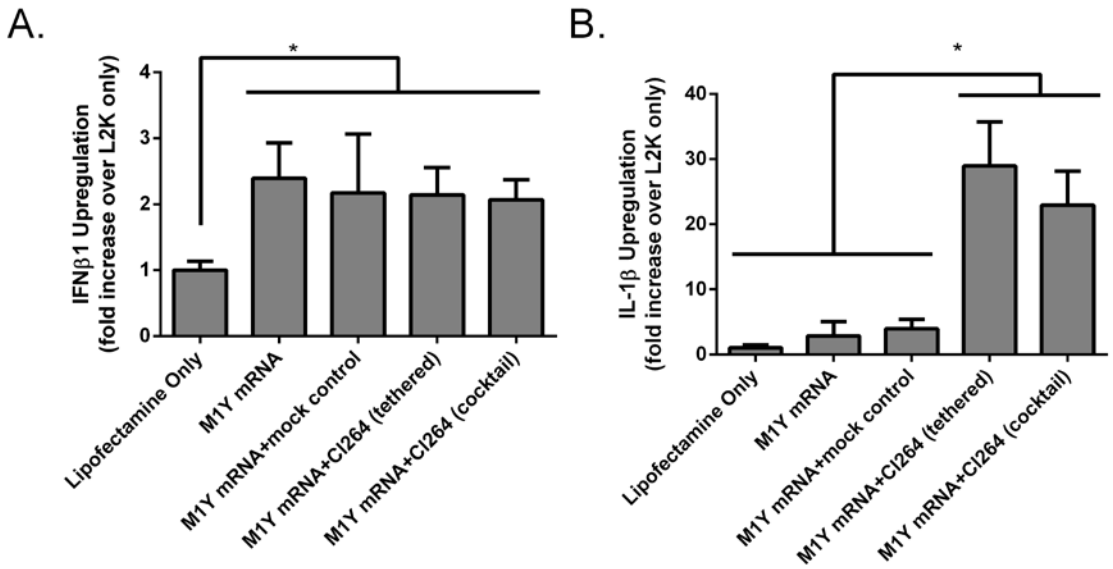

Figure 4.5 Effect of tethering the TLR7 adjuvant CL264 to IVT mRNA. RAW264.7 cells were transfected with ovalbumin IVT mRNA using Lipofectamine 2000. Five hours later, cellular responses were assayed using RT-qPCR. Where (A) shows that IFNβ1 are moderately increased where cells are transfected with ovalbumin IVT mRNA, (B) shows that IL-1β are significantly increased where IVT mRNA bearing CL264 is transfected compared to IVT mRNA alone. Fold change calculated in reference to β-Actin. Error bars show 95% confidence intervals. * Indicates significantly different ($p<0.05$, Tukey's test).

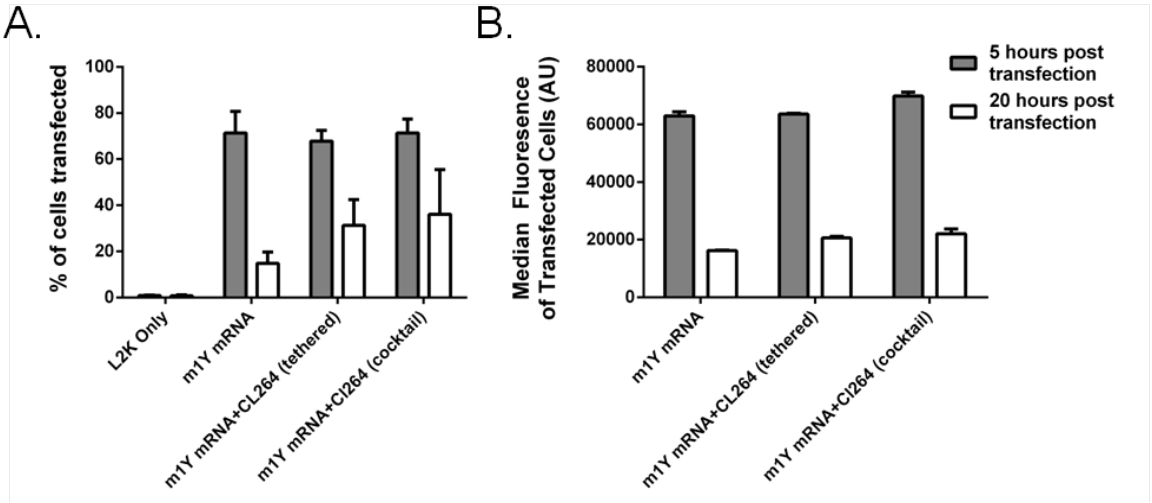

Figure 4.6. Protein expression of IVT mRNA delivered with and without tethered agonist. RAW 264.7 cells were transfected with ovalbumin M1Y mRNA alone or with the CL264 adjuvant. Five or 20 hours following transfection, cells were stained for ovalbumin protein content and analyzed with flow cytometry. As shown in (A), IVT mRNA co-delivery with CL264 leads to a higher percentage of cells transfected. (B) Shows that M1Y incorporation also lead to an increased intensity of ovalbumin staining compared to other IVT mRNA constructs. Error bars show standard deviation across three groups.

It is important that tethering an adjuvant to IVT mRNA still allows for protein translation. To assess if tethering an adjuvant to IVT mRNA affects protein expression, RAW264.7 cells were transfected with IVT mRNA with or without tethered adjuvant, and then protein content was assessed with flow cytometry. Figure 4.6 shows that tethering an adjuvant to IVT mRNA does not appreciably affect transgene production. While the result is not statistically significant, there is a noticeable trend that CL264 co-delivery leads to increased protein production.

We also compared how the incorporation of modified bases may affect cellular responses in response to CL264 tethered IVT mRNA. Figure 4.7 shows IVT mRNA composed of all unmodified bases, or the modified bases pseudouridine or m1Y. While unmodified mRNA leads to increased Il-1βresponses compared to m1Y mRNA, the difference is dramatically increased when CL264 is tethered to the mRNA. This

suggests that there may be some synergistic innate immune responses to unmodified mRNA with tethered Cl264.

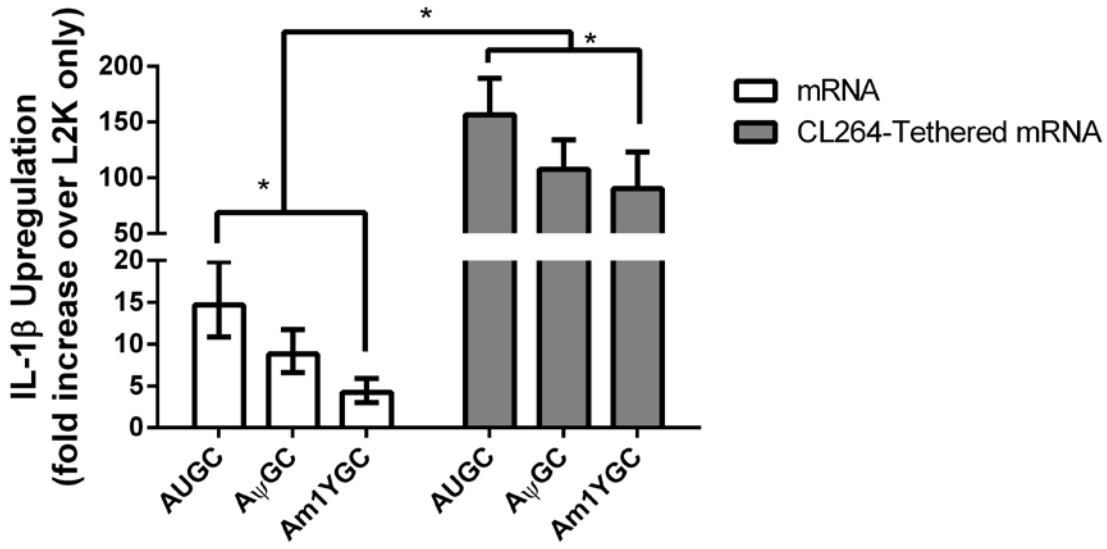

Figure 4.7. Effect of modified bases on immune response to CL264-tethered IVT mRNA. Fold change calculated in reference to β-Actin. Error bars show 95% confidence intervals. * Indicates significantly different ($p<0.05$, Tukey's test).

4.3.3 Tethering the cell membrane TLR2 adjuvant PAM2CSK4 to IVT mRNA

Studies in Chapter 3 of this thesis, as well as other studies done in the Santangelo lab, show that a significant portion of IVT mRNA is trapped inside cellular endosomal compartments. As TLR7 is active in the endosome, tethering CL264 to IVT mRNA is likely to interact with TLR7. We wanted to assess if tethering an adjuvant that is recognized by a membrane-bound PRR would also be functional. To do so, the TLR2 adjuvant PAM2CSK was tethered to IVT mRNA and then transfected into cells. Figure 4.8 shows that this adjuvant is indeed able to interact with its receptor when tethered to

IVT mRNA. Interestingly, when the adjuvant seems to be more active when it is tethered to IVT mRNA, than when it is delivered as a cocktail.

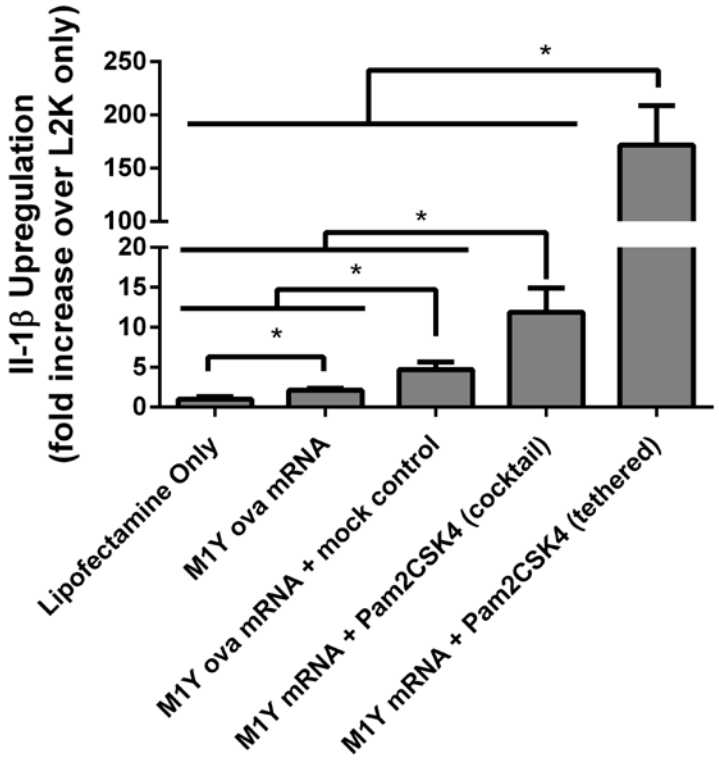

Figure 4.8. Effect of tethering the TLR2 adjuvant Pam2CSK4 to IVT mRNA. Fold change calculated in reference to β-Actin. Error bars show 95% confidence intervals. * Indicates significantly different ($p<0.05$, Tukey's test).

4.3.4 Effects of tethering agonist to IVT mRNA vs cocktail delivery following intramuscular injection

We next wanted to assess the functionality of our IVT mRNA construct following injection *in vivo*. We hypothesized that agonist tethered IVT mRNA would lead to stronger antiviral immune responses in the muscle compared to a cocktail of IVT mRNA and the agonist following injection. To test this hypothesis, M1Y modified IVT mRNA

was injected intramuscularly either tethered TLR7 agonist (CL264) or the TLR7 agonist delivered with mRNA as a cocktail. M1Y mRNA and CL264 each injected alone were also used as controls. Five hours following injection, the muscle was removed and processed for analysis via a mouse antiviral PCR array. Genes included in the PCR array are shown in Table 4.1.

Table 4.1 Genes assessed with PCR assay

Toll-Like Receptor Signaling:
Receptors and Chaperones: Cnpy3, Ctsb, Ctsl, Ctss, Tlr3, Tlr7, Tlr8, Tlr9.
Downstream Signaling: Chuk (Ikka), Fos, Ikbkb, Irak1, Irf3, Irf5, Irf7, Jun, Map2k1 (Mek1), Map2k3 (Mek3), Map3k7 (Tak1), Mapk1 (Erk2), Mapk14 (p38 Mapk), Mapk3 (Erk1), Mapk8 (Jnk1), Myd88, Nfkb1, Nfkbia (Ikba/Mad3), Rela, Ripk1, Spp1, Tbk1, Ticam1 (Trif), Tnf, Traf3, Traf6.
Responsive Genes: Ccl3 (Mip-1a), Ccl4 (Mip-1b), Ccl5 (Rantes), Cd40 (Tnfrsf5), Cd80, Cd86, Cxcl10 (Inp10), Cxcl11 (I-TAC/IP-9), Cxcl9 (Mig), Ifna2, Ifnb1, Il12a, Il12b, Il15, Il1b, Il6.
Nod-Like Receptor Signaling:
Receptors and Signaling: Aim2, Card9, Casp1 (Ice), Hsp90aa1, Mefv, Nlrp3, Nod2, Oas2, Pstpip1, Pycard (Tms1/Asc), Sugt1, Tank, Tbkbp1.
Responsive Genes: Il1b, Il18.
RIG-I-Like Receptor Signaling:
Receptors and Chaperones: Cyld, Dak, Ddx58 (RIG-I), Dhx58 (Lgp2), Ifih1 (Mda5), Isg15 (G1p2), Trim25.
Downstream Signaling: Atg5, Atg12, Azi2, Casp8 (Flice), Chuk (Ikka), Ddx3x, Fadd, Ikbkb, Irf3, Irf7, Map3k1 (Mekk1), Map3k7 (Tak1), Mapk14 (p38 Mapk), Mapk8 (Jnk1), Mavs, Nfkb1, Nfkbia, Pin1, Rela, Ripk1, Tbk1, Tnf, Tradd, Traf3, Traf6.
Responsive Genes: Cxcl10 (Inp10), Ifna2, Ifnb1, Il12a, Il12b.
Type-I-Interferon Signaling and Response:
Signaling Pathway: Ifna2, Ifnar1, Ifnb1, Stat1.
Interferon-Stimulated Genes (ISGs): Il15, Isg15 (G1p2), Mx1, Tlr3.

A heat map of the gene expression is shown in Figure 4.9. Figure 4.10 shows gene expression following injection with CL264 alone and M1Y ovalbumin mRNA alone relative to the sham injection control. To understand how co-delivery of the TLR7 agonist CL264 affected the local environment, normalized expression of mRNA delivered with CL264 is plotted against normalized gene expression of following M1Y mRNA alone (Figure 4.11). We see that a cocktail delivery of IVT mRNA with Cl264 agonist leads to a modest change in gene expression compared to IVT mRNA delivered alone. When IVT mRNA is delivered with CL264 tethered, there are more pronounced changed in gene expression. In Figure 4.11, nearly all of the genes (except for NLRP3, Pstp1, and Mefv) that show more than a threefold regulation change over the M1y mRNA treatment group are involved in Toll-like receptor signaling. Expression levels for TLR responsive genes that show more than a threefold increase in Figure 4.11 are shown in Figure 4.12. Tethered delivery of mRNA and CL264 consistently shows greater changes in gene expression levels compared to cocktail delivery for these genes.

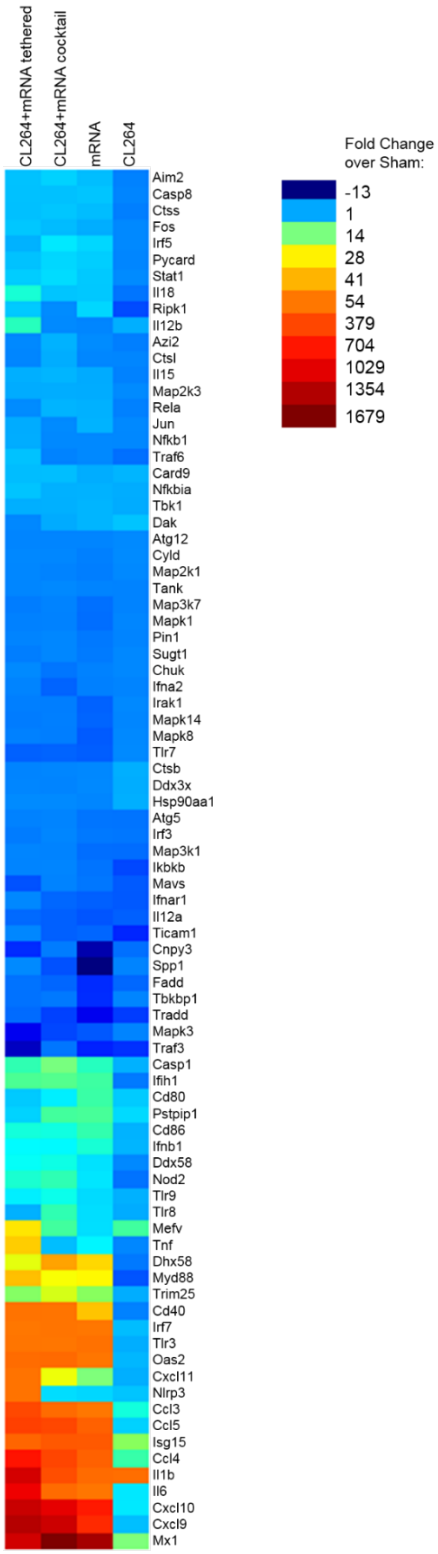

Figure 4.9. Heat map showing fold change of gene expression over a sham injection control in response to intramuscular injection with the indicated treatment. Five mice per group were injected intramuscularly in the anterior tibialis with the indicated treatment. Five hours following injection, the muscle was removed and analyzed for expression of the indicated genes.

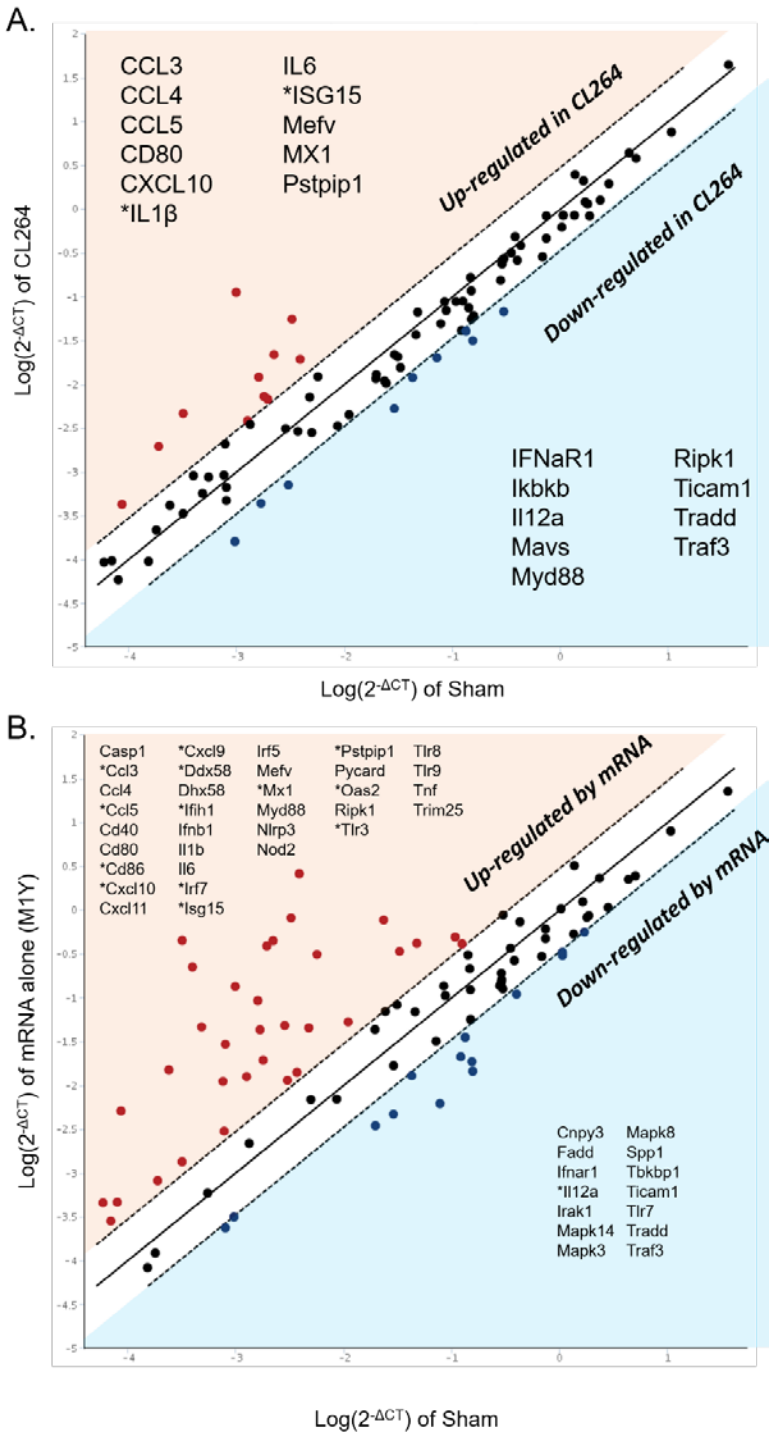

Figure 4.10. Gene expression in the muscle after injection with CL264 or IVT mRNA. (A) CL264 delivered alone and (B) M1Y mRNA delivered alone plotted against normalized expression of the sham injection control. Dashed lines indicate a fold regulation cut-off of 3. Genes listed indicate those that are 3-fold over or under expressed compared to the sham injection control. * indicates the difference in gene expression is statistically significant (student T's test, $p<0.05$).

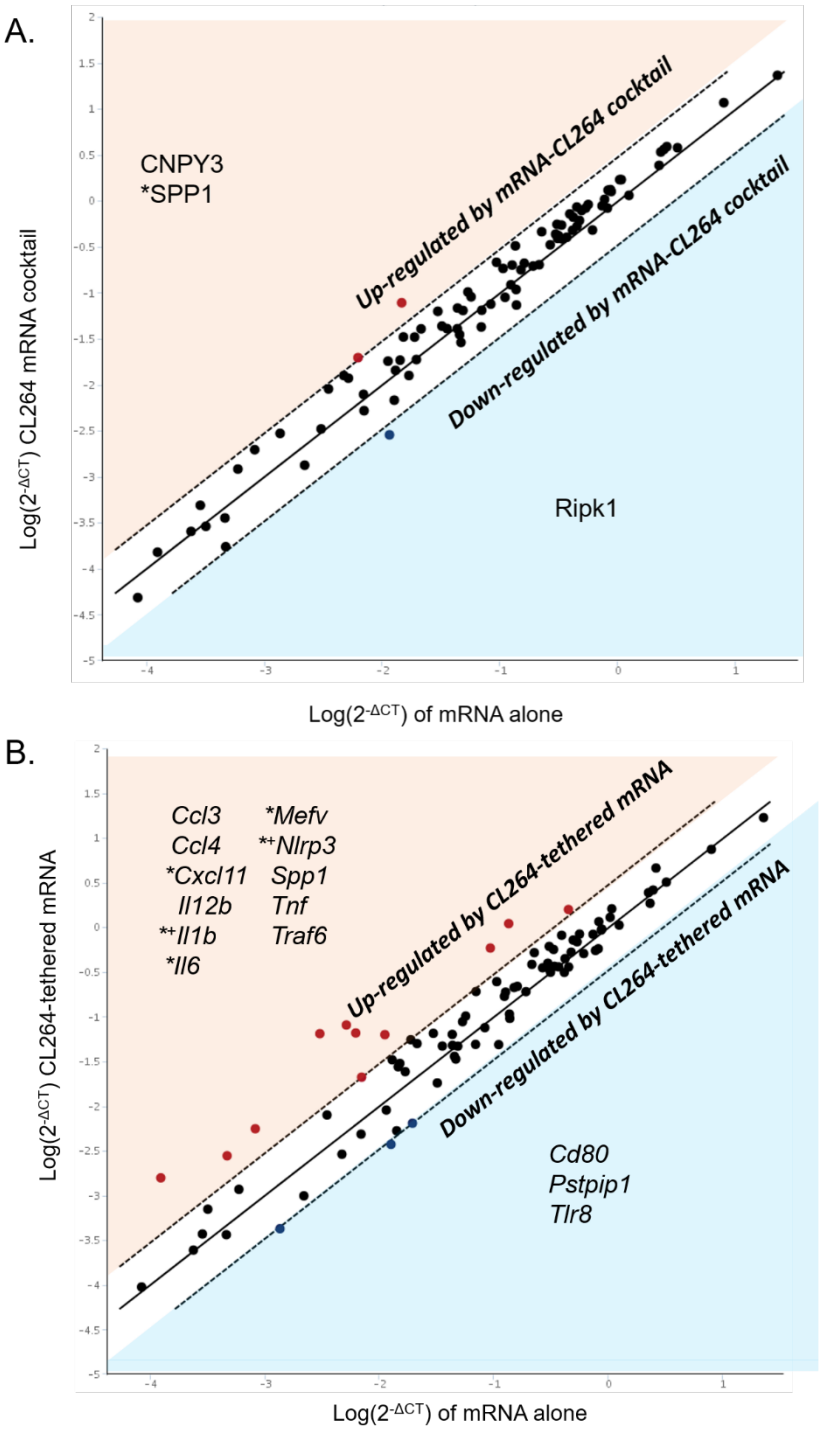

Figure 4.11. Gene expression after injection of IVT mRNA with CL264. (A) ovalbumin M1Y mRNA and CL264 delivered as a cocktail and (B) CL264 tethered to ovalbumin M1Y mRNA delivered against ovalbumin M1Y alone. Dashed lines indicate a fold regulation cut-off of 3. Genes listed indicate those that are 3-fold over or under expressed compared to the M1Y mRNA injection control. * indicates the difference in gene expression is statistically significant from M1Y mRNA only; $^{+}$ indicates gene expression is significantly different between Cl264 tethered to M1y mRNA compared CL264 delivered as a cocktail with mRNA (student t's test, $p<0.05$).

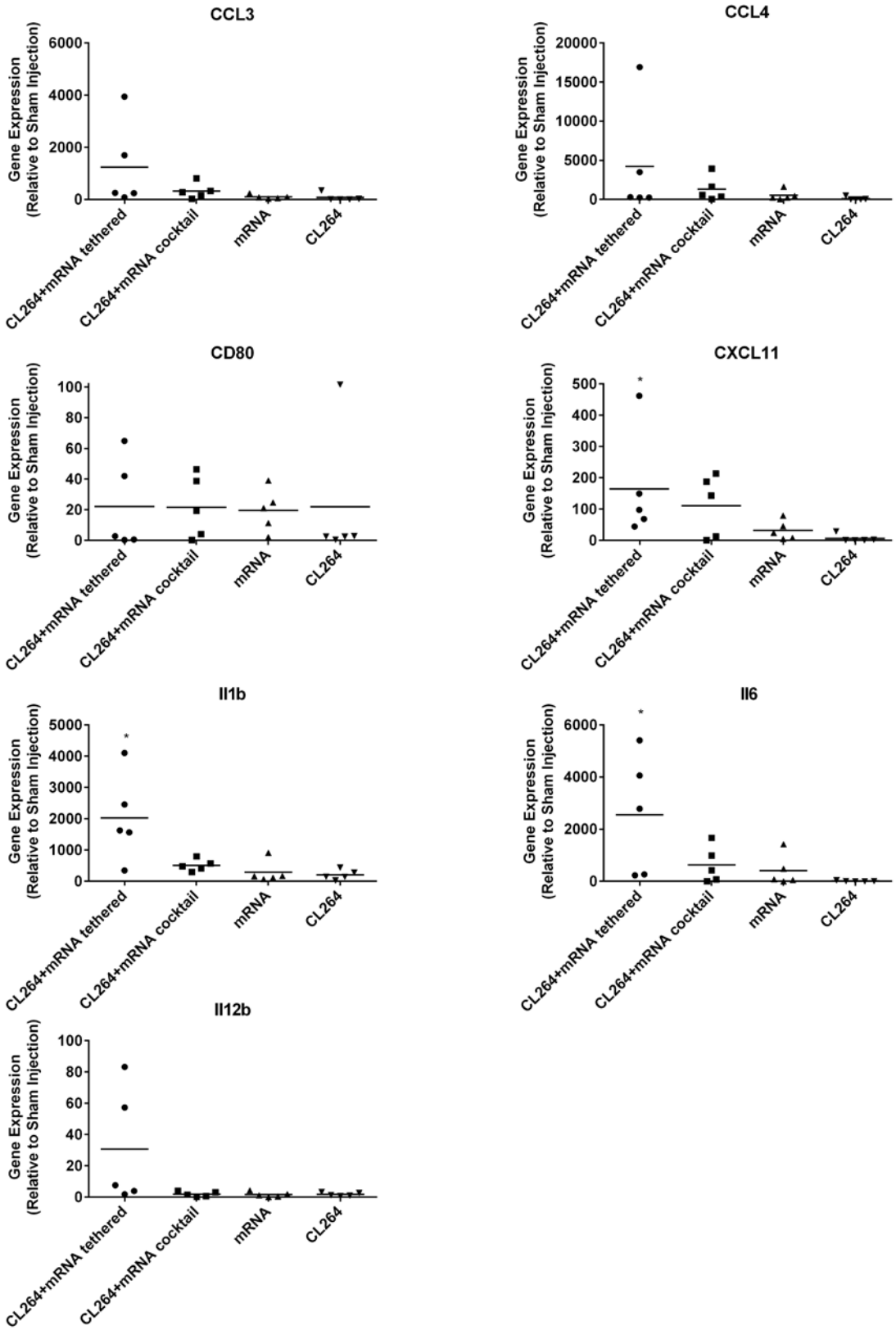

Figure 4.12 Gene expression of toll-like receptor responsive genes with more than a threefold increase in Figure 4.11. Each data point represents the expression levels from an individual animal.

4.4 Conclusion

This chapter outlines a methodology for the development of IVT mRNA with controllable adjuvant properties. Agonists targeting a variety of PRRs can be tethered to IVT mRNA to enhance its immunostimulatory properties. We showed that agonists tethered to IVT mRNA can functionally target either endosomal or cell membrane bound PRRs. The ability to target membrane bound receptors was tested using an adjuvant against TLR2. As shown in Figure 4.8, the tethered agonist condition leads to significantly increased cytokine responses compared to agonist delivered as a cocktail. This could possibly be because TLR2's activation is dependent upon dimer formation (165). Perhaps tethering TLR2 to IVT mRNA allowed for enhanced dimerization and thus activation.

This chapter also showed that upon i.m. injection, tethered IVT mRNA-agonist delivery enhances immune responses compared to cocktail delivery. We hypothesize that tethering the low molecular weight agonist to IVT mRNA enhances retention in the muscle and increases localization in the endosomal compartments. Previous studies have shown that imiquimod, another low molecular weight TLR7 agonist, is rapidly cleared following intramuscular injection. It has been shown to be ineffective as a co-delivered agonist for vaccination purposes (165).

This strategy enables comparisons between IVT mRNA vaccines that stimulate different PRRs. Further, this approach could also enable the delivery of other molecules that could affect IVT mRNA performance. Cell targeting peptides or cell penetrating peptides could be tethered to IVT mRNA to enhance intracellular uptake of IVT mRNA.

CHAPTER 5

PERSPECTIVES AND FUTURE DIRECTIONS

This thesis investigated innate immune responses to IVT mRNA and identified strategies to modulate these responses. Chapter 2 demonstrates that the substitution of modified bases in IVT mRNA alters the activation of antiviral sensors and also influences transgene protein expression in a gene-dependent manner. Chapter 3 identifies specific PRRs that interact with IVT mRNA. This chapter highlights the use of PLAs for studying PRR activation, further demonstrating that PRR activation could be modulated by nanoparticle-mediated delivery of IVT mRNA. Chapter 4 presents a strategy for tethering adjuvants to IVT mRNA, allowing for the controllable activation of PRRs. In this section, future directions for this work are discussed. The prospects for IVT mRNA vaccines and suggest general directions for future research and development.

5.1 Dendritic cell response to nucleic acid transfection

Other researchers have shown that modified bases, particularly 5mC and Ψ, reduce antiviral responses and increase transgene protein production of IVT mRNA (35). Chapter 2 illustrates that this observation does not hold true across all gene sequences. The protein expression of Ara h 2 IVT mRNA was higher when unmodified bases were incorporated but lower when 5mC and Ψ were used. On the contrary, transgene expression of ovalbumin IVT mRNA was higher when 5mC and Ψ were used but lower when composed of all unmodified bases.

This study presents multiple questions for future work:

- Can codon optimization be used to modulate the impact of modified bases on transgene protein production and antiviral responses?

- Do modified bases introduce codons that are difficult to translate (i.e., ineffective transfer RNA recognition of codon)?
- Is the secondary structure of 5mC/Ψ IVT mRNA altered such that protein translation is affected?
- Do modified bases in IVT mRNA affect PRR recognition in a sequence dependent manner?
- Do modified bases selectively impact transgene expression of secreted (e.g., Ara h 2) versus cytoplasmic proteins (e.g., ovalbumin)?

This chapter also compares the ability of IVT mRNA and plasmid DNA to induce BMDC maturation. IVT mRNA is largely regarded as more immunostimulatory than plasmid DNA, yet plasmid DNA induced BMDC maturation events and IVT mRNA did not. Chapter 2 explores the maturation of dendritic cells *in vitro*, thus presenting a limited picture of the actual immunostimulatory responses to each nucleic acid. Further, BMDCs are not fully representative of the complex phenotypes and characteristics of dendritic cells found *in vivo* (166). Moreover, dendritic cells are known to interact with a wide variety of cell types, which can influence their PRR expression levels, maturation, and other processes (167). *In vitro* studies do not account for these interactions, limiting implications of the findings. However, the study of BMDC maturation suggests an avenue to improve IVT mRNA vaccine design. IVT mRNA co-delivery with an adjuvant may enhance the development of adaptive immunity.

Surprisingly, $TLR7^{+}$and $TLR7^{-}$ cells had comparable NFKB responses to IVT mRNA transfection. This is interesting for several reasons. At least two other studies (65, 127) use the same cell line to find the opposite results. Also, our proximity ligation assays performed in Chapter 3 show that TLR7 is activated by IVT mRNA. Another study shows that IVT mRNA activates TLR7 in dendritic cells *only* when it is complexed

to protamine (68). Overall, there is substantial conflicting evidence on IVT mRNA activation of TLR7. One possible explanation is that TLR7 signal propagation is mediated by other factors. Perhaps a factor present in cell culture serum is required to enable TLR7 activation either by providing or upregulating a critical accessory molecule. Here, we are reminded of the extreme complexity of the innate immune system. Responses to pathogens are regulated on many different levels: multiple cell types, PRR, accessory proteins, and cytokines adjust each other's activity to develop a response. For example, TLR7, TLR8, and TLR9 all regulate each other's activity.(168, 169).

In light of this, we hypothesized that cell culture systems may not be appropriate for studying PRR activity. Moreover, knock-in and knock-out systems have the capacity to skew results. Therefore, we were motivated to develop a method that would allow for assessing PRR activity *in vivo* without perturbing the expression level of PRRs. These methods and their findings are described in Chapter 3.

5.2 In situ analysis of mRNA vaccine

In this chapter, we demonstrated the use of proximity ligation assays for detecting specific PRR activation. Using PLAs, we showed that cholk nanoparticle-mediated delivery of IVT mRNA affected PRR activation. The nanoparticle formulation reduced TLR7 and enhanced RIG-I and MDA5 activation. We also showed that nanoparticle-mediated delivery enhanced infiltration of immune cells to the injection site. We hypothesize this is due to increasing the size of IVT mRNA (by delivering it in a 300 nm particle), which enhanced its retention in the muscle. Thus, nanoparticle-mediated delivery led to a more localized distribution of IVT mRNA in the muscle. This may have enhanced infiltration of immune cells to the injection site.

PLA detection of PRR activation is a unique tool for probing innate immune responses. This technique is especially powerful for studying PRR activation when multiple receptors are expected to simultaneously be activated. While animal or cell systems that up or down regulate receptor levels are important to assess functional contributions of a PRR to the developed immune responses, they can mask the importance of other contributing PRRs that act in concert with the receptor being investigated. As researchers continue to explore strategies to modulate innate immune responses to IVT mRNA and other vaccines, PLAs offer insight on the impact these strategies have on PRR activation. This technique of innate immune surveillance may enable more understanding of IVT mRNA's interaction with innate immunity. Future work should use PLAs to determine how codon optimization and modified bases influence PRR activation. Also, can different genes expect to activate PRRs in the same way? Moreover, PLAs could be developed for studying IVT mRNA activation of other PRRs such as PKR and TLR3.

While we showed that nanoparticle-mediated delivery of IVT mRNA affected innate immune activation, adaptive immune responses were not investigated. Future work should focus on understanding how the nature of innate immune activation and transgene protein production by IVT mRNA affects the development of adaptive immune responses. Future directions could also focus on developing relationships between the measurement of the specific innate immune response elements presented in this chapter (such as immune cell infiltration to injection site, PRR activation, and lymph node trafficking) and adaptive immune responses. Could PRR activation levels, as detected through PLAs, be used as predictive measures of a vaccine’s success?

The data collected from PLAs for assessing PRR activation is limited in several regards. First, activity levels of two different PRRs cannot be compared, as antibody binding and proximity ligation are not always 100% efficient. Second, optimization of

assay conditions along with data collection and analysis are time consuming methods. Proximity ligation assays require several antibody binding and enzymatic steps that can be costly and time-consuming for a large number of samples. Analysis of the assay involves counting individual puncta per volume of tissue or per individual cell. This work was *highly* enabled by the use of an UltraVIEW spinning disk confocal microscope in the Santangelo lab. PLA analysis of tissue requires confocal microscopy with at least 40x magnification. As many images may be required to quantify PRR activity (at least 360 images were collected in this study for each PRR), the speed of image acquisition significantly impacts the ease of data collection. Researchers without access to imaging modalities with similar capabilities would face extreme handicap in collecting similar data sets. Efforts to develop a more high-throughput method for detecting PRR signaling complexes could enhance practicality of these experiments and facilitate future work. For example, developing methods for flow cytometric analysis would enable larger data sets to be analyzed.

5.3 IVT mRNA with programmable innate immune stimulation

This chapter outlines a strategy for directed control of innate immune responses by IVT mRNA. This work showed that PRR agonists tethered to IVT mRNA can activate PRRs without compromising IVT mRNA transgene protein production. Previously, researchers were only able to tune IVT mRNA characteristics by tweaking the molecule itself (e.g. substituting modified bases or altering the genetic sequence). This work enables altering IVT mRNA characteristics on a more significant scale to allow for more transformations of IVT mRNA's interaction with innate immunity.

Tethering adjuvants to IVT mRNA relies on the specific binding of a complementary oligonucleotide to IVT mRNA. Not every oligonucleotide binding site on the IVT mRNA was filled. While four oligonucleotides were designed to bind to each IVT

mRNA molecule, we found that on average, only one oligonucleotide molecule bearing 4 adjuvant molecules was bound to each IVT mRNA molecule. This technology could be improved through further research investigating the probe binding efficiency to IVT mRNA. Future directions could optimize probe sequence (length and binding region) as well as the spacing between oligonucleotide binding regions to enhance agonist tethering to IVT mRNA. Additionally, Neutravidin is conjugated to the oligonucleotide, and biotinylated agonists are bound to the Neutravidin. This protein complex may sterically interfere with oligonucleotide binding to IVT mRNA. Future work should investigate if an alternate conjugation strategy could improve binding.

Other molecules aside from PRR agonists could also be tethered to IVT mRNA. For example, ligands targeting certain cell types could direct entry into dendritic cells or liver cells. Additionally, molecules that affect transgene protein could also be tethered, such as translation factors. Moreover, cytokines, chemokines, or transcription factors could also be conjugated to IVT mRNA to modulate the immune responses.

Why should molecules be tethered to IVT mRNA, rather than delivered in a cocktail or combined in a nanoparticle formulation? Work presented in Chapter 4 shows how a TLR7 agonist to tethered IVT mRNA leads to more potent innate immune stimulation than cocktail delivery. Many PRR agonists are low molecular weight molecules that are quickly cleared from the muscle after injection (170, 171). Tethering these agonists to IVT mRNA molecules likely enhances their retention in the muscle. Moreover, when an endosomally active molecule such as CL264 is used, tethering it to IVT mRNA likely enhances its localization in endosomal compartments. When the extracellularly-active TLR2 agonist was bound to IVT mRNA, its activity was amplified compared to non-tethered delivery. This may be because this agonist dimerizes in order to activate TLR2. Thus, tethered adjuvant may have facilitated dimerization, enhancing activity.

As an alternative to tethered IVT mRNA delivery, nanoparticle-mediated delivery may also co-deliver adjuvant and IVT mRNA. Nanoparticle co-delivery may also enhance retention of adjuvants in the muscle by facilitating intracellular uptake and increasing the effective size of the adjuvant. As shown in Chapter 3, nanoparticle mediated delivery can also affect PRR activation of IVT mRNA and modulate other innate immune responses. However, while researched have developed a multitude of nanoparticle formulations to enhance nucleic acid delivery, it is unclear if nanoparticle-mediated delivery is advantageous over naked IVT mRNA delivery. Tethering adjuvants to IVT mRNA still allows for nanoparticle-mediated delivery, but does not rely on a technology that may be inessential. Thus, co-delivery of adjuvants by tethering them to IVT RNA allows for flexibility in vaccine design. This is notable, as IVT mRNA vaccines are in their infancy. Future directions should focus on determining what adjuvants are most useful for specific vaccine candidates.

5.4 Perspective

Several pre-clinical studies indicate that IVT mRNA could be an effective vaccination medium (20, 164, 172). While clinical success of IVT mRNA remains to be seen, there is significant design space to modulate the characteristics of IVT mRNA for a given application. This thesis identifies several design variables that modulate IVT mRNA characteristics and functionality. The impact of these strategies alludes to the sensitivity of PRR-ligand recognition, and unexplored possible strategies to further modulate innate immune responses to IVT mRNA.

Collectively, the design of IVT mRNA molecules affect both its characteristics and functionality. For example, two sequences encoding the same gene with different codon usage will have very different IVT mRNA characteristics. The secondary structures and nucleobase percentages will differ. As a result, the two sequences may

be recognized differently by PRRs. Codon usage and PRR activation also influence transgene protein expression. The full impact is unclear that a collective grouping of design criteria has on IVT mRNA characteristics. Future studies that focus on how these design criteria modulate characteristics and functionality would enable more thoughtful and rational design of IVT mRNA constructs.

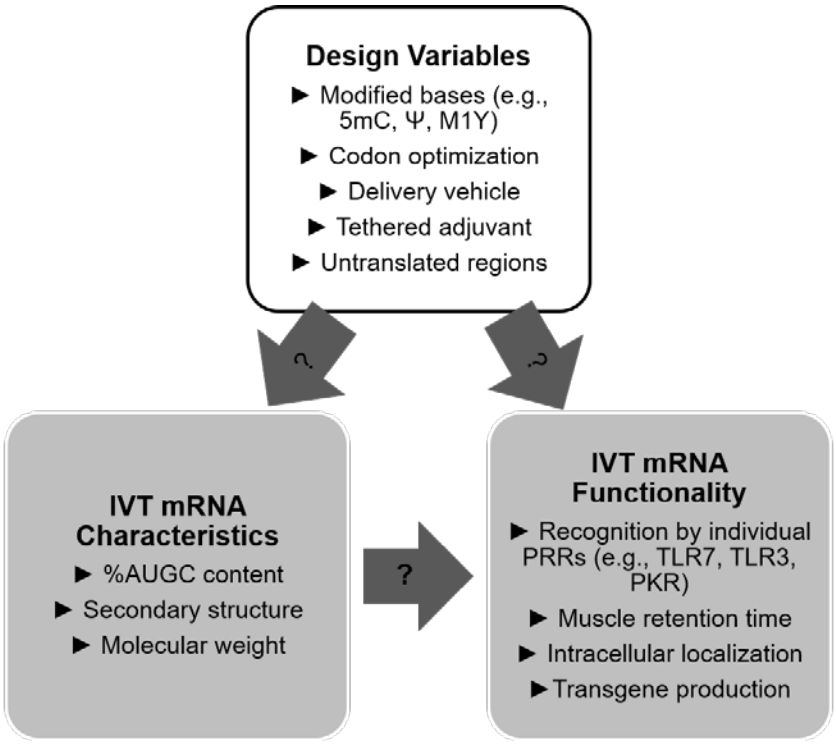

Figure 5.1. Design variables can modulate IVT mRNA characteristics and functionality. IVT mRNA design variables affect characteristics and functionality. The mechanisms regarding how consummate design criteria impact characteristics and functionality are unknown, a hurdle to rational design of IVT mRNA molecules.

Endogenous RNAs are nearly always exist in ribonucleoprotein complexes, likely reducing their interactions with antiviral PRRs. As IVT mRNA is delivered devoid of any bound proteins likely explains the activation of PRRs detecting cytoplasmic dsRNA. Strategies to shield recognition of IVT mRNA, either by reducing secondary structure through sequence engineering or alternative strategies could improve protein production. To mimic endogenous RNAs, small proteins or other molecules could be bound to IVT mRNA to reduce interactions with PRRs. In fact, modified bases are well-established to affect secondary structure of endogenous RNAs, and reduction of secondary structure could be the mechanism of modulating PRR recognition (72, 73).

Throughout this thesis work, as well as through other studies performed in the Santangelo lab, it is evident that IVT mRNA characteristics and functionality have sequence-to-sequence variation. As demonstrated in Chapter 2, substitution of modified bases enhance functionality of some sequences while impairing others. A systems-based approach to identify sequence design criteria, probing codon choice, gene characteristics, and substitution of modified bases would be warranted. This methodology could identify sequence motifs important for PRR activation or specific codons where modified bases impact translation rates.

One of the ultimate goals for IVT mRNA is the rapid manufacturing of vaccines in the case of an epidemic or other biological threats. To make progress toward this goal, future efforts could compare IVT mRNA vaccines with extant vaccines that are known to be effective. Very practical exercises could provide benchmarks for IVT mRNA performance. Important questions to answer include:

- What level of transgene antigenic protein is required?
- Do the kinetics of transgene antigenic protein production compare favorably to those in a vaccination?
- Does biodistribution vary between extant vaccines and IVT mRNA?

- Does biodistribution vary between extant vaccines and IVT mRNA of the antigenic protein?
- How do the characteristics (i.e., specific PRR activation, immune cell infiltration, lymph node uptake) of innate immunity differ?
- How do the characteristics of adaptive immunity differ?

To answer these questions, the innate immune responses to IVT mRNA vaccines could be compared to extant vaccines using PLAs, along with other methods, as described in Chapter 3. Based on the findings, IVT mRNA's interaction with the innate immune system could be engineered to mimic effective vaccines by tethering adjuvants or introducing modified bases described in Chapters 2 and 4.

Preclinical animal studies using DNA vaccines produced compelling evidence demonstrating their efficacy; however, clinical trials yielded surprisingly low immunological responses. While rodent models are practical for preliminary studies, there are significant limitations when translating the findings to humans that should be acknowledged. First, muscle sizes are different in rodents and humans, impacting retention time of i.m. delivered vaccine. The ratio of injection volume to muscle volume is also different in mouse models and humans, influencing vaccine retention time, entry into the lymphatics, systemic distribution, and localization of innate immune responses. Moreover, the innate immune systems differ between humans and mice, limiting the carryover of conclusions from mouse models (173). For instance, human and murine TL7 and TLR8 have variable specificity to certain ligands (136). Additionally, many inbred mouse strains have genetic abnormalities within the innate immune system that may augment or diminish innate immune responses (174, 175).

IVT mRNA is a unique tool for driving transient protein production. While this thesis focused on the production of antigenic protein for vaccination purposes, IVT mRNA can also be used for synthesis of therapeutic proteins. This approach would

enable faster, cost effective therapeutics compared to traditional protein manufacturing methods. Additionally, post-translational modifications of therapeutic proteins will be true-to-host, a nontrivial challenge for proteins manufactured in non-mammalian systems. Studying innate immune responses to IVT mRNA is important to further therapeutic applications. Activation of PKR and OAS-L, which impedes protein translation degrade intracellular RNAs respectively could dramatically impact transgene protein production and are significant hurdles to therapeutic applications.

APPENDIX A

STATISTICAL ANALYSIS OF PROXIMITY LIGATION ASSAYS

A.1. Statistical model to evaluate data from proximity ligation assays

Dr. Brani Vidakovic is acknowledged for his assistance and consultation for the work presented in Appendix A. The following describes the building of a statistical model to evaluate the data collected from the proximity ligation assays performed in Chapter 3. A model was built to fully match the experimental design and describe the data collected from each proximity ligation assay (PLA). The model is described as:

$y_{ijkl} = \mu + \alpha_i + \beta_j + (\alpha\beta)_{ij} + \gamma_{k(ij)} + \epsilon_{ijkl}$

Where:

y_{ijkl} = normally distributed data collected from MDA5, TLR7 or RIGI.
μ = mean of the data
α_i = contribution from treatment condition
β_j = contribution from time condition
$\alpha\beta_{ij}$ =contribution from any interaction between treatment and time condition
$\gamma_{k(ij)}$ = contribution from individual animal tested, nested in treatment and time
ϵ_{ijkl} = contributions from error
i = mRNA alone, mRNA+cholk, sham, isotype controls,
j = 1.5, 6, 16 hours
k = individual animal tested (1:4)
l = image taken (1:6)

We aimed to test the following hypotheses to determine if the treatment, time point, interaction between the treatment and time, and individual animal nested in treatment and time were significant factors in the data collected. These hypotheses are described as:

H_o: $\alpha_i = 0$
H_o: $\beta_j = 0$
H_o: $\gamma_{k(ij)} = 0$
H_o: $\alpha\beta_{ij} = 0$

A.2. Data from proximity ligation assays do not follow a normal distribution

The data were analyzed to determine if they followed normal distributions before performing an analysis of variance (ANOVA), which assumes a normal distributions of data. In the experimental design, this normality is expected from the model residuals. The residuals were calculated for each PLA experiment using MATLAB, and are presented in Figure A.1.

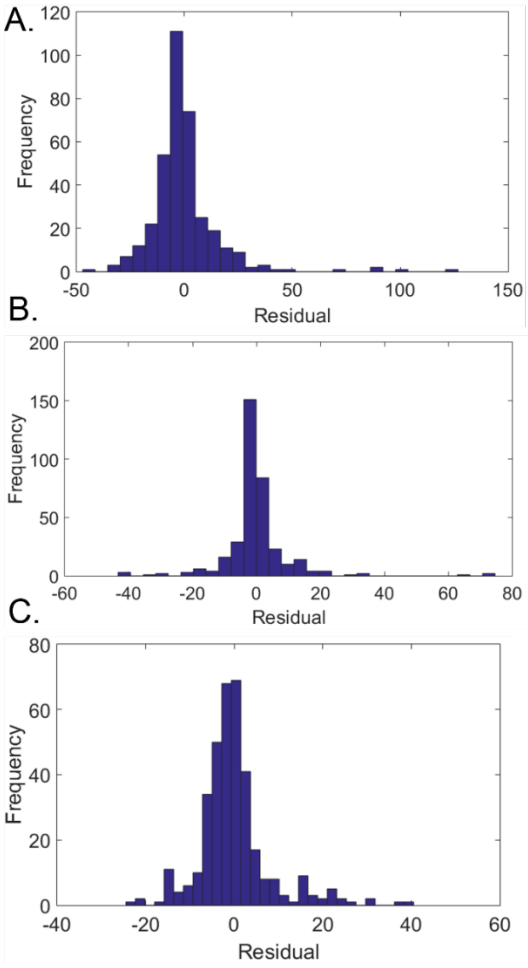

Figure A.1. Histograms of residuals from data of (A) TLR7, (B) MDA5, and (C) RIG-I PLAs. The ``fat'' tails and excessive kurtosis indicate that the distributions deviate from normality.

The residuals in Figure A.1 show a skewness to the right as well as a positive kurtosis reflecting a non-normal distribution. To further visualize if the data followed a normal distribution, q-q plots were formed (Figure A.2). The MATLAB function 'qqplot' was used to plot the empirical quantiles of the experimental data against the normal quantiles. A perfect normal distribution would show the blue data points collapsing on the red dotted line; however, the data shows an 'S' shape, which is the evidence that the experimental data does not conform to normality. Together, the q-q plots and residual plots shown in Figures A.1 and A.2 show that the distribution of the residuals is right skewed, heavy tailed, and with a positive kurtosis.

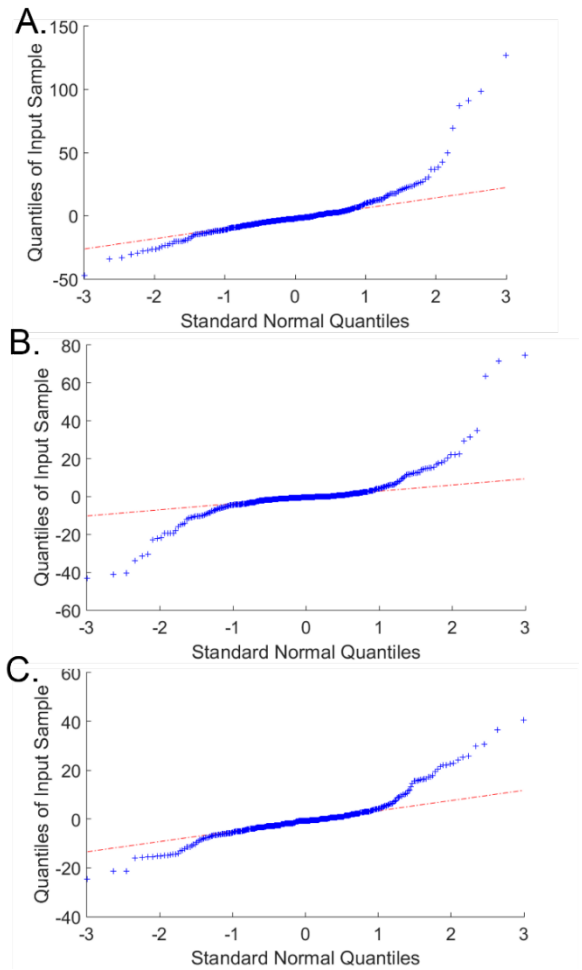

Figure A.2. q-q plots from data from (A) TLR7, (B) MDA5, and (C) RIG-I proximity ligation assays.

A.3. Transformation of proximity ligation data to meet normal distribution

To determine how well the data could be transformed to normality, we tested transforming the data points by raising to the exponent ‘q’, where q varied in steps of 0.01 from 0.01 to 0.5. The Jarque-Bera statistic (JB) was calculated for each q value as a measure of discrepancy from normality. The JB statistic describes how well experimental data fits skewness and kurtosis, two important aspects of the normal distribution. JB is defined as:

$$JB = \frac{n}{6}(S^2 + \frac{(C-3)^2}{4})$$

Where:

n is the sample size,
S is the sample skewness,
C is the sample kurtosis.

S and C were calculated by MATLAB's statistical toolbox using 'skewness' and 'kurtosis' commands. Figure A.3 shows the JB statistic calculated for each q value for each PLA. We see that the JB statistic reaches a value very close to zero approximately where q = 0.28 for TLR7, q= 0.33 for MDA5 and q= 0.35 for RIG-I.

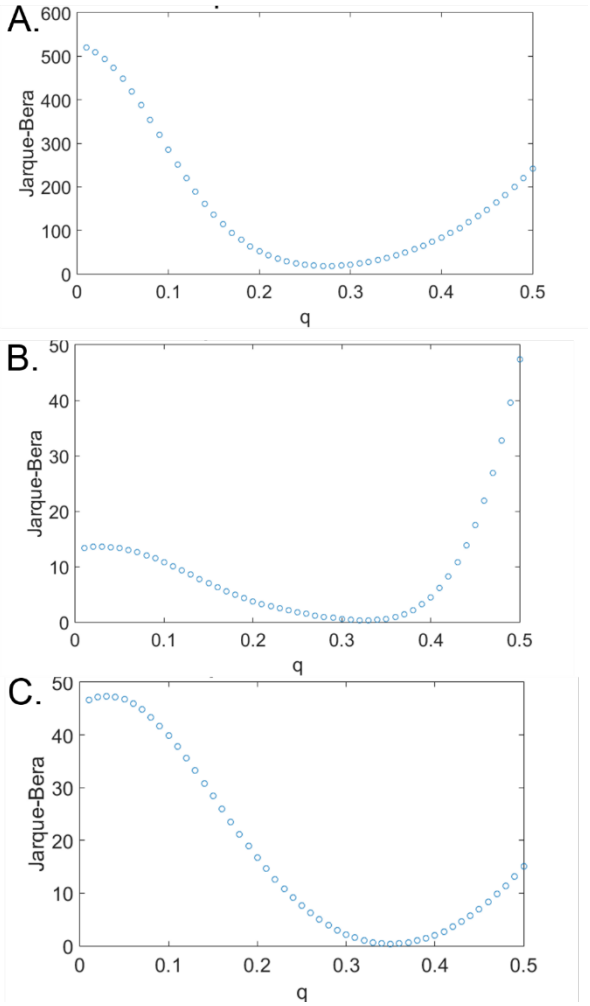

Figure A.3. Calculated JB statistic for each q value from PLAs for (A) TLR7 (B) MDA5 and (C) RIG-I.

To treat all of the collected data equally, we took the cubed root of the collected data points for each PRR PLA. Residual plots and q-qplots were generated on the transformed data to qualitatively determine if they followed normal distributions. Residuals plots and q-qplots are shown in Figures A.4 and A.5, respectively. The Jarques-Bera test was also performed on the transformed data to test if it followed a normal distribution.

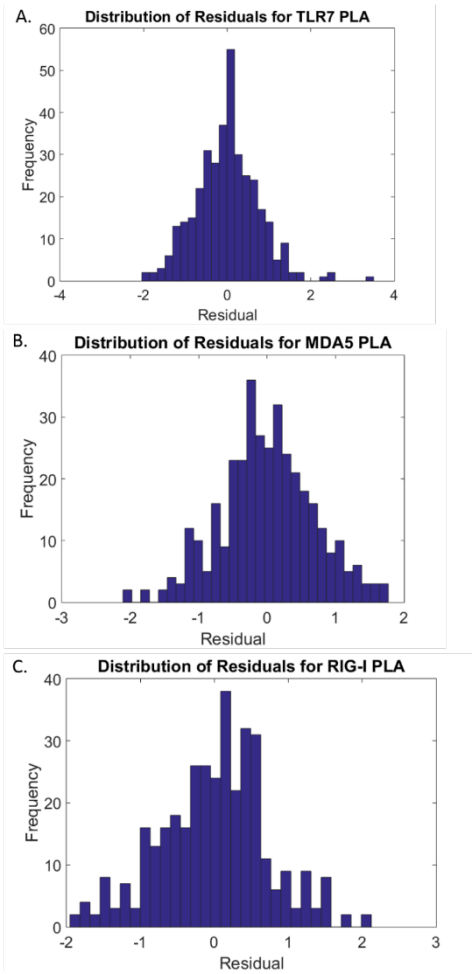

Figure A.4. Histograms of residual plots from data from PLAs of (A) TLR7, (B) MDA5, and (C) RIG-I. Data is transformed by taking the cubed root.

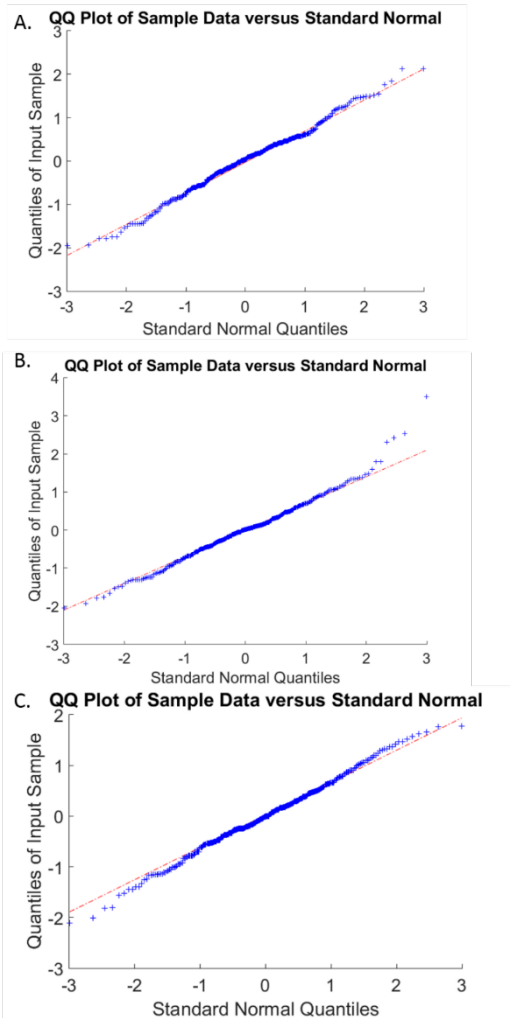

Figure A.5. q-q plots from data from PLAs of (A) TLR7, (B) MDA5, and (C) RIG-I. Data is transformed by taking the cubed root.

Figures A.4 and A.5 show that the transformed data now better approximates a normal distribution. Inspection of the function $y=x^{1/3}$, which is shown in Figure A.6, demonstrates why this transformation makes the collected data better fit a Gaussian distribution. When the cubic root is taken of low x values (values in the solid box), small differences between the values are magnified. When the cubic root is taken of higher x values (regions in the dashed box), differences between the x values are reduced. This reduced the heavy tails and right skewness and enhanced the left skewness of the initial residual histograms shown in Figure A.1.

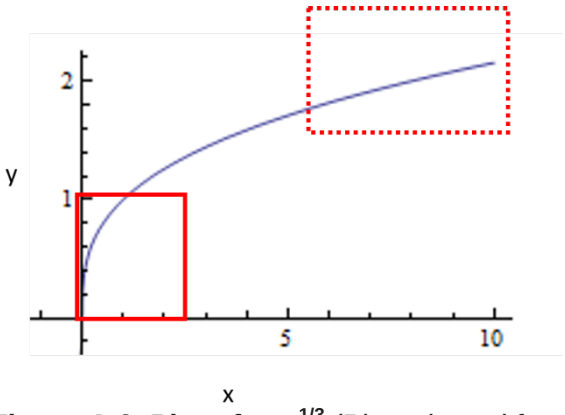

Figure A.6. Plot of $y=x^{1/3}$ (Plot adapted from http://mathematica.stackexchange.com).

A.4. Analysis of variance on proximity ligation assays

Now that the data better approximated a normal distribution, a hierarchical ANOVA was performed for each PLA. This nested the animals within the treatment and time, following the experimental design. Treatment, time, and individual animals were each tested to determine if they were significant contributors to total variability in data. For the PLAs of all PRRs, the treatment group was found to be a significant factor. For RIGI-I and MDA5 PLAs, time was also found to be a significant contributor. The 'multcompare' MATLAB function was then used to conduct pairwise comparisons among treatment groups and time points. Findings found from each treatment group are shown in Chapter 3, in Figures 3.10-3.12. Here, we also show the effects of time (Figure A.7), which shows the mean and 95% confidence intervals for each time point, considering data collected at all treatment groups. These plots allow us to distill more information from the collected data.

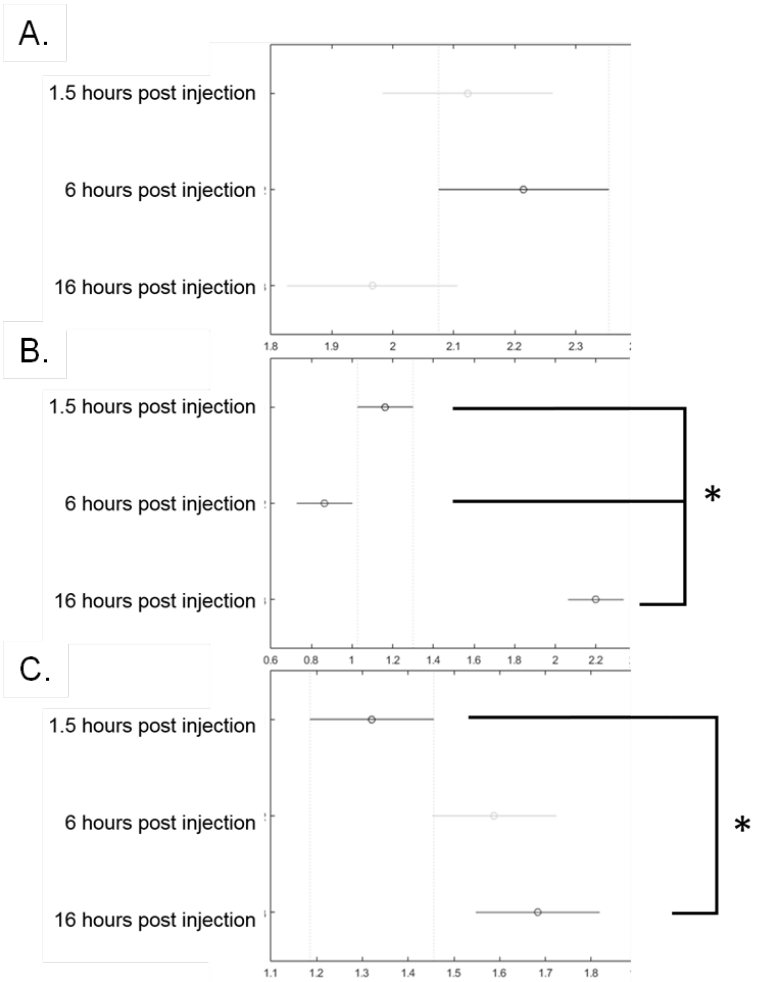

Figure A.7. Effect of time on activation of (A) TLR7 (B) MDA-5 and (C) RIG-I. Data is transformed to the cubed root. Mean values of the number of proximity ligation assay puncta per imaging frame and relative confidence intervals are shown.

A.5. MATLAB scripts

Below is the MATLAB code used for calculating JB statistic for multiple q values.

```
load mda5.dat; mda5=mda5(:);
load times.dat;
load animal.dat;
load treatment.dat;
times=times(:);
animal=animal(:);
treatment=treatment(:);
mynest = [0 0 0;
          0 0 0;
          1 1 0];
mymodel =[0 0 0;   %intercept effect
```

```
                1 0 0;   %treatment effect
                0 1 0;   %time  effect
                0 0 1;   %animal effect
                1 1 0];  %treatment * time effect (interaction)
close all force;

%Find transformation with the lowest JB statistic
jabe = @(sample) length(sample)/6 * (skewness(sample)^2 + (kurtosis(sample)-3)^2/4 );
jaber=[];

for q = 0.02:0.01:0.5;  % define transformations data set
        [p tab stats]=anovan(mda5.^q , {treatment, times, animal}, ...;
            'random', [3],...
            'nested', mynest,...
            'varnames', {'Treatment', 'Time', 'Animals'},...
            'model', mymodel);

        y=stats.resid;

        jaber = [jaber jabe(stats.resid)];
end

close all force
 figure;
 plot(0.02:0.01:.5, jaber,'o')
 title('Jarque-Bera for RIGI PLA^q')
 xlabel('q')
 ylabel('Jarque-Bera')

close all force
 figure;
 plot(0.02:0.01:.4, jaber,'o') %plot of JB statistic for all of q

%% Show QQplot of data
qqplot(stats.resid)
title('qqplot for MDA-5 PLA ')
set(gca, 'FontSize', 20)

%% Show histogram of residuals
figure;
hist(stats.resid, 30)
title('Distribution of Residuals for MDA5 PLA')
xlabel('Residual')
ylabel('Frequency')
set(gca,                                    'FontSize',                                    20)
```

Below is the MATLAB code used for performing the hierarchical ANOVA.

```
load mda5.dat; mda5=mda5(:);
load times.dat;
load animal.dat;
load treatment.dat;
times=times(:);
animal=animal(:);
treatment=treatment(:);

mynest = [0 0 0;
          0 0 0;
          1 1 0];
%
mymodel =[0 0 0;   %intercept effect
          1 0 0;   %treatment effect
          0 1 0;   %time  effect
          0 0 1;   %animal effect
          1 1 0];  %treatment * time effect (interaction)

 close all force;
 [p tab stats]=anovan(mda5.^(1/3) , {treatment, times, animal}, ...;
    'random', [3],...
    'nested', mynest,...
    'varnames', {'Treatment', 'Time', 'Animals'},...
    'model', mymodel);

y=stats.resid;

%%
n= length(y);
corrs=[]
range = 0.1:0.05:2;
for h = range
c=corr(sort(y).^h, norminv([0.5/n :1/n :1])');
corrs=[corrs c];
end

%% Perform multiple comparisons and calculate p values
   [p tab stats]=anovan(mda5.^(1/3), {treatment, times, animal}, ...
    'varnames', {'Treatment', 'Time','animal'},...
    'model', 'linear');
figure; multcompare(stats, 'dimension',1)
figure; multcompare(stats, 'dimension',2)
figure; multcompare(stats, 'dimension',[1 2])
```

APPENDIX B

DNA TEMPLATES FOR IVT MRNA

Below are the sequences for the DNA templates used for preparation of IVT mRNA. Prior to transcription, each sequence is digested with a restriction enzyme at the 3' end. The sequence for the T7 RNA polymerase promoter is underlined. The restriction digestion site is bolded. After transcription, a poly(A) tail is added enzymatically.

B.1 DNA Template for Ara h 2

CTAATACGACTCACTATAGGGAGAGCCGCCACCATGGCCAAGCTGACCATCCTGGT
CGCCCTGGCCCTGTTCCTGCTCGCTGCCCACGCTTCTGCCAGACAGCAGTGGGAG
CTGCAGGGCGACAGAAGATGCCAGAGCCAGCTGGAAAGAGCCAACCTGAGGCCC
TGCGAGCAGCACCTGATGCAGAAGATCCAGCGGGACGAGGACAGCTACGAGAGG
GACCCCTACAGCCCCAGCCAGGACCCCTACTCCCCTAGCCCCTACGACAGAAGAG
GCGCTGGCTCCAGCCAACACCAAGAAAGATGCTGCAACGAGCTGAACGAGTTCGA
GAACAACCAGAGATGCATGTGCGAGGCTCTGCAGCAGATCATGGAAAACCAGAGC
GACAGACTGCAGGGCAGGCAGCAAGAACAGCAGTTCAAGAGAGAGCTGAGAAACC
TGCCCCAGCAGTGCGGCCTGAGAGCCCCCCAGAGATGCGACCTGGACGTGGAAA
GCGGCGGCGACTACAAAGACCATGACGGTGATTATAAAGATCATGACATCGACTAC
AAGGATGACGATGACAAGTAGT**GCGGCCGC**AAAA

B.2 DNA template for cytoplasmic ovalbumin

TAATACGACTCACTATAGGCTAGCCTCGAGCCACCATGGGCTCCATCGGCGCAGC
AAGCATGGAATTTTGTTTTGATGTATTCAAGGAGCTCATCAATTCCTGGGTAGAAAG
TCAGACAAATGGAATTATCAGAAATGTCCTTCAGCCAAGCTCCGTGGATTCTCAAAC
TGCAATGGTTCTGGTTAATGCCATTGTCTTCAAAGGACTGTGGGAGAAAACATTTAA
GGATGAAGACACACAAGCAATGCCTTTCAGAGTGACTGAGCAAGAAAGCAAACCTG
TGCAGATGATGTACCAGATTGGTTTATTTAGAGTGGCATCAATGGCTTCTGAGAAAA
TGAAGATCCTGGAGCTTCCATTTGCCAGTGGGACAATGAGCATGTTGGTGCTGTTG
CCTGATGAAGTCTCAGGCCTTGAGCAGCTTGAGAGTATAATCAACTTTGAAAAACTG
ACTGAATGGACCAGTTCTAATGTTATGGAAGAGAGGAAGATCAAAGTGTACTTACCT
CGCATGAAGATGGAGGAAAAATACAACCTCACATCTGTCTTAATGGCTATGGGCAT
TACTGACGTGTTTAGCTCTTCAGCCAATCTGTCTGGCATCTCCTCAGCAGAGAGCC
TGAAGATATCTCAAGCTGTCCATGCAGCACATGCAGAAATCAATGAAGCAGGCAGA
GAGGTGGTAGGGTCAGCAGAGGCTGGAGTGGATGCTGCAAGCGTCTCTGAAGAAT
TTAGGGCTGACCATCCATTCCTCTTCTGTATCAAGCACATCGCAACCAACGCCGTT
CTCTTCTTTGGCAGATGTGTTTCCCCTTAAGGCTGCCTTCTGCGGGGCTTGCCTTC
TGGCCATGCCCTTCTTCTCTCCCTTGCACCTGTACCTCTTGGTCTTTGAATAAAGCC
TGAGTAGGAAG**GCGGCCGC**TTT

APPENDIX C

PRIMER SEQUENCES FOR QRT-PCR

Below are the primer sequences used for qRT-PCR, primarily for experiments in Chapter 2. All other primers used were purchased from QIAGEN and the sequences were not provided.

Table C.1 Primer sequences used in Chapter 2

Target	Forward Primer	Reverse Primer	Design RefSeq
IVT mRNA Specific Primers			
Ovalbumin	GCTCCATCGGCGCAGCAAGC	CCACGGAGCTTGGCTGAAGGACA	n/a
Ara h 2	CTGCTCGCTGCCCACGCTTCT	TCGCAGGGCCTCAGGTTGGCT	n/a
Human Specific Primers			
GAPDH (human)	TGGACCTGACCTGCCGTCTA	TAGCCCAGGATGCCCTTGA	NM_001289745.1|
Mouse Specific Primers			
Actb	CCCTAAGGCCAACCGTGAAA	CAGCCTGGATGGCTACGTAC	NM_007393.3
IL27B	AAGTACCGACTCCGCTACC	GGTGAAAGTCGTGGCTTCAA	NM_015766.2
Fcgr1	ATCTGCAGGAGTGTCCATCA	AGATGACACGGATGCTCTCA	NM_010186.5
Gapdh	AGACGGCCGCATCTTCTT	TTCACACCGACCTTCACCAT	NM_008084.2
IFNalpha	TCCACCAGCAGCTCAATGAC	TCTTCCTGGGTCAGGGGAAA	NM_010502.2
Ifnb1	AGCTCCAAGAAAGGACGAACA	TGGATGGCAAAGGCAGTGTA	NM_010510.1
Il10	AAAGGACCAGCTGGACAACA	TAAGGCTTGGCAACCCAAGTA	NM_010548.2
Il12a	AAACCAGCACATTGAAGACC	GGAAGAAGTCTCTCTAGTAGCC	NM_001159424.1
Il12b	ATCGTTTTGCTGGTGTCTCC	GGAGTCCAGTCCACCTCTAC	NM_008352.2
Il18	CAAAGAAAGCCGCCTCAAAC	GACGCAAGAGTCTTCTGACA	NM_008360.1
Il1a	AGATGGCCAAAGTTCCTGAC	AGAGATGGTCAATGGCAGAAC	NM_010554.4
Il1b	TGGCAACTGTTCCTGAACTCA	GGGTCCGTCAACTTCAAAGAAC	NM_008361.3
Il1rn	AGCTCATTGCTGGGTACTTACA	TGGATGCCCAAGAACACACTA	NM_001039701.3
Il2	CCCAGGATGCTCACCTTCAAA	CCGCAGAGGTCCAAGTTCA	NM_008366.3
Il4	ACGGAGATGGATGTGCCAAA	GCACCTTGGAAGCCCTACA	NM_021283.2
Il6	CCAGAAACCGCTATGAAGTTCC	GTTGTCACCAGCATCAGTCC	NM_031168.1
Nos2	GAGGAGCAGGTGGAAGACTA	GGAAAAGACTGCACCGAAGATA	NM_010927.3
Rere	AAGGAGCTGCTTCCCAGTA	GCCTCTGGTGTTTTCTTCCA	NM_001085492.1
RPL13a	CATTGTGGCCAAGCAGGTA	CCAGAAATGTTGATGCCTTCAC	NM_009438.5
Tgfb1	GCTGCGCTTGCAGAGATTAA	GTAACGCCAGGAATTGTTGCTA	NM_011577.1
Tnf	CAAATGGCCTCCCTCTCATCA	TGGGCTACAGGCTTGTCAC	NM_013693.2

APPENDIX D

ANTIVIRAL PCR ARRAY DATA

Below are the average calculated fold changes of gene expression from the PCR array data in Chapter 4. In Table D.1, fold changes are calculated relative to gene expression by cells treated with Lipofectamine 2000 only. RAW264.7 cells were used for the experiment.

Table D.1. Fold change of antiviral genes after transfection with IVT mRNA

Gene Symbol	Refseq	AUGC	AψGC	AM1YGC
Aim2	NM_001013779	1.9354	0.4638	0.1473
Atg12	NM_026217	1.5949	3.3048	2.3828
Atg5	NM_053069	1.7018	0.523	0.1533
Azi2	NM_013727	0.3609	0.041	0.0216
Card9	NM_001037747	0.839	1.5683	1.3048
Casp1	NM_009807	0.8286	0.1829	0.0993
Casp8	NM_009812	2.2761	3.0357	2.6649
Ccl3	NM_011337	2.8055	0.309	0.1854
Ccl4	NM_013652	6.8036	0.2844	0.2233
Ccl5	NM_013653	6.98	1.1511	0.7222
Cd40	NM_011611	745.462	299.5782	428.8825
Cd80	NM_009855	4.2811	1.5111	0.2376
Cd86	NM_019388	14.4949	9.1289	8.2766
Chuk	NM_007700	0.6498	1.2741	4.4614
Cnpy3	NM_028065	0.891	0.2447	0.0759
Ctsb	NM_007798	1.059	1.0851	0.4776
Ctsl	NM_009984	0.2879	0.0274	0.0115
Ctss	NM_021281	2.139	1.4585	0.7444
Cxcl10	NM_021274	24.2982	1.7197	2.4267
Cxcl11	NM_019494	15.9105	10.3207	2.5225
Cxcl9	NM_008599	2.5156	1.0394	3.5395
Cyld	NM_173369	2.6095	2.3353	1.1495
Dak	NM_145496	1.1168	2.4204	0.3815
Ddx3x	NM_010028	1.0247	1.4682	0.8716
Ddx58	NM_172689	9.6414	2.4742	1.2648
Dhx58	NM_030150	1.9617	0.1867	0.1723
Fadd	NM_010175	1.6671	0.5418	0.1239
Fos	NM_010234	2.6467	0.5763	0.2182

Hsp90aa1	NM_010480	1.4161	1.8853	1.1366
Ifih1	NM_027835	5.0718	1.8108	2.0456
Ifna2	NM_010503	62.8081	2.3347	10.1487
Ifnar1	NM_010508	0.776	1.7578	1.4636
Ifnb1	NM_010510	169.6908	13.1087	25.5929
Ikbkb	NM_010546	1.3678	0.4789	0.1726
Il12a	NM_008351	0.983	0.7755	5.9258
Il12b	NM_008352	0.9631	0.6985	5.9258
Il15	NM_008357	7.7074	0.4765	0.2376
Il18	NM_008360	6.6631	0.9394	0.3976
Il1b	NM_008361	140.3898	42.2601	24.0378
Il6	NM_031168	2.3951	0.479	5.9258
Irak1	NM_008363	2.2568	0.8373	0.2824
Irf3	NM_016849	0.8138	0.1096	0.043
Irf5	NM_012057	0.6536	0.831	2.5204
Irf7	NM_016850	2.5538	1.1859	4.1795
Isg15	NM_015783	14.9381	3.3808	5.9083
Jun	NM_010591	1.5443	1.8624	10.3427
Map2k1	NM_008927	1.9362	2.409	1.3082
Map2k3	NM_008928	1.2022	1.3765	2.343
Map3k1	NM_011945	2.127	2.1433	0.1754
Map3k7	NM_172688	0.97	0.3573	0.1573
Mapk1	NM_011949	1.3775	0.5079	0.1854
Mapk14	NM_011951	1.6515	1.2865	0.3836
Mapk3	NM_011952	1.1035	0.653	0.3026
Mapk8	NM_016700	2.3516	1.2322	0.3445
Mavs	NM_144888	0.256	1.2835	0.9801
Mefv	NM_019453	1.5422	2.0631	3.4909
Mx1	NM_010846	158.5699	9.9972	6.6625
Myd88	NM_010851	0.3698	0.4873	2.2214
Nfkb1	NM_008689	1.498	1.7318	1.4879
Nfkbia	NM_010907	1.953	1.4492	4.9488
Nlrp3	NM_145827	3.2236	1.958	0.8855
Nod2	NM_145857	1.6467	0.1009	0.0233
Oas2	NM_145227	1.1808	1.0424	2.815
Pin1	NM_023371	1.4961	0.4644	0.1928
Pstpip1	NM_011193	1.6748	1.3874	0.7922
Pycard	NM_023258	0.1786	0.0842	0.007
Rela	NM_009045	0.4029	1.2439	1.6087
Ripk1	NM_009068	0.5214	1.5786	2.6328
Spp1	NM_009263	1.6448	1.9139	2.0449

Stat1	NM_009283	5.1479	1.3076	0.9869
Sugt1	NM_026474	1.0645	0.2564	0.0897
Tank	NM_011529	1.233	0.5734	0.3255
Tbk1	NM_019786	1.0736	1.46	0.8444
Tbkbp1	NM_198100	1.047	0.9623	0.3034
Ticam1	NM_174989	0.5411	0.2306	1.7396
Tlr3	NM_126166	3.0583	9.6668	7.6708
Tlr7	NM_133211	0.4564	1.9068	2.6746
Tlr8	NM_133212	0.4921	24.3462	6.5493
Tlr9	NM_031178	0.6565	0.6127	2.0639
Tnf	NM_013693	2.5682	1.1852	5.804
Tradd	NM_001033161	2.2947	0.706	0.2172
Traf3	NM_011632	1.1049	2.4589	2.0381
Traf6	NM_009424	1.6417	3.9082	5.5084
Trim25	NM_009546	0.4777	0.6304	2.3975

Table D.2. Fold regulation of antiviral genes over sham injection control following IVT mRNA injection in anterior tibialis

	Refseq	**RNA+CL264 (Tethered)**	**RNA+CL264 (cocktail)**	**RNA**	**CL264**
Aim2	NM_001013779	2.4711	3.5283	2.2396	-1.6698
Atg12	NM_026217	-1.5054	-1.4749	-1.515	-1.1888
Atg5	NM_053069	-1.7195	-1.569	-2.3139	-2.3896
Azi2	NM_013727	-1.2638	1.4522	-1.0155	-1.8597
Card9	NM_001037747	2.1643	2.2388	1.0898	1.6123
Casp1	NM_009807	9.4321	13.9943	8.8204	1.4084
Casp8	NM_009812	2.4354	2.4349	2.6804	-1.505
Ccl3	NM_011337	369.813	135.5505	58.6417	7.6069
Ccl4	NM_013652	719.616	390.5616	203.6388	9.9239
Ccl5	NM_013653	423.6943	374.7567	202.8934	3.5083
Cd40	NM_011611	82.3805	79.4861	37.2352	-1.6808
Cd80	NM_009855	2.9911	5.4615	10.0874	3.0693
Cd86	NM_019388	7.645	7.4741	9.5735	1.5119
Chuk	NM_007700	-1.185	-2.2845	-1.718	-1.3205
Cnpy3	NM_028065	-5.6779	-2.0087	-10.7389	-2.5724
Ctsb	NM_007798	-1.5487	-1.4271	-1.3225	1.2807
Ctsl	NM_009984	-1.4434	1.09	-1.3563	-1.4204
Ctss	NM_021281	2.3797	2.7715	2.1744	-1.8918
Cxcl10	NM_021274	1199.5084	1011.1903	676.5128	5.0313
Cxcl11	NM_019494	83.7961	24.0028	14.7843	1.2188
Cxcl9	NM_008599	1330.1414	1175.6172	572.9969	2.3168

Cyld	NM_173369	-1.3279	-1.3852	-1.8162	-1.1029
Dak	NM_145496	-1.3272	1.012	1.655	2.6455
Ddx3x	NM_010028	-1.4529	-1.535	-1.2187	1.1237
Ddx58	NM_172689	6.7027	7.324	4.5696	-1.2235
Dhx58	NM_030150	23.5987	44.4451	33.0014	-2.1372
Fadd	NM_010175	-2.4128	-2.9857	-5.6917	-2.9352
Fos	NM_010234	2.8412	2.1206	1.2136	-1.2498
Hsp90aa1	NM_010480	-1.079	-1.1422	-1.4312	1.2709
Ifih1	NM_027835	11.2064	11.7689	10.2912	-2.1051
Ifna2	NM_010503	-1.5801	-3.1003	-1.8013	-1.5771
Ifnar1	NM_010508	-1.2887	-2.9563	-3.2947	-3.5713
Ifnb1	NM_010510	6.2894	6.143	7.9089	1.6104
Ikbkb	NM_010546	-1.5774	-1.4846	-2.3609	-4.4045
Il12a	NM_008351	-2.8239	-3.2651	-3.7653	-3.2804
Il12b	NM_008352	8.8954	-1.1695	-1.4436	1.2286
Il15	NM_008357	1.2538	1.6465	1.0026	-1.661
Il18	NM_008360	7.919	2.6717	2.8797	-2.3542
Il1b	NM_008361	1125.1571	331.1941	137.3022	114.3997
Il6	NM_031168	947.4906	138.236	60.1918	5.0038
Irak1	NM_008363	-1.8767	-1.9458	-3.2023	-1.2527
Irf3	NM_016849	-2.0045	-1.4099	-2.1628	-2.2411
Irf5	NM_012057	1.454	5.0626	3.8562	-1.2582
Irf7	NM_016850	56.06	74.5723	55.4838	2.1727
Isg15	NM_015783	178.5567	258.69	252.338	17.175
Jun	NM_010591	1.0766	-1.0728	1.5123	-1.2425
Map2k1	NM_008927	-1.3574	-1.6154	-1.9206	-1.2224
Map2k3	NM_008928	1.0329	1.1469	1.0479	-1.111
Map3k1	NM_011945	-1.4688	-1.6514	-2.6412	-2.6993
Map3k7	NM_172688	-1.9593	-1.6183	-2.5392	-1.5975
Mapk1	NM_011949	-1.7505	-1.6572	-2.6415	-1.4522
Mapk14	NM_011951	-2.0197	-1.8597	-3.0425	-1.4147
Mapk3	NM_011952	-8.1512	-4.4548	-3.6257	-1.5288
Mapk8	NM_016700	-1.7364	-1.9116	-3.5029	-1.2586
Mavs	NM_144888	-3.9239	-1.6419	-2.2337	-3.5534
Mefv	NM_019453	29.983	10.5731	4.4008	10.4909
Mx1	NM_010846	1144.4342	1678.6093	1423.8644	14.7032
Myd88	NM_010851	38.1556	24.4941	25.9858	-3.7954
Nfkb1	NM_008689	1.1372	-1.2142	-1.2079	-1.2745
Nfkbia	NM_010907	2.6319	1.3794	1.4599	1.1301
Nlrp3	NM_145827	83.6227	4.2805	3.8934	2.693
Nod2	NM_145857	8.0679	9.3562	4.8564	-2.4341

Oas2	NM_145227	126.7129	139.7291	63.4598	1.7493
Pin1	NM_023371	-1.5423	-1.3688	-2.1747	-1.5609
Pstpip1	NM_011193	3.6209	10.5955	10.9122	4.0768
Pycard	NM_023258	2.5194	3.8527	3.3056	-1.4017
Rela	NM_009045	-1.0132	1.5992	1.4014	-1.7475
Ripk1	NM_009068	3.0326	-1.0465	3.839	-4.2023
Spp1	NM_009263	-1.1818	-3.9357	-12.5284	-1.578
Stat1	NM_009283	3.1908	4.2142	2.9279	-1.098
Sugt1	NM_026474	-1.9284	-1.3924	-2.0554	-1.327
Tank	NM_011529	-1.4031	-1.2076	-1.5692	-1.5944
Tbk1	NM_019786	1.2727	1.2941	1.6197	1.0414
Tbkbp1	NM_198100	-2.453	-2.171	-5.6205	-1.5131
Ticam1	NM_174989	-1.3535	-3.2897	-3.0107	-5.9365
Tlr3	NM_126166	70.5748	60.523	97.2897	1.1955
Tlr7	NM_133211	-3.2334	-3.1117	-3.3507	-1.189
Tlr8	NM_133212	1.3536	9.4079	4.2909	1.0652
Tlr9	NM_031178	5.4253	7.1368	4.1323	1.408
Tnf	NM_013693	35.4211	2.2049	5.9195	-1.3416
Tradd	NM_001033161	-2.78	-4.6513	-8.2109	-4.8998
Traf3	NM_011632	-9.9291	-2.2777	-6.1218	-5.4464
Traf6	NM_009424	2.4693	-1.6374	-1.2268	-2.5581
Trim25	NM_009546	16.6749	22.8674	17.1369	1.1073

REFERENCES

1. (WHO) WHO (2014) The top 10 causes of death. in *Fact Sheets*, ed Organization Wh (http://www.who.int/mediacentre/factsheets/fs310/en/index1.html).

2. Holmgren J & Czerkinsky C (2005) Mucosal immunity and vaccines. *Nat Med* 11(4 Suppl):S45-53.

3. Iwasaki A & Medzhitov R (2015) Control of adaptive immunity by the innate immune system. *Nat Immunol* 16(4):343-353.

4. Finco O & Rappuoli R (2014) Designing vaccines for the twenty-first century society. *Front Immunol* 5.

5. Rappuoli R, Mandl CW, Black S, & De Gregorio E (2012) Vaccines for the twenty-first century society (vol 11, pg 865, 2011). *Nat Rev Immunol* 12(3):225-225.

6. Flynn NM*, et al.* (2005) Placebo-controlled phase 3 trial of a recombinant glycoprotein 120 vaccine to prevent HIV-1 infection. *J Infect Dis* 191(5):654-665.

7. Gilbert PB*, et al.* (2005) Correlation between immunologic responses to a recombinant glycoprotein 120 vaccine and incidence of HIV-1 infection in a phase 3 HIV-1 preventive vaccine trial. *J Infect Dis* 191(5):666-677.

8. Liu L*, et al.* (2012) Global, regional, and national causes of child mortality: an updated systematic analysis for 2010 with time trends since 2000. *Lancet* 379(9832):2151-2161.

9. Spies B*, et al.* (2003) Vaccination with plasmid DNA activates dendritic cells via Toll-like receptor 9 (TLR9) but functions in TLR9-deficient mice. *J Immunol* 171(11):5908-5912.

10. Suschak JJ, Wang S, Fitzgerald KA, & Lu S (2015) Identification of Aim2 as a sensor for DNA vaccines. *J Immunol* 194(2):630-636.

11. Cristillo AD*, et al.* (2011) Induction of mucosal and systemic antibody and T-cell responses following prime-boost immunization with novel adjuvanted human immunodeficiency virus-1-vaccine formulations. *The Journal of general virology* 92(Pt 1):128-140.

12. Lobigs M*, et al.* (2010) An inactivated Vero cell-grown Japanese encephalitis vaccine formulated with Advax, a novel inulin-based adjuvant, induces protective neutralizing antibody against homologous and heterologous flaviviruses. *The Journal of general virology* 91(Pt 6):1407-1417.

13. Jeon BY*, et al.* (2011) Co-immunization of plasmid DNA encoding IL-12 and IL-18 with Bacillus Calmette-Guerin vaccine against progressive tuberculosis. *Yonsei medical journal* 52(6):1008-1015.

14. Li L, Saade F, & Petrovsky N (2012) The future of human DNA vaccines. *Journal of biotechnology* 162(2-3):171-182.

15. Singh A*, et al.* (2008) Efficient modulation of T-cell response by dual-mode, single-carrier delivery of cytokine-targeted siRNA and DNA vaccine to antigen-presenting cells. *Molecular therapy : the journal of the American Society of Gene Therapy* 16(12):2011-2021.

16. Redding L & Weiner DB (2009) DNA vaccines in veterinary use. *Expert review of vaccines* 8(9):1251-1276.

17. Dhama K, Mahendran M, Gupta PK, & Rai A (2008) DNA vaccines and their applications in veterinary practice: current perspectives. *Veterinary research communications* 32(5):341-356.

18. Li J*, et al.* (2014) Messenger RNA vaccine based on recombinant MS2 virus-like particles against prostate cancer. *International journal of cancer. Journal international du cancer* 134(7):1683-1694.

19. Roesler E*, et al.* (2009) Immunize and disappear-Safety-optimized mRNA vaccination with a panel of 29 allergens. *J Allergy Clin Immun* 124(5):1070-1077.

20. Petsch B*, et al.* (2012) Protective efficacy of in vitro synthesized, specific mRNA vaccines against influenza A virus infection. *Nat Biotechnol* 30(12):1210-1216.

21. Kubler H*, et al.* (2015) Self-adjuvanted mRNA vaccination in advanced prostate cancer patients: a first-in-man phase I/IIa study. *Journal for immunotherapy of cancer* 3:26.

22. Weide B*, et al.* (2009) Direct Injection of Protamine-protected mRNA: Results of a Phase 1/2 Vaccination Trial in Metastatic Melanoma Patients. *J Immunother* 32(5):498-507.

23. Rittig SM*, et al.* (2011) Intradermal vaccinations with RNA coding for TAA generate CD8+ and CD4+ immune responses and induce clinical benefit in vaccinated patients. *Molecular therapy : the journal of the American Society of Gene Therapy* 19(5):990-999.

24. Van Tendeloo VFI*, et al.* (2001) Highly efficient gene delivery by mRNA electroporation in human hematopoietic cells: superiority to lipofection and passive pulsing of mRNA and to electroporation of plasmid cDNA for tumor antigen loading of dendritic cells. *Blood* 98(1):49-56.

25. Zou S, Scarfo K, Nantz MH, & Hecker JG (2010) Lipid-mediated delivery of RNA is more efficient than delivery of DNA in non-dividing cells. *Int J Pharmaceut* 389(1-2):232-243.

26. Wang YH*, et al.* (2013) Systemic Delivery of Modified mRNA Encoding Herpes Simplex Virus 1 Thymidine Kinase for Targeted Cancer Gene Therapy. *Molecular Therapy* 21(2):358-367.

27. Hogan DJ, Riordan DP, Gerber AP, Herschlag D, & Brown PO (2008) Diverse RNA-Binding Proteins Interact with Functionally Related Sets of RNAs, Suggesting an Extensive Regulatory System. *Plos Biol* 6(10):2297-2313.

28. Singh G*, et al.* (2012) The Cellular EJC Interactome Reveals Higher-Order mRNP Structure and an EJC-SR Protein Nexus. *Cell* 151(4):750-764.

29. Bregman A*, et al.* (2011) Promoter Elements Regulate Cytoplasmic mRNA Decay. *Cell* 147(7):1473-1483.

30. Maquat LE, Tarn WY, & Isken O (2010) The Pioneer Round of Translation: Features and Functions. *Cell* 142(3):368-374.

31. Sauliere J*, et al.* (2010) The exon junction complex differentially marks spliced junctions. *Nature structural & molecular biology* 17(10):1269-1271.

32. Mendez R & Richter JD (2001) Translational control by CPEB: a means to the end. *Nature reviews. Molecular cell biology* 2(7):521-529.

33. Lorenz C*, et al.* (2011) Protein expression from exogenous mRNA Uptake by receptor-mediated endocytosis and trafficking via the lysosomal pathway. *Rna Biol* 8(4):627-636.

34. Bire S*, et al.* (2013) Exogenous mRNA delivery and bioavailability in gene transfer mediated by piggyBac transposition. *Bmc Biotechnol* 13.

35. Warren L*, et al.* (2010) Highly efficient reprogramming to pluripotency and directed differentiation of human cells with synthetic modified mRNA. *Cell Stem Cell* 7(5):618-630.

36. Andreas Thess SG, Barbara L Mui, Michael J Hope, Patrick Baumhof, Mariola Fotin-Mleczek and Thomas Schlake (2015) Sequence-engineered mRNA Without Chemical Nucleoside Modifications Enables an Effective Protein Therapy in Large Animals. *Molecular Therapy*

37. Kormann MSD*, et al.* (2011) Expression of therapeutic proteins after delivery of chemically modified mRNA in mice. *Nature Biotechnology* 29(2):154-U196.

38. Holtkamp S*, et al.* (2006) Modification of antigen-encoding RNA increases stability, translational efficacy, and T-cell stimulatory capacity of dendritic cells. *Blood* 108(13):4009-4017.

39. Azmi F, Fuaad AAA, Skwarczynski M, & Toth I (2014) Recent progress in adjuvant discovery for peptide-based subunit vaccines. *Hum Vacc Immunother* 10(3):778-796.

40. Coffman RL, Sher A, & Seder RA (2010) Vaccine Adjuvants: Putting Innate Immunity to Work. *Immunity* 33(4):492-503.

41. Pulendran B & Ahmed R (2006) Translating innate immunity into immunological memory: Implications for vaccine development. *Cell* 124(4):849-863.

42. Pollard C*, et al.* (2013) Type I IFN Counteracts the Induction of Antigen-Specific Immune Responses by Lipid-Based Delivery of mRNA Vaccines. *Molecular Therapy* 21(1):251-259.

43. Kariko K, Ni HP, Capodici J, Lamphier M, & Weissman D (2004) mRNA is an endogenous ligand for Toll-like receptor 3. *J Biol Chem* 279(13):12542-12550.

44. Fotin-Mleczek M*, et al.* (2011) Messenger RNA-based Vaccines With Dual Activity Induce Balanced TLR-7 Dependent Adaptive Immune Responses and Provide Antitumor Activity. *J Immunother* 34(1):1-15.

45. Kariko K*, et al.* (2008) Incorporation of Pseudouridine Into mRNA Yields Superior Nonimmunogenic Vector With Increased Translational Capacity and Biological Stability. *Molecular Therapy* 16(11):1833-1840.

46. Anderson BR*, et al.* (2010) Incorporation of pseudouridine into mRNA enhances translation by diminishing PKR activation. *Nucleic Acids Res* 38(17):5884-5892.

47. Anderson BR*, et al.* (2011) Nucleoside modifications in RNA limit activation of 2'-5'-oligoadenylate synthetase and increase resistance to cleavage by RNase L. *Nucleic Acids Res* 39(21):9329-9338.

48. Randall RE & Goodbourn S (2008) Interferons and viruses: an interplay between induction, signalling, antiviral responses and virus countermeasures. *The Journal of general virology* 89(Pt 1):1-47.

49. Zhu JZ*, et al.* (2014) Antiviral Activity of Human OASL Protein Is Mediated by Enhancing Signaling of the RIG-I RNA Sensor. *Immunity* 40(6):936-948.

50. Akira S, Takeda K, & Kaisho T (2001) Toll-like receptors: critical proteins linking innate and acquired immunity. *Nature Immunology* 2(8):675-680.

51. Kulkarni RR*, et al.* (2014) Activation of the RIG-I Pathway during Influenza Vaccination Enhances the Germinal Center Reaction, Promotes T Follicular Helper Cell Induction, and Provides a Dose-Sparing Effect and Protective Immunity. *J Virol* 88(24):13990-14001.

52. Martins KAO*, et al.* (2014) Toll-Like Receptor Agonist Augments Virus-Like Particle-Mediated Protection from Ebola Virus with Transient Immune Activation. *Plos One* 9(2).

53. Nallagatla SR*, et al.* (2007) 5 '-triphosphate-dependent activation of PKR by RNAs with short stem-loops. *Science* 318(5855):1455-1458.

54. Heinicke LA, Nallagatla SR, Hull CM, & Bevilacqua PC (2011) RNA helical imperfections regulate activation of the protein kinase PKR: Effects of bulge position, size, and geometry. *Rna* 17(5):957-966.

55. Silverman RH (2007) Viral encounters with 2 ',5 '-oligoadenylate synthetase and RNase L during the interferon antiviral response. *J Virol* 81(23):12720-12729.

56. Hornung V, Hartmann R, Ablasser A, & Hopfner KP (2014) OAS proteins and cGAS: unifying concepts in sensing and responding to cytosolic nucleic acids. *Nat Rev Immunol* 14(8):521-528.

57. Harman AN*, et al.* (2013) Identification of Lineage Relationships and Novel Markers of Blood and Skin Human Dendritic Cells. *Journal of Immunology* 190(1):66-79.

58. Yoneyama M*, et al.* (2004) The RNA helicase RIG-I has an essential function in double-stranded RNA-induced innate antiviral responses. *Nature Immunology* 5(7):730-737.

59. Wu B*, et al.* (2013) Structural Basis for dsRNA Recognition, Filament Formation, and Antiviral Signal Activation by MDA5. *Cell* 152(1-2):276-289.

60. Schmidt A*, et al.* (2009) 5 '-triphosphate RNA requires base-paired structures to activate antiviral signaling via RIG-I. *P Natl Acad Sci USA* 106(29):12067-12072.

61. Schlee M & Hartmann G (2010) The Chase for the RIG-I Ligand-Recent Advances. *Molecular Therapy* 18(7):1254-1262.

62. Malathi K, Dong BH, Gale M, & Silverman RH (2007) Small self RNA generated by RNASE L amplifies antiviral innate immunity. *J Interf Cytok Res* 27(8):700-700.

63. Bruns AM, Leser GP, Lamb RA, & Horvath CM (2014) The Innate Immune Sensor LGP2 Activates Antiviral Signaling by Regulating MDA5-RNA Interaction and Filament Assembly. *Mol Cell* 55(5):771-781.

64. Muzio M*, et al.* (2000) Differential expression and regulation of toll-like receptors (TLR) in human leukocytes: Selective expression of TLR3 in dendritic cells. *Journal of Immunology* 164(11):5998-6004.

65. Diebold SS, Kaisho T, Hemmi H, Akira S, & Sousa CRE (2004) Innate antiviral responses by means of TLR7-mediated recognition of single-stranded RNA. *Science* 303(5663):1529-1531.

66. Forsbach A*, et al.* (2008) Identification of RNA sequence motifs stimulating sequence-specific TLR8-dependent immune responses. *Journal of Immunology* 180(6):3729-3738.

67. Larange A, Antonios D, Pallardy M, & Kerdine-Romer S (2009) TLR7 and TLR8 agonists trigger different signaling pathways for human dendritic cell maturation. *J Leukocyte Biol* 85(4):673-683.

68. Rettig L*, et al.* (2010) Particle size and activation threshold: a new dimension of danger signaling. *Blood* 115(22):4533-4541.

69. Zheng GQ*, et al.* (2013) Sprouts of RNA epigenetics The discovery of mammalian RNA demethylases. *Rna Biol* 10(6):915-918.

70. Kierzek E*, et al.* (2014) The contribution of pseudouridine to stabilities and structure of RNAs. *Nucleic Acids Res* 42(5):3492-3501.

71. Chen Y, Sierzputowskagracz H, Guenther R, Everett K, & Agris PF (1993) 5-Methylcytidine Is Required for Cooperative Binding of Mg2+ and a Conformational Transition at the Anticodon Stem-Loop of Yeast Phenylalanine Transfer-Rna. *Biochemistry-Us* 32(38):10249-10253.

72. Motorin Y & Helm M (2010) tRNA Stabilization by Modified Nucleotides. *Biochemistry-Us* 49(24):4934-4944.

73. Sydow D, Leonarski F, D'Ascenzo L, & Auffinger P (2015) Stabilization effects induced by modified nucleotides in tRNA T-loop motifs. *J Biomol Struct Dyn* 33:66-66.

74. Palama IE, Cortese B, D'Amone S, & Gigli G (2015) mRNA delivery using non-viral PCL nanoparticles. *Biomater Sci-Uk* 3(1):144-151.

75. Carlile TM*, et al.* (2014) Pseudouridine profiling reveals regulated mRNA pseudouridylation in yeast and human cells. *Nature* 515(7525):143-+.

76. Schwartz S*, et al.* (2014) Transcriptome-wide Mapping Reveals Widespread Dynamic-Regulated Pseudouridylation of ncRNA and mRNA. *Cell* 159(1):148-162.

77. Wang X*, et al.* (2014) N-6-methyladenosine-dependent regulation of messenger RNA stability. *Nature* 505(7481):117-+.

78. Motorin Y & Helm M (2011) RNA nucleotide methylation. *Wires Rna* 2(5):611-631.

79. Nallagatla SR*, et al.* (2013) Native Tertiary Structure and Nucleoside Modifications Suppress tRNA's Intrinsic Ability to Activate the Innate Immune Sensor PKR. *Plos One* 8(3).

80. Nallagatla SR & Bevilacqua PC (2008) Nucleoside modifications modulate activation of the protein kinase PKR in an RNA structure-specific manner. *Rna* 14(6):1201-1213.

81. Mays LE*, et al.* (2013) Modified Foxp3 mRNA protects against asthma through an IL-10 dependent mechanism. *J Clin Invest* 123(3):1216-1228.

82. Kariko K, Muramatsu H, Keller JM, & Weissman D (2012) Increased Erythropoiesis in Mice Injected With Submicrogram Quantities of Pseudouridine-containing mRNA Encoding Erythropoietin. *Molecular Therapy* 20(5):948-953.

83. Fernandez IS*, et al.* (2013) Unusual base pairing during the decoding of a stop codon by the ribosome. *Nature* 500(7460):107-U136.

84. Karijolich J & Yu YT (2011) Converting nonsense codons into sense codons by targeted pseudouridylation. *Nature* 474(7351):395-+.

85. Parisien M, Yi C, & Pan T (2012) Rationalization and prediction of selective decoding of pseudouridine-modified nonsense and sense codons. *Rna* 18(3):355-367.

86. Gustafsson C, Govindarajan S, & Minshull J (2004) Codon bias and heterologous protein expression. *Trends Biotechnol* 22(7):346-353.

87. Duan JB*, et al.* (2013) Genome-wide survey of interindividual differences of RNA stability in human lymphoblastoid cell lines. *Sci Rep-Uk* 3.

88. Saunders R & Deane CM (2010) Synonymous codon usage influences the local protein structure observed. *Nucleic Acids Res* 38(19):6719-6728.

89. Plotkin JB & Kudla G (2011) Synonymous but not the same: the causes and consequences of codon bias. *Nat Rev Genet* 12(1):32-42.

90. Ngumbela KC*, et al.* (2008) Quantitative Effect of Suboptimal Codon Usage on Translational Efficiency of mRNA Encoding HIV-1 gag in Intact T Cells. *Plos One* 3(6).

91. Fath S*, et al.* (2011) Multiparameter RNA and Codon Optimization: A Standardized Tool to Assess and Enhance Autologous Mammalian Gene Expression. *Plos One* 6(3).

92. Gustafsson C*, et al.* (2012) Engineering genes for predictable protein expression. *Protein Expres Purif* 83(1):37-46.

93. Gaspar P, Moura G, Santos MAS, & Oliveira JL (2013) mRNA secondary structure optimization using a correlated stem-loop prediction. *Nucleic Acids Res* 41(6).

94. Griswold KE, Mahmood NA, Iverson BL, & Georgiou G (2003) Effects of codon usage versus putative 5 '-mRNA structure on the expression of Fusarium solani cutinase in the Escherichia coli cytoplasm. *Protein Expres Purif* 27(1):134-142.

95. Zhang WC, Xiao WH, Wei HM, Zhang J, & Tian ZG (2006) mRNA secondary structure at start AUG codon is a key limiting factor for human protein expression in Escherichia coli. *Biochem Bioph Res Co* 349(1):69-78.

96. Probst J*, et al.* (2009) Spontaneous cellular uptake of exogenous messenger RNA *in vivo* is nucleic acid-specific, saturable and ion dependent (vol 14, pg 1175, 2007). *Gene Ther* 16(5):706-706.

97. Phua KKL, Leong KW, & Nair SK (2013) Transfection efficiency and transgene expression kinetics of mRNA delivered in naked and nanoparticle format. *J Control Release* 166(3):227-233.

98. Zohra FT, Chowdhury EH, & Akaike T (2009) High performance mRNA transfection through carbonate apatite-cationic liposome conjugates. *Biomaterials* 30(23-24):4006-4013.

99. Phua KKL, Staats HF, Leong KW, & Nair SK (2014) Intranasal mRNA nanoparticle vaccination induces prophylactic and therapeutic anti-tumor immunity. *Sci Rep-Uk* 4.

100. Anderson DM*, et al.* (2003) Stability of mRNA/cationic lipid lipoplexes in human and rat cerebrospinal fluid: Methods and evidence for nonviral mRNA gene delivery to the central nervous system. *Hum Gene Ther* 14(3):191-202.

101. Su XF, Fricke J, Kavanagh DG, & Irvine DJ (2011) In Vitro and *in vivo* mRNA Delivery Using Lipid-Enveloped pH-Responsive Polymer Nanoparticles. *Mol Pharmaceut* 8(3):774-787.

102. Scheel B*, et al.* (2006) Therapeutic anti-tumor immunity triggered by injections of immunostimulating single-stranded RNA. *Eur J Immunol* 36(10):2807-2816.

103. Gantier MP*, et al.* (2008) TLR7 is involved in sequence-specific sensing of single-stranded RNAs in human macrophages. *Journal of Immunology* 180(4):2117-2124.

104. Sahin U, Kariko K, & Tureci O (2014) mRNA-based therapeutics - developing a new class of drugs. *Nat Rev Drug Discov* 13(10):759-780.

105. Scheel B*, et al.* (2005) Toll-like receptor-dependent activation of several human blood cell types by protamine-condensed mRNA. *Eur J Immunol* 35(5):1557-1566.

106. Nguyen DN*, et al.* (2012) Lipid-derived nanoparticles for immunostimulatory RNA adjuvant delivery. *P Natl Acad Sci USA* 109(14):E797-E803.

107. Cheng C, Convertine AJ, Stayton PS, & Bryers JD (2012) Multifunctional triblock copolymers for intracellular messenger RNA delivery. *Biomaterials* 33(28):6868-6876.

108. Uchida S*, et al.* (2013) *In vivo* Messenger RNA Introduction into the Central Nervous System Using Polyplex Nanomicelle. *Plos One* 8(2).

109. Perche F*, et al.* (2011) Enhancement of dendritic cells transfection *in vivo* and of vaccination against B16F10 melanoma with mannosylated histidylated lipopolyplexes loaded with tumor antigen messenger RNA. *Nanomed-Nanotechnol* 7(4):445-453.

110. Crowley P, Baumhover and Rice (2015) Efficient expression of stabilized mRNA PEG-peptide polyplexes in liver. *Gene Ther*.

111. Rittig SM*, et al.* (2011) Intradermal Vaccinations With RNA Coding for TAA Generate CD8(+) and CD4(+) Immune Responses and Induce Clinical Benefit in Vaccinated Patients. *Molecular Therapy* 19(5):990-999.

112. Hung IFN*, et al.* (2014) Immunogenicity of Intradermal Trivalent Influenza Vaccine With Topical Imiquimod: A Double Blind Randomized Controlled Trial. *Clin Infect Dis* 59(9):1246-1255.

113. Kreiter S*, et al.* (2010) Intranodal vaccination with naked antigen-encoding RNA elicits potent prophylactic and therapeutic antitumoral immunity. *Cancer research* 70(22):9031-9040.

114. Fasbender A, Zabner J, Zeiher BG, & Welsh MJ (1997) A low rate of cell proliferation and reduced DNA uptake limit cationic lipid-mediated gene transfer to primary cultures of ciliated human airway epithelia. *Gene Ther* 4(11):1173-1180.

115. Matsui H, Johnson LG, Randell SH, & Boucher RC (1997) Loss of binding and entry of liposome-DNA complexes decreases transfection efficiency in differentiated airway epithelial cells. *J Biol Chem* 272(2):1117-1126.

116. Li WJ & Szoka FC (2007) Lipid-based nanoparticles for nucleic acid delivery. *Pharm Res* 24(3):438-449.

117. Manthorpe M*, et al.* (1993) Gene-Therapy by Intramuscular Injection of Plasmid DNA - Studies on Firefly Luciferase Gene-Expression in Mice. *Hum Gene Ther* 4(4):419-431.

118. Shi YF, Parhar RS, Zou MJ, Al-Mohanna FA, & Paterson MC (2002) Gene therapy of melanoma pulmonary metastasis by intramuscular injection of plasmid DNA encoding tissue inhibitor of metalloproteinases-1. *Cancer Gene Ther* 9(2):126-132.

119. Ferraro B*, et al.* (2011) Clinical applications of DNA vaccines: current progress. *Clin Infect Dis* 53(3):296-302.

120. Ponsaerts P, Van Tendeloo VF, & Berneman ZN (2003) Cancer immunotherapy using RNA-loaded dendritic cells. *Clin Exp Immunol* 134(3):378-384.

121. Mockey M*, et al.* (2006) mRNA transfection of dendritic cells: synergistic effect of ARCA mRNA capping with Poly(A) chains in cis and in trans for a high protein expression level. *Biochem Biophys Res Commun* 340(4):1062-1068.

122. Yamamoto A, Kormann M, Rosenecker J, & Rudolph C (2009) Current prospects for mRNA gene delivery. *Eur J Pharm Biopharm* 71(3):484-489.

123. Rizzuto G*, et al.* (1999) Efficient and regulated erythropoietin production by naked DNA injection and muscle electroporation. *Proc Natl Acad Sci U S A* 96(11):6417-6422.

124. Roy K, Mao HQ, Huang SK, & Leong KW (1999) Oral gene delivery with chitosan--DNA nanoparticles generates immunologic protection in a murine model of peanut allergy. *Nat Med* 5(4):387-391.

125. Chua KY, Kuo IC, & Huang CH (2009) DNA vaccines for the prevention and treatment of allergy. *Curr Opin Allergy Clin Immunol* 9(1):50-54.

126. Zuker M (2003) Mfold web server for nucleic acid folding and hybridization prediction. *Nucleic Acids Res* 31(13):3406-3415.

127. Kariko K, Buckstein M, Ni H, & Weissman D (2005) Suppression of RNA recognition by Toll-like receptors: the impact of nucleoside modification and the evolutionary origin of RNA. *Immunity* 23(2):165-175.

128. Kormann MS*, et al.* (2011) Expression of therapeutic proteins after delivery of chemically modified mRNA in mice. *Nat Biotechnol* 29(2):154-157.

129. Fotin-Mleczek M*, et al.* (2011) Messenger RNA-based vaccines with dual activity induce balanced TLR-7 dependent adaptive immune responses and provide antitumor activity. *J Immunother* 34(1):1-15.

130. Diebold SS, Kaisho T, Hemmi H, Akira S, & Reis e Sousa C (2004) Innate antiviral responses by means of TLR7-mediated recognition of single-stranded RNA. *Science* 303(5663):1529-1531.

131. Schlake T, Thess A, Fotin-Mleczek M, & Kallen KJ (2012) Developing mRNA-vaccine technologies. *Rna Biol* 9(11):1319-1330.

132. Kramps T & Probst J (2013) Messenger RNA-based vaccines: progress, challenges, applications. *Wiley interdisciplinary reviews. RNA* 4(6):737-749.

133. Pashine A, Valiante NM, & Ulmer JB (2005) Targeting the innate immune response with improved vaccine adjuvants. *Nature Medicine* 11(4):S63-S68.

134. Kasturi SP*, et al.* (2011) Programming the magnitude and persistence of antibody responses with innate immunity. *Nature* 470(7335):543-U136.

135. Reed SG, Orr MT, & Fox CB (2013) Key roles of adjuvants in modern vaccines. *Nat Med* 19(12):1597-1608.

136. Heil F*, et al.* (2004) Species-specific recognition of single-stranded RNA via toll-like receptor 7 and 8. *Science* 303(5663):1526-1529.

137. Goubau D*, et al.* (2014) Antiviral immunity via RIG-I-mediated recognition of RNA bearing 5'-diphosphates. *Nature* 514(7522):372-375.

138. Reikine S, Nguyen JB, & Modis Y (2014) Pattern recognition and signaling mechanisms of RIG-I and MDA5. *Front Immunol* 5.

139. Triantafilou K*, et al.* (2012) Visualisation of direct interaction of MDA5 and the dsRNA replicative intermediate form of positive strand RNA viruses. *Journal of cell science* 125(Pt 20):4761-4769.

140. Zarember KA & Godowski PJ (2002) Tissue expression of human toll-like receptors and differential regulation of toll-like receptor mRNAs in leukocytes in response to microbes, their products, and cytokines (vol 168, pg 554, 2002). *Journal of Immunology* 169(2):1136-1136.

141. Soderberg O*, et al.* (2006) Direct observation of individual endogenous protein complexes in situ by proximity ligation. *Nat Methods* 3(12):995-1000.

142. Lin SC, Lo YC, & Wu H (2010) Helical assembly in the MyD88-IRAK4-IRAK2 complex in TLR/IL-1R signalling. *Nature* 465(7300):885-U882.

143. Gay NJ, Symmons MF, Gangloff M, & Bryant CE (2014) Assembly and localization of Toll-like receptor signalling complexes. *Nat Rev Immunol* 14(8):546-558.

144. Barral PM*, et al.* (2009) Functions of the cytoplasmic RNA sensors RIG-I and MDA-5: Key regulators of innate immunity. *Pharmacol Therapeut* 124(2):219-234.

145. Kawai T*, et al.* (2005) IPS-1, an adaptor triggering RIG-I- and Mda5-mediated type I interferon induction. *Nature Immunology* 6(10):981-988.

146. Santangelo PJ*, et al.* (2009) Single molecule-sensitive probes for imaging RNA in live cells. *Nat Methods* 6(5):347-U346.

147. Lifland AW, Zurla C, Yu JN, & Santangelo PJ (2011) Dynamics of Native beta-actin mRNA Transport in the Cytoplasm. *Traffic* 12(8):1000-1011.

148. Zurla C, Lifland AW, & Santangelo PJ (2011) Characterizing mRNA Interactions with RNA Granules during Translation Initiation Inhibition. *Plos One* 6(5).

149. Alonas E*, et al.* (2014) Combining Single RNA Sensitive Probes with Subdiffraction-Limited and Live-Cell Imaging Enables the Characterization of Virus Dynamics in Cells. *Acs Nano* 8(1):302-315.

150. Lifland AW*, et al.* (2012) Human Respiratory Syncytial Virus Nucleoprotein and Inclusion Bodies Antagonize the Innate Immune Response Mediated by MDA5 and MAVS. *J Virol* 86(15):8245-8258.

151. Kawai T & Akira S (2010) The role of pattern-recognition receptors in innate immunity: update on Toll-like receptors. *Nature Immunology* 11(5):373-384.

152. Ramos HJ & Gale M (2011) RIG-I like receptors and their signaling crosstalk in the regulation of antiviral immunity. *Curr Opin Virol* 1(3):167-176.

153. Rouskin S, Zubradt M, Washietl S, Kellis M, & Weissman JS (2014) Genome-wide probing of RNA structure reveals active unfolding of mRNA structures *in vivo*. *Nature* 505(7485):701-705.

154. Choi UY, Kang JS, Hwang YS, & Kim YJ (2015) Oligoadenylate synthase-like (OASL) proteins: dual functions and associations with diseases. *Exp Mol Med* 47:e144.

155. Donovan J, Dufner M, & Korennykh A (2013) Structural basis for cytosolic double-stranded RNA surveillance by human oligoadenylate synthetase 1. *Proc Natl Acad Sci U S A* 110(5):1652-1657.

156. Hartmann R, Justesen J, Sarkar SN, Sen GC, & Yee VC (2003) Crystal structure of the 2'-specific and double-stranded RNA-activated interferon-induced antiviral protein 2'-5'-oligoadenylate synthetase. *Mol Cell* 12(5):1173-1185.

157. Othoro C*, et al.* (2009) Enhanced immunogenicity of Plasmodium falciparum peptide vaccines using a topical adjuvant containing a potent synthetic Toll-like receptor 7 agonist, imiquimod. *Infection and immunity* 77(2):739-748.

158. Johnson TR, Rao S, Seder RA, Chen M, & Graham BS (2009) TLR9 agonist, but not TLR7/8, functions as an adjuvant to diminish FI-RSV vaccine-enhanced disease, while either agonist used as therapy during primary RSV infection increases disease severity. *Vaccine* 27(23):3045-3052.

159. Broquet AH, Hirata Y, McAllister CS, & Kagnoff MF (2011) RIG-I/MDA5/MAVS Are Required To Signal a Protective IFN Response in Rotavirus-Infected Intestinal Epithelium. *Journal of Immunology* 186(3):1618-1626.

160. McNab F, Mayer-Barber K, Sher A, Wack A, & O'Garra A (2015) Type I interferons in infectious disease. *Nat Rev Immunol* 15(2):87-103.

161. Rouzaut A*, et al.* (2010) Dendritic cells adhere to and transmigrate across lymphatic endothelium in response to IFN-alpha. *Eur J Immunol* 40(11):3054-3063.

162. Wille-Reece U*, et al.* (2005) HIV Gag protein conjugated to a toll-like receptor 7/8 agonist improves the magnitude and quality of Th1 and CD8(+) T cell responses in nonhuman primates. *P Natl Acad Sci USA* 102(42):15190-15194.

163. Napolitani G, Rinaldi A, Bertoni F, Sallusto F, & Lanzavecchia A (2005) Selected Toll-like receptor agonist combinations synergistically trigger a T helper type 1-polarizing program in dendritic cells. *Nature Immunology* 6(8):769-776.

164. Hess PR, Boczkowski D, Nair SK, Snyder D, & Gilboa E (2006) Vaccination with mRNAs encoding tumor-associated antigens and granulocyte-macrophage colony-stimulating factor efficiently primes CTL responses, but is insufficient to overcome tolerance to a model tumor/self antigen. *Cancer Immunol Immunother* 55(6):672-683.

165. Jin MS*, et al.* (2007) Crystal structure of the TLR1-TLR2 heterodimer induced by binding of a tri-acylated lipopeptide. *Cell* 130(6):1071-1082.

166. Joffre OP, Segura E, Savina A, & Amigorena S (2012) Cross-presentation by dendritic cells. *Nat Rev Immunol* 12(8):557-569.

167. Holmes TD*, et al.* (2014) Licensed human natural killer cells aid dendritic cell maturation via TNFSF14/LIGHT. *Proc Natl Acad Sci U S A* 111(52):E5688-5696.

168. Desnues B*, et al.* (2014) TLR8 on dendritic cells and TLR9 on B cells restrain TLR7-mediated spontaneous autoimmunity in C57BL/6 mice. *Proc Natl Acad Sci U S A* 111(4):1497-1502.

169. Wang J*, et al.* (2006) The functional effects of physical interactions among Toll-like receptors 7, 8, and 9. *J Biol Chem* 281(49):37427-37434.

170. Zhang WW & Matlashewski G (2008) Immunization with a Toll-like receptor 7 and/or 8 agonist vaccine adjuvant increases protective immunity against Leishmania major in BALB/c mice. *Infection and immunity* 76(8):3777-3783.

171. Vasilakos JP & Tomai MA (2013) The use of Toll-like receptor 7/8 agonists as vaccine adjuvants. *Expert review of vaccines* 12(7):809-819.

172. Mockey M*, et al.* (2007) mRNA-based cancer vaccine: prevention of B16 melanoma progression and metastasis by systemic injection of MART1 mRNA histidylated lipopolyplexes. *Cancer Gene Ther* 14(9):802-814.

173. Iwasaki A & Pillai PS (2014) Innate immunity to influenza virus infection. *Nat Rev Immunol* 14(5):315-328.

174. Stephan K, Smirnova I, Jacque B, & Poltorak A (2007) Genetic analysis of the innate immune responses in wild-derived inbred strains of mice. *Eur J Immunol* 37(1):212-223.

175. Sellers RS, Clifford CB, Treuting PM, & Brayton C (2012) Immunological variation between inbred laboratory mouse strains: points to consider in phenotyping genetically immunomodified mice. *Veterinary pathology* 49(1):32-43.